Fermi National Accelerator Laboratory

FERMILAB-TM-1834
Revision 3

Topics in Radiation at Accelerators: Radiation Physics for Personnel and Environmental Protection

J.D. Cossairt

Fermi National Accelerator Laboratory
P.O. Box 500, Batavia, Illinois 60510

October 1996

Operated by Universities Research Association Inc. under Contract No. DE-AC02-76CH03000 with the United States Department of Energy

Disclaimer

Distribution

RADIATION PHYSICS FOR PERSONNEL AND ENVIRONMENTAL PROTECTION

J. DONALD COSSAIRT
FERMI NATIONAL ACCELERATOR LABORATORY

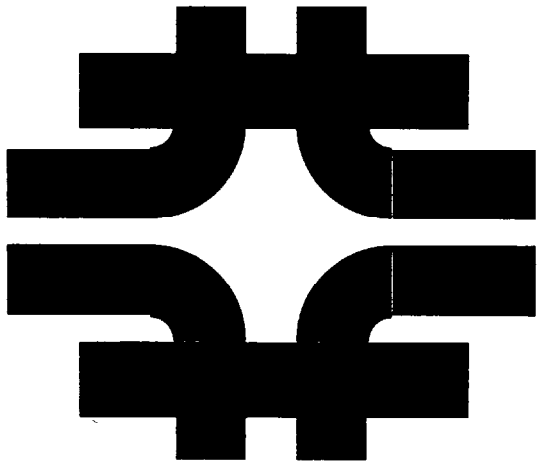

US PARTICLE ACCELERATOR SCHOOL
FLORIDA STATE UNIVERSITY-1993
DUKE UNIVERSITY-1995
TM-1834
Revised June 1995
Revised October 1996

This page is intentionally left blank.

ACKNOWLEDGMENTS

These lecture notes are dedicated to my wife Claudia, and our children, Joe and Sally, who accommodated my long hours spent in the preparation of these notes with love, cheerfulness, and support. I acknowledge the opportunity provided by the Fermilab Director, John Peoples, to participate in this endeavor. I greatly appreciate the encouragement of Mel Month and A. Lincoln Read to participate in the USPAS. I have also greatly appreciated the support and advice of several members of the Fermilab Environment, Safety and Health Section during the preparation and revision of these materials: Alex Elwyn provided a great deal of helpful advice while these materials were initially developed. Nancy Grossman and Kamran Vaziri have offered many suggestions for improvement in these materials. I especially acknowledge Nancy's improvement of the problems. Many other helpful suggestions have been provided by Elaine Marshall, Vernon Cupps, and David Boehnlein. All of these individuals were not timid in calling to my attention my many minor errors and a few major ones which I have hopefully corrected in this revision.

J. Donald Cossairt
October 1996

PREFACE

The original version of this text was presented as part of a course taught at the session of the U. S. Particle Accelerator School held at Florida State University in January, 1993. Upon completion of the USPAS school, the notes were further refined and presented informally as a course at Fermilab in the Spring of 1993. Following this second presentation of the course, the materials were improved by taking into account the many suggestions of course participants. This third revision was prepared after the course was presented in depth at Fermilab in the autumn of 1994, at the U. S. Particle Accelerator School at Duke University in January 1995, and at the Health Physics Society Meeting in Boston in July 1995. This text represents a compilation of the work of many, many people and it is hoped that the reference citations leads the reader to those individuals who have developed this field of applied physics. The problems supplied with each chapter were developed with the goal of promoting better understanding of the text. Solutions to all of the problems are available by contacting the author.

Table of Contents

Chapter 1 Composition of Accelerator Radiation Fields

In this chapter, terminology, physical and radiological quantities, and units of measurement used to describe the properties of accelerator radiation fields are reviewed. The general considerations of primary radiation fields pertinent to accelerators are discussed. The primary radiation fields produced by electron beams are described qualitatively and quantitatively. In the same manner the primary radiation fields produced by proton and ion beams are described.

I. Review of Units and Terminology and Physical Constants and Properties

Radiological Units

In this section common units and terminology used in accelerator radiation protection are described or defined.

energy: The unit of energy in common use when dealing with energetic particles is the electron volt (eV) 1 eV= 1.602×10^{-12} ergs or 1.602×10^{-19} Joule; multiples in common use at accelerators are the keV (10^3 eV), MeV (10^6 eV), GeV(10^9 eV), and TeV (10^{12} eV)

absorbed dose: The energy absorbed per unit mass of material. It is usually denoted by the symbol "D". The customary unit of absorbed dose is the rad while the *Système Internationale* (SI) unit of absorbed dose is the Gray:

1 rad = 100 ergs/gram = 6.24×10^{13} eV/gm
1 Gray (Gy) = 1 J/kg = 100 rads = 6.24×10^{15} eV/gm.

dose equivalent: This quantity has the same dimensions as absorbed dose. It is used to take into account the fact that different particle types have biological effects which are enhanced, per given absorbed dose, over those due to 200 keV photons (a "standard" reference particle). It is usually denoted by the symbol "H".

quality factor: This factor takes into account the relative enhancement in biological effects of various types of ionizing radiation. It is usually denoted by Q, and is used to obtain H from D through the following equation:

$$H = QD. \qquad (1.1)$$

Q is dependent on both particle type and energy and, thus, for any radiation field its value is an average over all components. It is specifically defined to be equal to unity for 200 keV photons. Q ranges from unity for photons electrons, and high energy muons to a value as high as 20 for α–particles (^{4}He nuclei) of a few MeV in energy. For neutrons, Q ranges from 2 to greater than 10, although recent guidance by the International Council on Radiation Protection (ICRP) and the U. S. National Council on Radiation Protection and Measurements (NCRP) recommends that Q be increased by a factor of 2 for neutrons. [Values have been proposed for photons and electrons that differ from unity!]

Q is presently defined to be a function of **linear energy transfer** (LET), L, which, crudely, is equivalent to **stopping power**, or rate of energy loss for charged particles (conventionally, in units of keV/micron). [All ionizing radiation ultimately manifests itself through charged particles so that LET is a "universal" parameterization of localized radiation damage.]

Quality Factor Relationship Graphs Taken from (Sw79)

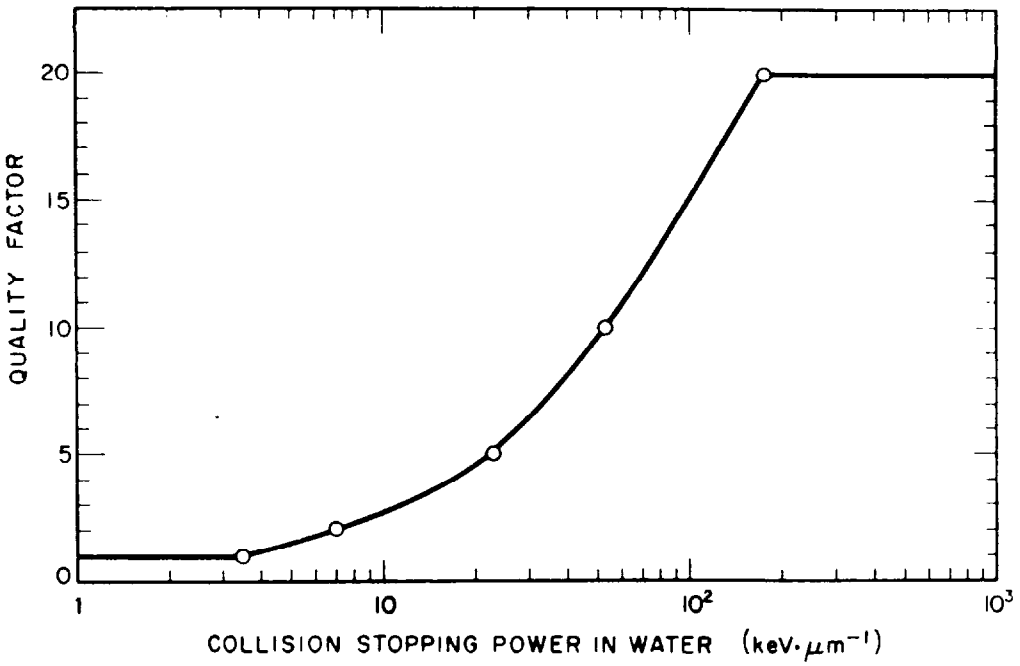

Fig. 1.1 Quality Factor, Q, of charged particles as a function of collision stopping power (LET_∞) in water as recommended by ICRP [Reproduced from (Pa73) and (IC73)].

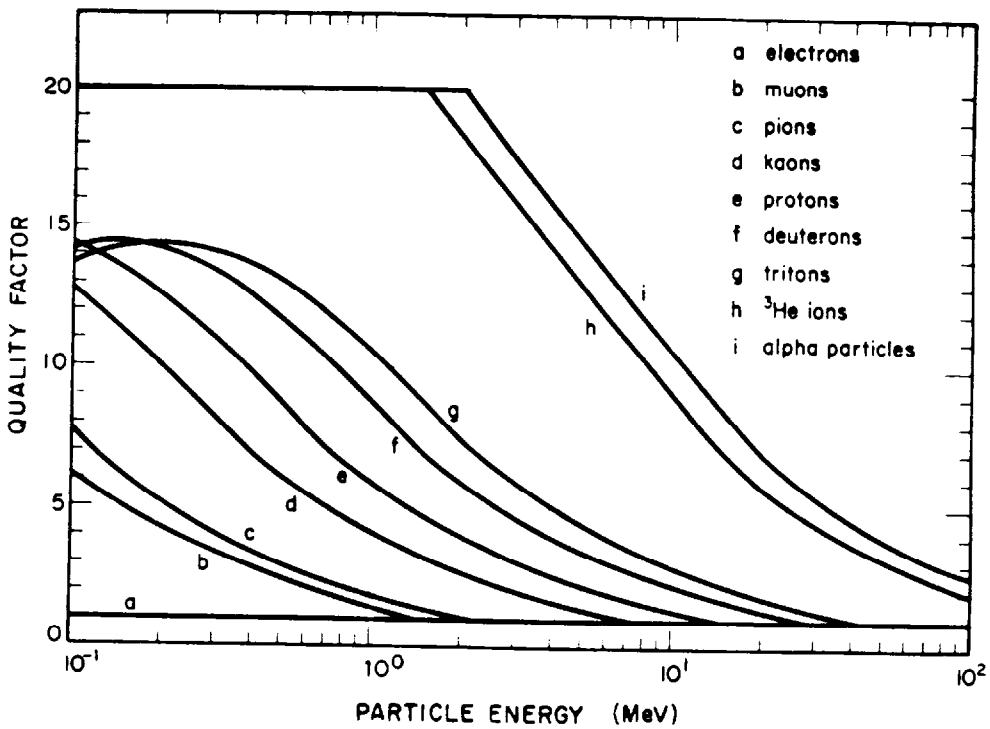

Fig. 1.2 Quality factors of charged particles as a function of energy, as recommended by ICRP. [Reproduced from (Pa73) and (IC73)].

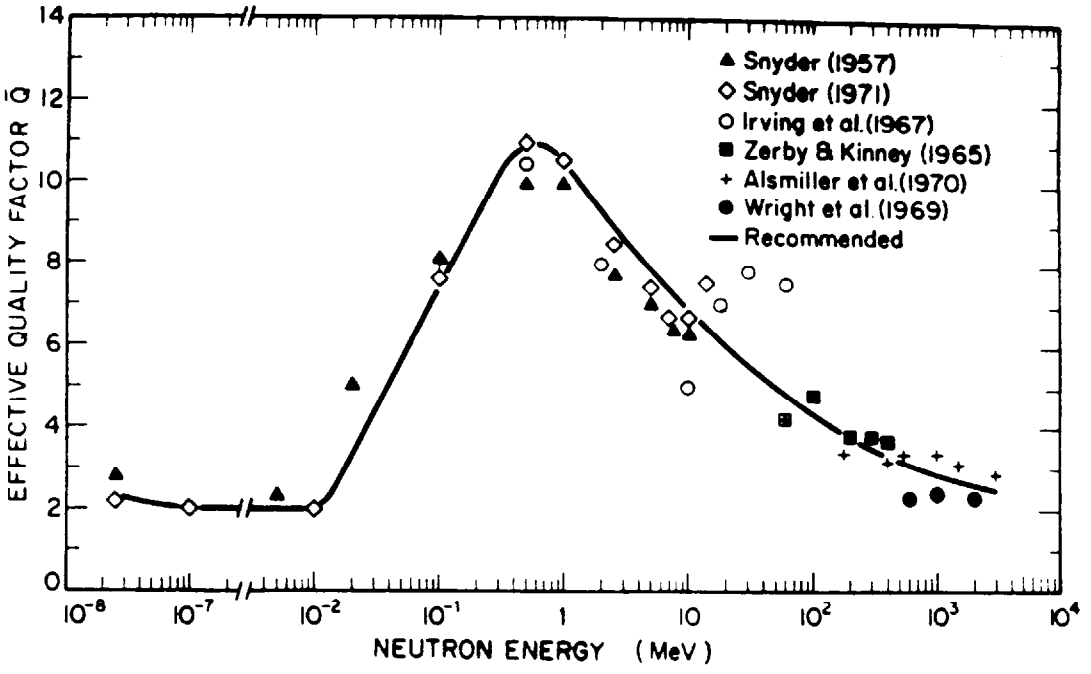

Fig. 1.3 Effective quality factor, Q, for neutrons as a function of neutron kinetic energy: the maximum dose equivalent divided by the absorbed dose where the maximum dose equivalent occurs. The curve indicates values recommended by ICRP. [Reproduced from (Pa73) and (IC73).]

Most commonly, the "quality factor" actually used is an average over the spectrum of LET present:

$$\langle Q \rangle = \int_0^\infty Q(L)D(L)dL \Big/ \int_0^\infty D(L)dL. \qquad (1.2)$$

Thus, H (rem) = QD when D is in rads (customary) and H (Sievert (Sv)) = QD when D is in Gy (SI). Figures 1.1, 1.2, and 1.3 from (Sw79) give the relationship between Q and LET and also between Q and particle energy for a variety of particles.

flux density-The number of particles that traverse a unit area in unit time, generally denoted by the symbol "ϕ",

$$\phi = \frac{d^2n}{dAdt} \qquad (1.3)$$

where d^2n is the differential number of particles traversing surface area element dA during time dt. For radiation fields where the constituent particles move in a multitude of directions, ϕ is determined from the number of transversals of a sphere of revolution of a small element of circular area dA.

fluence, denoted by Φ, is simply the integral over some time interval of the flux density,

$$\Phi = \int_{t_i}^{t_f} \phi(t)dt. \qquad (1.4)$$

The units of flux density are $cm^{-2}s^{-1}$ (customary) and $m^{-2}s^{-1}$ (SI) while the units of fluence are, of course, inverse area without the units of inverse time. Beware! Other units of time such as hours, minutes, days, years, etc cm^{-2} and m^{-2} are routinely used in the literature of radiation protection.

fluence or flux density-to-dose (or dose equivalent) conversion factors - Such factors have been derived through complex calculations supported in a limited way by measurements. These calculations also include effects due to the finite thicknesses of the material of reference (usually "tissue") and include secondary effects. Figures 1.4, 1.5, 1.6, and 1.7 give some graphs of typical fluence or flux density to dose equivalent conversion factors. Figures 1.4, 1.5, and 1.7 are taken from (Pa73) while Fig. 1.6 is taken from (Sw79).

For a radiation field containing a mixture of n different components (e.g., different particle types), one determines the dose equivalent, H, from:

$$H = \sum_{i=1}^{n} \int_{E_{min}}^{E_{max}} P_i(E)\Phi_i(E)dE \qquad (1.5)$$

where $\Phi_i(E)$ is the fluence of particles of type i with energy between E and dE and $P_i(E)$ is a parameter that converts fluence to dose equivalent.

The **cross section** is an extremely important physical concept in describing particle interactions. The cross section represents the "size" of the atom or nucleus for some particular interaction. Consider a beam of particles of fluence Φ (particles/cm^2) incident on a thin slab of absorber of thickness dx. The absorbing medium will contain N atoms/cm^3. The number of incident particles which interact, $d\Phi$, will be given by:

$$-d\Phi = \sigma N \Phi dx \qquad (1.6)$$

where σ is the cross section in units of cm^2. But, $N = \rho N_A/A$, where ρ is the density (g/cm^3), N_A is Avagadro's number (6.02×10^{23} mol^{-1}) and A is the atomic weight. Cross sections are often given in units of barns where 1 barn = 10^{-24} cm^2. If only one interaction is present with no other processes operative, this integrates, after some distance x (e.g., in cm), to:

$$\Phi(x) = \Phi(0)e^{-N\sigma x}. \qquad (1.7)$$

Thus, the **linear absorption coefficient**, μ, and its reciprocal, the **attenuation length**, λ, are given by:

$$\mu = N\sigma \ (cm^{-1}) \quad \text{and} \quad \lambda = 1/N\sigma \ (cm). \qquad (1.8)$$

Sometimes the mass attenuation length, $\lambda = \rho/N\sigma$ (g/cm^2) is used where ρ is the density in g/cm^3. In the literature, the symbols are, unfortunately, often "confused" and one has to be careful to understand the particular definition of "λ" involved.

Flux Density to Dose Conversion Factors

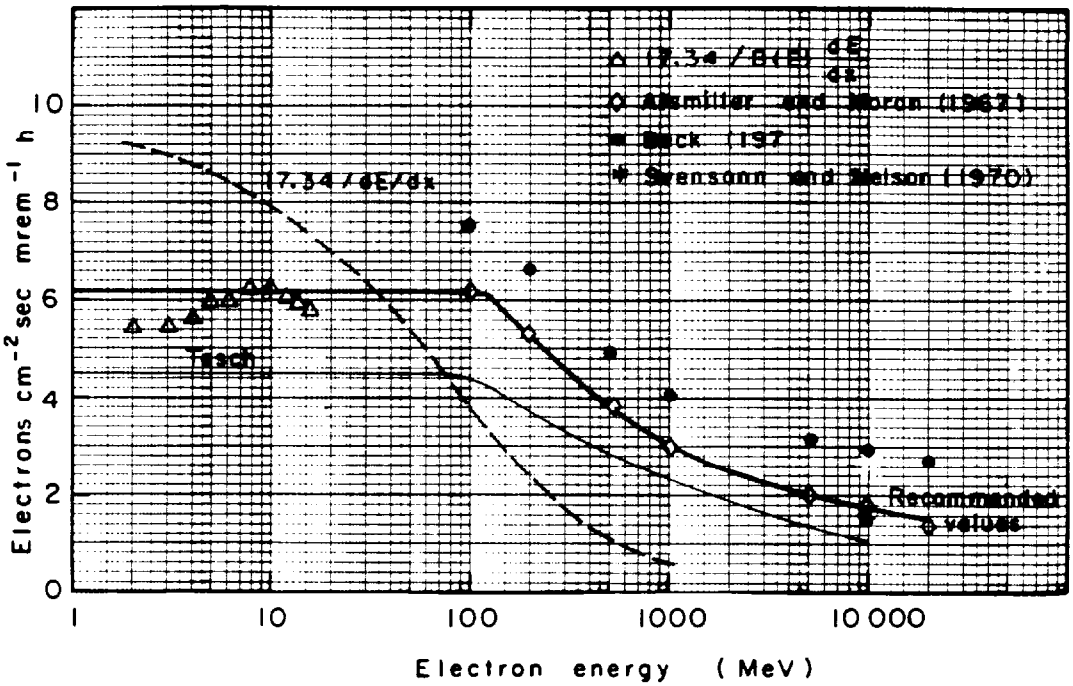

Fig. 1.4 Conversion factors for flux density to dose-equivalent rate for electrons. [Reproduced from (Pa73) and references cited therein.]

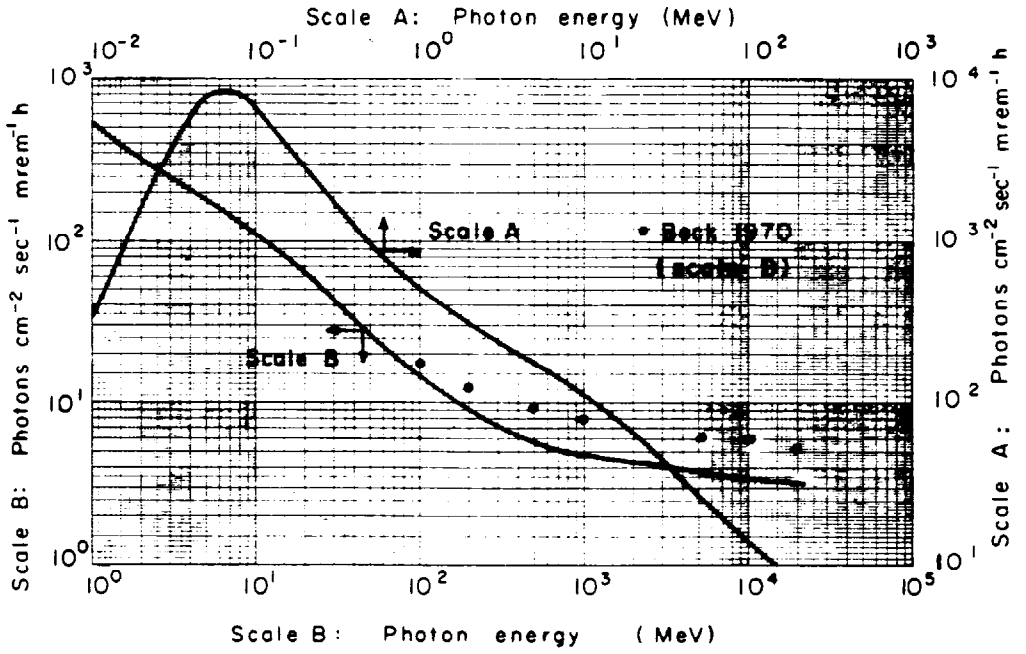

Fig. 1.5 Conversion factors for flux density to dose-equivalent rate for photons. [Reproduced from (Pa73) and references cited therein.]

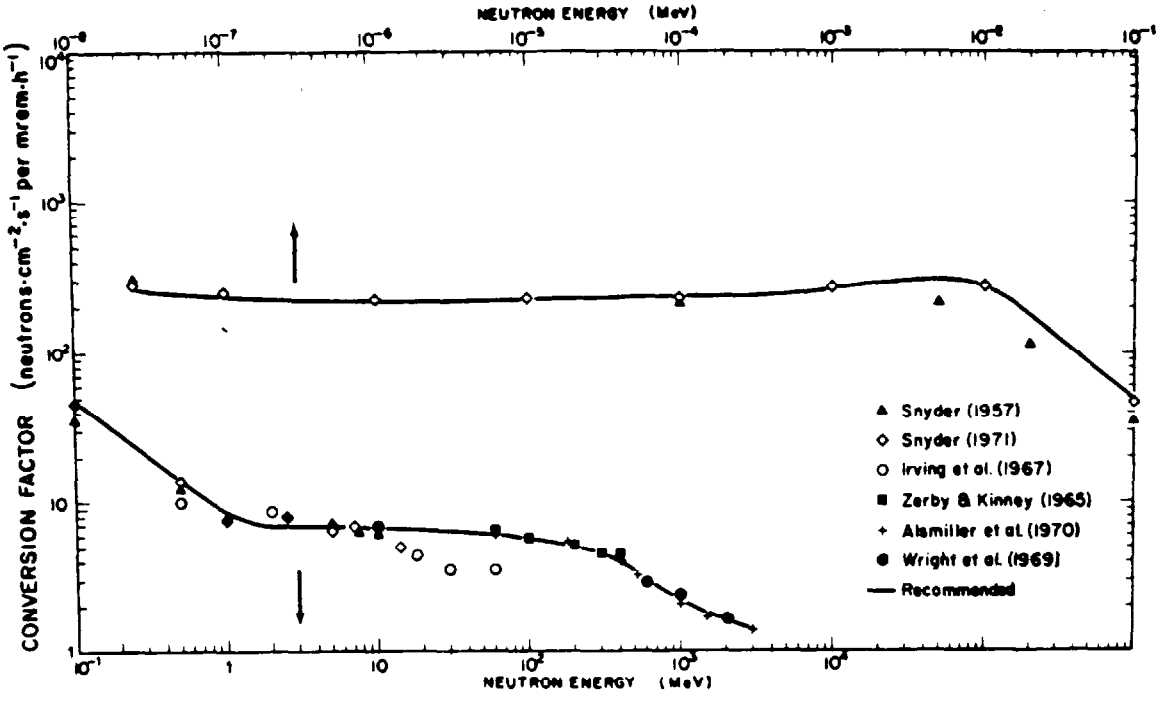

Fig. 1.6 Conversion factors for neutrons as a function of incident neutron kinetic energy for unidirectional broad beam, normal incidence. The curves indicate the values recommended by ICRP. [Reproduced from (Sw79) and from (IC73).]

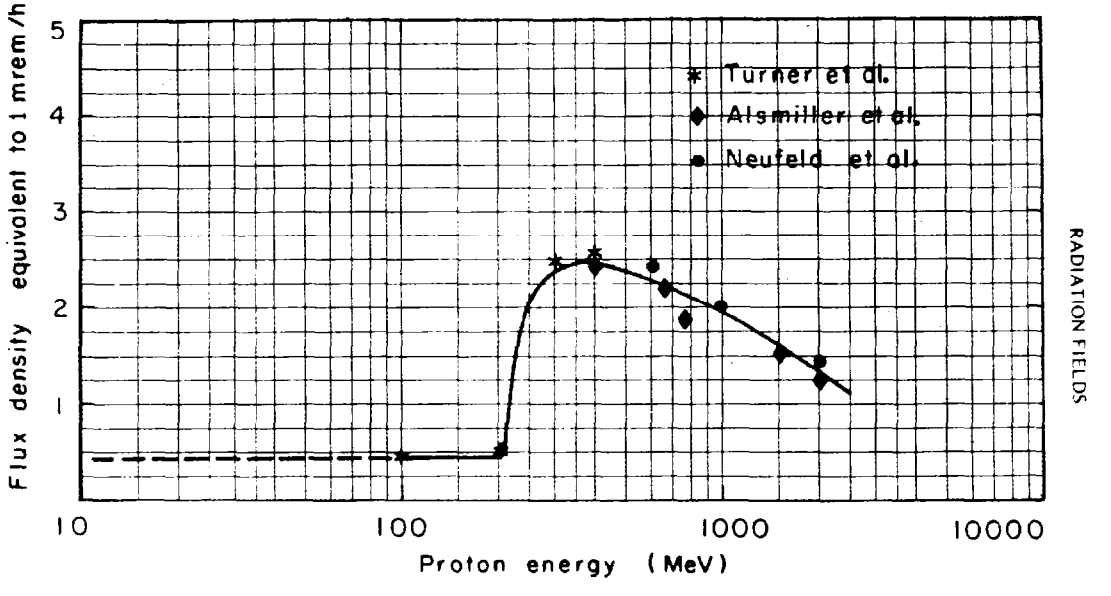

Fig. 1.7 Conversion factors for flux density to dose-equivalent rate for protons as a function of incident proton kinetic energy (protons cm^{-2} s^{-1} per mrem hr^{1}) [Reproduced from (Pa73).]

Physical Constants and Atomic and Nuclear Properties

Tables 1.1 and 1.2 give physical constants and atomic and nuclear properties taken from (PR92). A number of these constants and properties will be used throughout the rest of this text. and in the solutions of the problems.

II. Summary of relativistic relationships

The **rest energy**, W_0, of a particle of rest mass m_0 is given by,

$$W_0 = m_0c^2 \qquad (1.9)$$

where c is the velocity of light.

The **total energy** in free space, W, is then given by

$$W = mc^2 = m_0c^2(1-\beta^2)^{-1/2}, \qquad (1.10)$$

where $\beta = v/c$ and v is the velocity of the particle in a given frame of reference.

The **relativistic mass**, m, of a particle moving at β is another name for the total energy and is given by

$$mc^2 = \frac{1}{\sqrt{1-\beta^2}}m_0c^2 = \gamma m_0c^2 \qquad (1.11)$$

The **kinetic energy**, E, is then;

$$E = W - W_0 = (m - m_0)c^2 \quad \text{and} \qquad (1.12)$$

$$\beta = \sqrt{\left[1 - \left(\frac{W_0}{W}\right)^2\right]}. \qquad (1.13)$$

The **momentum**, p, of a particle is

$$p = mv = m\beta c = (1/c)(W^2 - W_0^2)^{1/2} = \frac{1}{c}\sqrt{[E(E + 2W_0)]}, \qquad (1.14)$$

so that at high energies, $p \approx E/c \approx W/c$.

It is usually most convenient to work in a system of units where energy is in units of eV, MeV, etc., velocities are expressed in units of the speed of light (β), momenta are expressed as energy divided by c (e.g., MeV/c, etc.), and masses are expressed as energy divided by c^2 (e.g., MeV/c^2, etc.).

Table 1.1 Physical Constants [Reproduced from (PR92)]

Reviewed 1991 by B.N. Taylor. Based mainly on the "1986 Adjustment of the Fundamental Physical Constants" by E.R. Cohen and B.N. Taylor, Rev. Mod. Phys. **59**, 1121 (1987). The figures in parentheses after the values give the 1-standard-deviation uncertainties in the last digits; the uncertainties in parts per million (ppm) are given in the last column. The uncertainties of the values from a least-squares adjustment are in general correlated, and the laws of error propagation must be used in calculating additional quantities; the full variance matrix is given in the cited paper. The set of constants resulting from the 1986 adjustment has been recommended for international use by CODATA (Committee on Data for Science and Technology).

Since the 1986 adjustment, new experiments have yielded improved values for a number of constants, including the Rydberg constant R_∞, the Planck constant h, the fine-structure constant α, and the molar gas constant R, and hence also for constants directly derived from these, such as the Boltzmann constant k and Stefan-Boltzmann constant σ. The new results and their impact on the 1986 recommended values are discussed extensively in "Recommended Values of the Fundamental Physical Constants: A Status Report," B.N. Taylor and E.R. Cohen, J. Res. Natl. Inst. Stand. Technol. **95**, 497 (1990). In general, the new results give uncertainties for the affected constants that are 5 to 7 times smaller than the 1986 uncertainties, but the changes in the values themselves are smaller than twice the 1986 uncertainties. Until there are more experiments and a complete readjustment of the constants, the 1986 CODATA set, given (in part) below, remains the set of choice.

Quantity	Symbol, equation	Value	Uncert. (ppm)
speed of light	c	299 792 458 m s^{-1}	(exact)*
Planck constant	h	6.626 075 5(40)$\times 10^{-34}$ J s	0.60
Planck constant, reduced	$\hbar \equiv h/2\pi$	1.054 572 66(63)$\times 10^{-34}$ J s	0.60
		= 6.582 122 0(20)$\times 10^{-22}$ MeV s	0.30
electron charge magnitude	e	1.602 177 33(49)$\times 10^{-19}$ C = 4.803 206 8(15)$\times 10^{-10}$ esu	0.30, 0.03
conversion constant	$\hbar c$	197.327 053(59) MeV fm	0.30
conversion constant	$(\hbar c)^2$	0.389 379 66(23) GeV^2 mbarn	0.59
electron mass	m_e	0.510 999 06(15) MeV/c^2 = 9.109 389 7(54)$\times 10^{-31}$ kg	0.30, 0.59
proton mass	m_p	938.272 31(28) MeV/c^2 = 1.672 623 1(10)$\times 10^{-27}$ kg	0.30, 0.59
		= 1.007 276 470(12) u = 1836.152 701(37) m_e	0.012, 0.020
deuteron mass	m_d	1875.613 39(57) MeV/c^2	0.30
unified atomic mass unit (u)	(mass C^{12} atom)/12 = (1 g)/N_A	931.494 32(28) MeV/c^2 = 1.660 540 2(10)$\times 10^{-27}$ kg	0.30, 0.59
permittivity of free space	ϵ_0	8.854 187 817 ... $\times 10^{-12}$ F m^{-1}	(exact)
permeability of free space	μ_0 ; $\epsilon_0\mu_0 = 1/c^2$	$4\pi \times 10^{-7}$ N A^{-2} = 12.566 370 614 ... $\times 10^{-7}$ N A^{-2}	(exact)
fine structure constant	$\alpha = e^2/4\pi\epsilon_0\hbar c$	*1/137.035 989 5(61)*†	*0.045*
classical electron radius	$r_e = e^2/4\pi\epsilon_0 m_e c^2$	2.817 940 92(38)$\times 10^{-15}$ m	0.13
electron Compton wavelength	$\lambda\!\!\!^{-}_e = \hbar/m_e c = r_e\alpha^{-1}$	3.861 593 23(35)$\times 10^{-13}$ m	0.089
Bohr radius ($m_{\text{nucleus}} = \infty$)	$a_\infty = 4\pi\epsilon_0\hbar^2/m_e e^2 = r_e\alpha^{-2}$	0.529 177 249(24)$\times 10^{-10}$ m	0.045
wavelength of 1 eV/c particle	hc/e	1.239 842 44(37)$\times 10^{-6}$ m	0.30
Rydberg energy	$hcR_\infty = m_e e^4/2(4\pi\epsilon_0)^2\hbar^2 = m_e c^2\alpha^2/2$	13.605 698 1(40) eV	0.30
Thomson cross section	$\sigma_T = 8\pi r_e^2/3$	0.665 246 16(18) barn	0.27
Bohr magneton	$\mu_B = e\hbar/2m_e$	5.788 382 63(52)$\times 10^{-11}$ MeV T^{-1}	0.089
nuclear magneton	$\mu_N = e\hbar/2m_p$	3.152 451 66(28)$\times 10^{-14}$ MeV T^{-1}	0.089
electron cyclotron freq./field	$\omega^e_{\text{cycl}}/B = e/m_e$	1.758 819 62(53)$\times 10^{11}$ rad s^{-1} T^{-1}	0.30
proton cyclotron freq./field	$\omega^p_{\text{cycl}}/B = e/m_p$	9.578 830 9(29)$\times 10^{7}$ rad s^{-1} T^{-1}	0.30
gravitational constant	G_N	6.672 59(85)$\times 10^{-11}$ m^3 kg^{-1} s^{-2}	128
		= 6.707 11(86)$\times 10^{-39}$ $\hbar c$ $(GeV/c^2)^{-2}$	128
standard grav. accel., sea level	g	9.806 65 m s^{-2}	(exact)
Avogadro number	N_A	*6.022 136 7(36)*$\times 10^{23}$ mol^{-1}	0.59
Boltzmann constant	k	1.380 658(12)$\times 10^{-23}$ J K^{-1}	8.5
		= 8.617 385(73)$\times 10^{-5}$ eV K^{-1}	8.4
Wien displacement law constant	$b = \lambda_{\max}T$	2.897 756(24)$\times 10^{-3}$ m K	8.4
molar volume, ideal gas at STP	$N_A k$(273.15 K)/(1 atmosphere)	22.414 10(19)$\times 10^{-3}$ m^3 mol^{-1}	8.4
Stefan-Boltzmann constant	$\sigma = \pi^2 k^4/60\hbar^3 c^2$	5.670 51(19)$\times 10^{-8}$ W m^{-2} K^{-4}	34
Fermi coupling constant	$G_F/(\hbar c)^3$	1.166 39(2)$\times 10^{-5}$ GeV^{-2}	17
weak mixing angle	$\sin^2\theta_W$ ($\overline{\text{MS}}$)	0.2325±0.0008	3441
$W^\pm$ boson mass	m_W	80.22±0.26 GeV/c^2	3241
Z^0 boson mass	m_Z	91.173±0.020 GeV/c^2	219
strong coupling constant	$\alpha_s(m_Z)$	0.1134±0.0035	3.1 × 10^4

π = 3.141 592 653 589 793 238 e = 2.718 281 828 459 045 235 γ = 0.577 215 664 901 532 861

1 in ≡ 0.0254 m 1 barn ≡ 10^{-28} m^2 1 eV = 1.602 177 33(49) × 10^{-19} J 1 gauss (G) ≡ 10^{-4} tesla (T)

1 Å ≡ 10^{-10} m 1 dyne ≡ 10^{-5} newton (N) 1 eV/c^2 = 1.782 662 70(54) × 10^{-36} kg 0° C ≡ 273.15 K

1 fm ≡ 10^{-15} m 1 *erg* ≡ 10^{-7} joule (J) 2.997 924 58 × 10^9 esu = 1 coulomb (C) 1 atmosphere ≡ 760 torr ≡ 1.013 25 × 10^5 N m^2

* The meter is now defined to be the length of the path traveled by light in 1/299792458 second. See B.W. Petley, Nature **303**, 373 (1983).

† At $Q^2 = m_e^2$. At $Q^2 \approx m_W^2$ the value is approximately 1/128.

Table 1.2 Atomic and Nuclear Properties of Materials [Reproduced from (PR92)]

Material	Z	A	Nuclear[a] total cross section σ_T [barn]	Nuclear[b] inelastic cross section σ_I [barn]	Nuclear[c] collision length λ_T [g/cm^2]	Nuclear[c] interaction length λ_I [g/cm^2]	$\left[\frac{dE}{dx}\right]_{min}^{d}$ $\left[\frac{\text{MeV}}{\text{g/cm}^2}\right]$	Radiation length[e] X_0 [g/cm^2]	[cm] () is for gas	Density[f] [g/cm^3] () is for gas [g/ℓ]	Refractive index n[f] () is $(n-1)\times10^6$ for gas
H_2	1	1.01	0.0387	0.033	43.3	50.8	4.12	61.28	865	0.0708(0.090)	1.112(140)
D_2	1	2.01	0.073	0.061	45.7	54.7	2.07	122.6	757	0.162(0.177)	1.128
He	2	4.00	0.133	0.102	49.9	65.1	1.94	94.32	755	0.125(0.178)	1.024(35)
Li	3	6.94	0.211	0.157	54.6	73.4	1.58	82.76	155	0.534	—
Be	4	9.01	0.268	0.199	55.8	75.2	1.61	65.19	35.3	1.848	—
C	6	12.01	0.331	0.231	60.2	86.3	1.78	42.70	18.8	2.265[g]	—
N_2	7	14.01	0.379	0.265	61.4	87.8	1.82	37.99	47.0	0.808(1.25)	1.205(300)
O_2	8	16.00	0.420	0.292	63.2	91.0	1.82	34.24	30.0	1.14(1.43)	1.22(266)
Ne	10	20.18	0.507	0.347	66.1	96.6	1.73	28.94	24.0	1.207(0.90)	1.092(67)
Al	13	26.98	0.634	0.421	70.6	106.4	1.62	24.01	8.9	2.70	—
Si	14	28.09	0.660	0.440	70.6	106.0	1.66	21.82	9.36	2.33	—
Ar	18	39.95	0.868	0.566	76.4	117.2	1.51	19.55	14.0	1.40(1.78)	1.233(283)
Ti	22	47.88	0.995	0.637	79.9	124.9	1.51	16.17	3.56	4.54	—
Fe	26	55.85	1.120	0.703	82.8	131.9	1.48	13.84	1.76	7.87	—
Cu	29	63.55	1.232	0.782	85.6	134.9	1.44	12.86	1.43	8.96	—
Ge	32	72.59	1.365	0.858	88.3	140.5	1.40	12.25	2.30	5.323	—
Sn	50	118.69	1.967	1.21	100.2	163	1.26	8.82	1.21	7.31	—
Xe	54	131.29	2.120	1.29	102.8	169	1.24	8.48	2.77	3.057(5.89)	(705)
W	74	183.85	2.767	1.65	110.3	185	1.16	6.76	0.35	19.3	—
Pt	78	195.08	2.861	1.708	113.3	189.7	1.15	6.54	0.305	21.45	—
Pb	82	207.19	2.960	1.77	116.2	194	1.13	6.37	0.56	11.35	—
U	92	238.03	3.378	1.98	117.0	199	1.09	6.00	≈0.32	≈18.95	—
Air, 20°C, 1 atm. (STP in paren.)					62.0	90.0	1.82	36.66	(30420)	0.001205(1.29)	1.000273(293)
H_2O					60.1	84.9	2.03	36.08	36.1	1.00	1.33
Shielding concrete[h]					67.4	99.9	1.70	26.7	10.7	2.5	—
SiO_2 (quartz)					67.0	99.2	1.72	27.05	12.3	2.64	1.458
H_2 (bubble chamber 26°K)					43.3	50.8	4.12	61.28	≈1000	≈ 0.063[i]	1.100
D_2 (bubble chamber 31°K)					45.7	54.7	2.07	122.6	≈900	≈ 0.140[i]	1.110
H-Ne mixture (50 mole percent)[j]					65.0	94.5	1.84	29.70	73.0	0.407	1.092
Ilford emulsion G5					82.0	134	1.44	11.0	2.89	3.815	—
NaI					94.8	152	1.32	9.49	2.59	3.67	1.775
BaF_2					92.1	146	1.35	9.91	2.05	4.89	1.56
BGO ($Bi_4Ge_3O_{12}$)					97.4	156	1.27	7.98	1.12	7.1	2.15
Polystyrene, scintillator (CH)[k]					58.4	82.0	1.95	43.8	42.4	1.032	1.581
Lucite, Plexiglas ($C_5H_8O_2$)					59.2	83.6	1.95	40.55	≈34.4	1.16–1.20	≈ 1.49
Polyethylene (CH_2)					56.9	78.8	2.09	44.8	≈47.9	0.92–0.95	—
Mylar ($C_5H_4O_2$)					60.2	85.7	1.86	39.95	28.7	1.39	—
Borosilicate glass (Pyrex)[l]					66.2	97.6	1.72	28.3	12.7	2.23	1.474
CO_2					62.4	90.5	1.82	36.2	(18310)	(1.977)	(410)
Ethane C_2H_6					55.73	75.71	2.25	45.66	(34035)	0.509(1.356)[m]	(1.038)[m]
Methane CH_4					54.7	74.0	2.41	46.5	(64850)	0.423(0.717)	(444)
Isobutane C_4H_{10}					56.3	77.4	2.22	45.2	(16930)	(2.67)	(1270)
NaF					66.78	97.57	1.69	29.87	11.68	2.558	1.336
LiF					62.00	88.24	1.66	39.25	14.91	2.632	1.392
Freon 12 (CCl_2F_2) gas, 26°C, 1 atm.[n]					70.6	106	1.62	23.7	4810	(4.93)	1.001080
Silica Aerogel[o]					65.5	95.7	1.83	29.85	≈150	0.1–0.3	$1.0+0.25\rho$
NEMA G10 plate[p]					62.6	90.2	1.87	33.0	19.4	1.7	—

For moderately relativistic particles, the mean rate of energy loss (**stopping power**) is given approximately by (PR92):

$$-\frac{dE}{dx} = 4\pi N_A r_e^2 m_e c^2 z^2 \frac{Z}{A}\frac{1}{\beta^2}\left[\ln\left\{\frac{2m_e c^2\gamma^2\beta^2}{I}\right\} - \beta^2 - \frac{\delta}{2}\right], \qquad (1.15)$$

where N_A is Avogadro's number, Z and A are the atomic number and weight of the material transversed, z is the atomic number of the projectile, m_e and r_e are the mass and "classical radius" of the electron and I is the ionization constant. δ is a small correction factor which approaches 2 lnγ. Substituting constants,

$$-\frac{dE}{dx} = (0.3071)z^2\frac{Z}{A}\frac{1}{\beta^2}\left[\ln\left\{\frac{2m_e c^2\gamma^2\beta^2}{I}\right\} - \beta^2 - \frac{\delta}{2}\right] \text{ (MeV cm}^2\text{g}^{-1}\text{)} \qquad (1.16)$$

where $I \approx 16Z^{0.9}$ eV for $Z > 1$ and has the value of approximately 20 eV for diatomic hydrogen).

The **decay length** at a given velocity of a particle with a finite meanlife (at rest), τ, can be obtained from the product of the speed of light and the meanlife, $c\tau$, which is often tabulated. The decay length is given by $\gamma\beta c\tau$, where relativistic time dilation is taken into account. This length is to be distinguised from that called the **decay path**. The latter represents a distance in space in which a given particle is allowed to decay with no or minimal competition from other effects exemplified by scattering or absorption.

III. Primary Radiation Fields at Accelerators-General Considerations

The particle yield is a crucial parameter. It is typically a function of both angle and particle energy and is defined according to Fig. 1.8. Such particle yields are reported in terms of particle type, energy, fluence, and angular distributions. Scattered reaction products are found at a hypothetical "detector" or located at radius, r, and polar angle, θ, relative to the direction of the incident particle along the positive Z-axis.

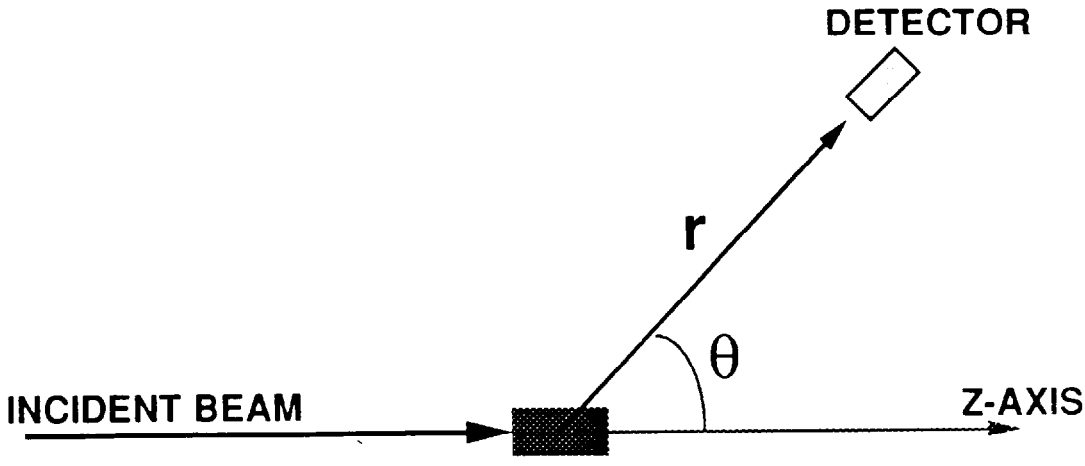

Fig. 1.8 Conceptual interaction of incident beam with material which produces radiation at the location of a hypothetical detector located at polar coordinates (r, θ).

The rate of production of the desired reaction products and their energy spectra is, in general, a strong function of both θ and the incident particle energy E_o.

With a single exception, there is no dependence on the azimuthal angle, α, in this spherical coordinate scheme.[1] [With coordinates (r,θ,α) α is used, unconventionally, as the azimuthal angle to avoid confusion with ϕ, the flux density.]

In principle, calculations of the particle yield could be taken directly from differential cross sections for given incident particle energy E (E usually denotes kinetic energy),

$$\frac{d\sigma(\theta,E)}{d\Omega},$$

where $\sigma(\Omega, E)$ is the cross section as a function of energy and Ω is the solid angle into which the secondary particles are produced. (The angular dependence is only on θ and not also on α due to the lack of azimuthal dependence.)

In general calculations of the radiation field which directly use the cross sections are not practical because targets hit by beam are not really thin (i.e., one cannot ignore energy loss or secondary interactions in the target) and there is incomplete knowledge of cross sections at all energies so one cannot integrate over θ and E to get the total yield.

For many applications, the details of the angular distributions of total secondary particle **yield**, $dY(\theta)/d\Omega$, and the **angular dependence of the emitted particle energy spectrum**, $d^2Y(\theta,E)/dEd\Omega$, of the emitted particle spectra are very important.

Often, the particle fluence is needed at a particular location at coordinates (r,θ) from a known point source of beam loss while the angular distributions of $dY/d\Omega$ are generally expressed in units of particles/(steradian · incident particle).

To obtain the total fluence $\Phi(\theta)$ [e.g., "particles"/(cm^2·incident particle)], or differential fluence $d\Phi(E,\theta)/dE$ [e.g., "particles"/(cm^2·MeV·incident particle)] at a given distance r (cm) at a specified angle θ, one must simply multiply the plotted values by r^{-2} (cm^2):

$$\Phi(\theta) = \frac{1}{r^2}\frac{dY(\theta)}{d\Omega} \quad \text{and} \quad \frac{d\Phi(E,\theta)}{dE} = \frac{1}{r^2}\frac{d^2Y(\theta,E)}{dEd\Omega}. \tag{1.17}$$

[1]The single exception is the case in which the spins of the target nuclei and/or the incident particle are oriented along some chosen direction in a "polarization" experiment.

IV. Radiation Production by Electron Accelerators *(Most of this material is adapted from (Sw79), the work of the late William P. Swanson of SLAC and LBL.)*

At all energies photons produced by bremsstrahlung dominate the radiation field aside from the hazard of the direct beam. As the energy increases, neutrons become a significant problem. For $E_0 > 100$ MeV, the electromagnetic cascade must be considered (see Chapter 2)

An interesting rule of thumb is that electrons have a finite range in material proportional to the initial kinetic energy of the electron:

For $2 < E_0 < 10$ MeV, $R = 0.6E_0$ g cm^{-2}. (In air, $R \approx 5\ E_0$ meters with E_0 in MeV). (1.18)

Above approximately 10 MeV, radiative losses begin to dominate.

Direct Beam

Swanson (Sw79) has given what he expressed as an approximate, "conservative" rule of thumb for the energy domain of $1 < E_0 < 100$ MeV:

$$\frac{dH}{dt} = 1.6 \times 10^{-4}\,\phi$$ where $\frac{dH}{dt}$ is the dose equivalent rate (rem h^{-1} and ϕ is the flux density (electrons cm^{-2} s^{-1}) (1.19)

Others have calculated the conversion factor as a function of energy as in Fig. 1.9 taken from (Sw79). (The results in Fig. 1.9 should be regarded as more recent improvements to the results of Fig. 1.4.)

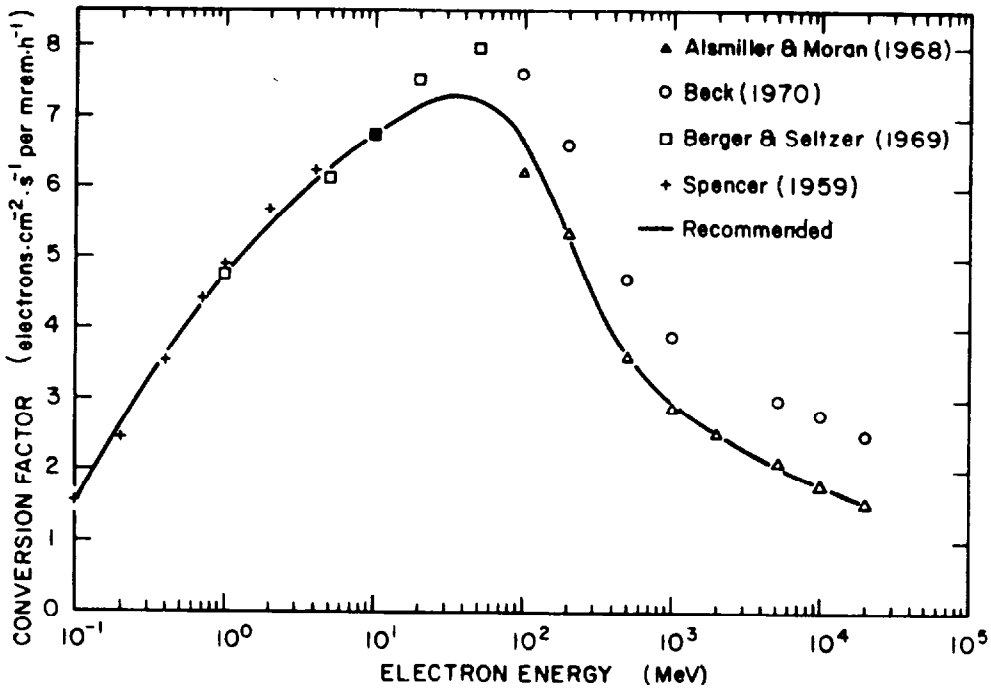

Fig. 1.9 Conversion factor as a function of incident energy E_0 for a unidirectional broad beam of monoenergetic electrons at normal incidence. The curve indicates values represented by the ICRP. [Reproduced from (Sw79). See (Sw79) for references indicated on figure.]

Bremsstrahlung

Bremsstrahlung is the radiative energy loss of electrons as they interact with materials. It appears in the form of photons. An important parameter when considering radiative energy loss of electrons in matter is the **critical energy,** E_c. E_c is that energy above which the energy loss due to radiation exceeds that due to ionization for electrons. The value E_c is a smooth function of atomic number;

$$E_c = 800/(Z + 1.2)\ (\text{MeV}), \tag{1.20}$$

where Z is the atomic number of the material.

The transition from ionization to radiation is also a smooth one. The stopping power for electrons may be written as the sum of collisional and radiative components (Pa73):

$$\left(\frac{dE}{dx}\right)_{tot} = \left(\frac{dE}{dx}\right)_{coll} + \left(\frac{dE}{dx}\right)_{rad}. \tag{1.21}$$

A parameter of significant importance for electrons is the **radiation length,** X_o, which (PR92) is the mean thickness of material over which a high energy electron loses all but 1/e of its energy by bremsstrahlung and is the approximate scale length for describing high-energy electromagnetic cascades. This parameter also plays a role in the "scaling" of multiple scattering for all charged particles. This parameter is approximated by:

$$X_o = \frac{716.4\ \text{g cm}^{-2}\text{A}}{Z(Z + 1)\ln\left(287/\sqrt{Z}\right)} \tag{1.22}$$

where Z and A are the atomic number and weight of the material medium.

It turns out for high energy electrons that: $\left(\frac{dE}{dx}\right)_{rad} = -\frac{E}{X_o}$, (1.23)

so that under these conditions (where ionization can be neglected)

$$E(x) = E_0 e^{-x/X_o} \tag{1.24}$$

where the energy of the incident particle is E_o.

Figure 1.10 taken from (SW79) gives the percentage of E_o which appears as radiation for various materials as a function of energy. External bremsstrahlung develops as a function of target thickness and is described by a "transition" curve. As the thickness increases, the radiation increases until reabsorption begins to take effect. Then, self-shielding begins to take over. One talks about the maximum as a "thick-target" bremsstrahlung spectrum. This can be used as a basis for conservative assumptions related to quantities of radiological concern. Figure 1.11 from (Sw79) shows the behavior for a high-Z target. This type of behavior has been developed into three "rules of thumb" by Swanson in (Sw79).

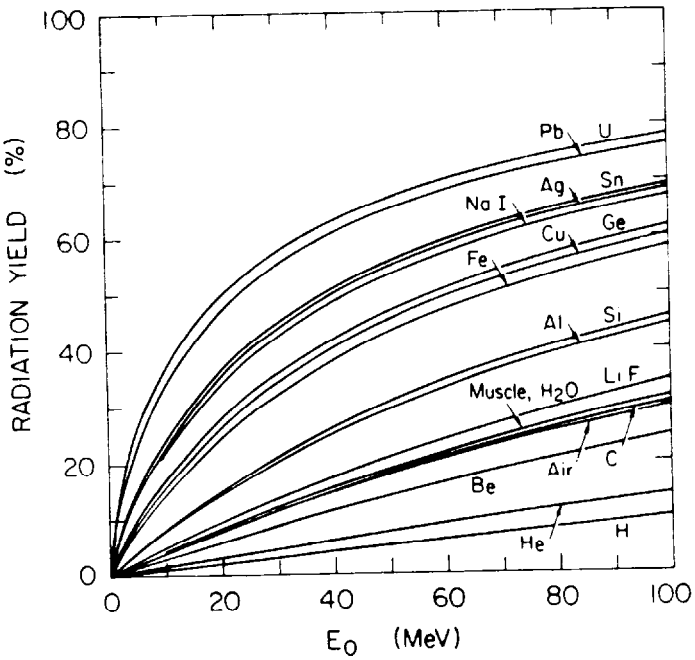

Fig. 1.10 Radiation yield (or bremsstrahlung efficiency) for electrons stopped in various materials. Fraction (in per cent) of kinetic energy of incident electrons converted to radiation as a function of incident energy E_0. The remainder is transferred to the medium by ionization. [Reproduced from (Sw79)].

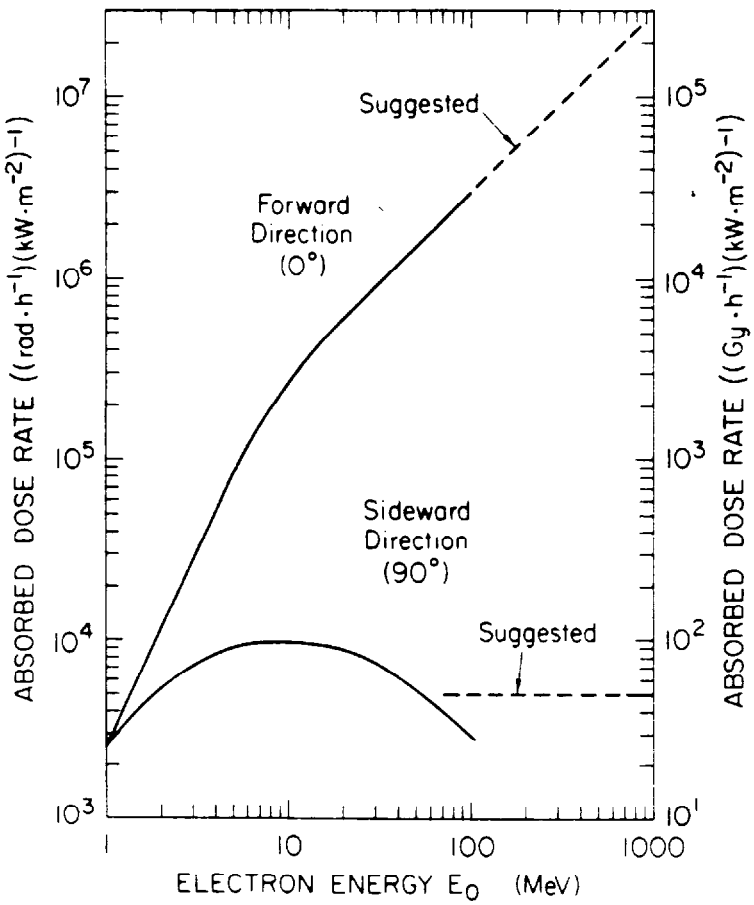

Fig. 1.11 Thick target bremsstrahlung from a high-Z target. Absorbed dose rates at 1 meter per unit incident electron beam power (kW) as a function of incident electron energy E_0. The dashed line at 0° represents a reasonable extrapolation of the measured values. The dose rates measured in the sideward direction (smoothed for this figure) depend strongly on target and detector geometry and vary by more than a factor of two. The dashed line at 90° represents the more penetrating radiation component to be considered in room shielding. [Reproduced from (Sw79).]

These "Rules of Thumb" parameterize this behavior for the absorbed dose rates, $\dot{D}$, at 1 meter and normalized to one kW of incident beam power:

Rule of Thumb 1:

$$\dot{D} = [(Gy \cdot h^{-1})(kW \cdot m^{-2})^{-1}] \approx 20\ E_0^2 \qquad \text{at } \theta = 0^o,\ E_0 < 15 \text{ MeV}. \tag{1.25}$$

Rule of Thumb 2:

$$\dot{D} = [(Gy \cdot h^{-1})(kW \cdot m^{-2})^{-1}] \approx 300\ E_0 \qquad \text{at } \theta = 0^o,\ E_0 > 15 \text{ MeV}. \tag{1.26}$$

Rule of Thumb 3:

$$\dot{D} = [(Gy \cdot h^{-1})(kW \cdot m^{-2})^{-1}] \approx 50 \qquad \text{at } \theta = 90^o,\ E_0 > 100 \text{ MeV}. \tag{1.27}$$

One can scale to other distances by using the "inverse square" law. It should be noted that one can get higher dose rates at 90° in certain circumstances due to softer radiation components. The forward intensity is a slowly varying function of target material except at very low Z. The angular width, $\theta_{1/2}$, of the forward lobe (half-intensity) is approximately given by the relation:

$$E_0\theta_{1/2} \approx 100 \text{ (MeV degrees)}. \tag{1.28}$$

This is displayed graphically in Fig. 1.12 taken from (Sw79).

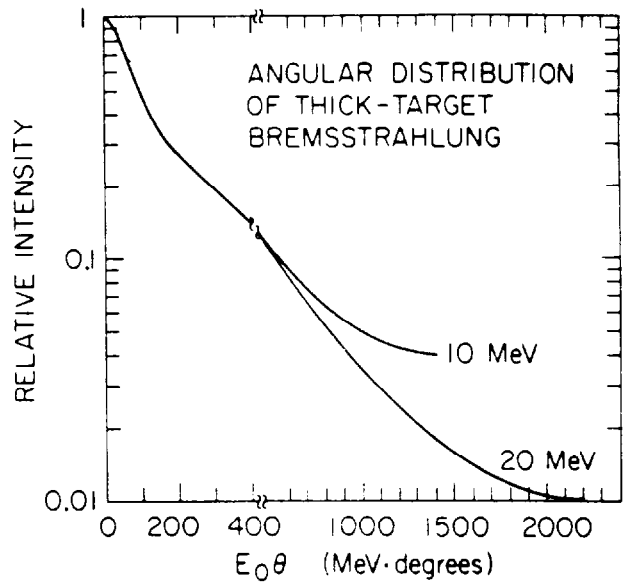

Fig. 1.12 Angular distribution of bremsstrahlung intensity from high-Z targets (relative units), plotted as a function of the variable $E_0\theta$. [Reproduced from (Sw79).]

Figure 1.13 taken from Ref. 4 shows bremsstrahlung spectra at $\theta = 0^o$ for electrons incident on a high-Z material of intermediate thickness at a variety of energies.

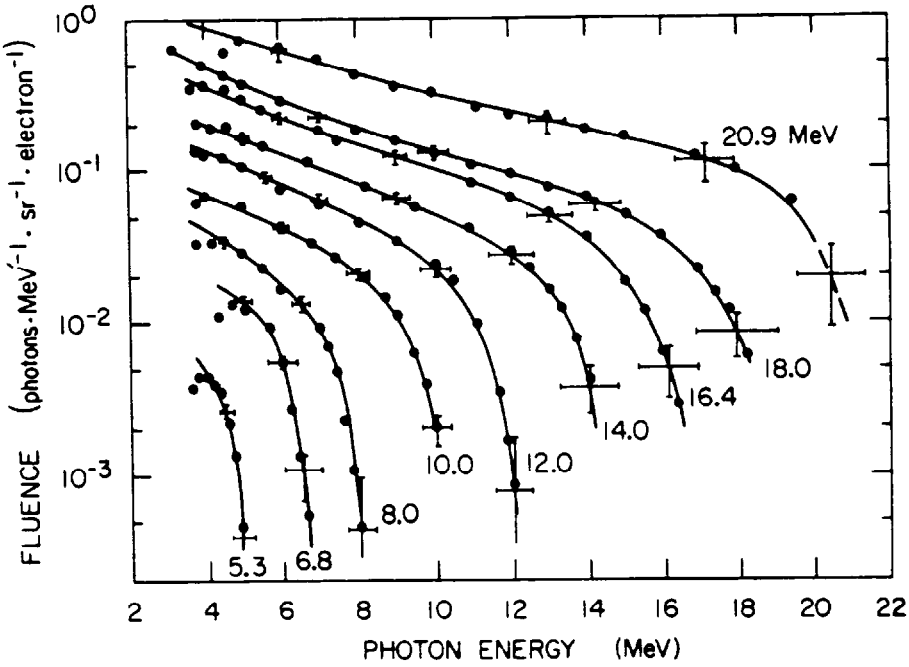

Fig. 1.13 Bremsstrahlung spectra measured at $\theta = 0^o$ from intermediate-thickness (0.2 X_o) targets of high-Z material. The data points are measurements. [Reproduced from (Sw79).]

Figure 1.14 from (Sw79) shows typical spectra for 30 and 60 MeV electrons at various angles. Note the prominence of the 0.511 MeV peak which corresponds to positron annihilations each of which produce two photons of that energy.

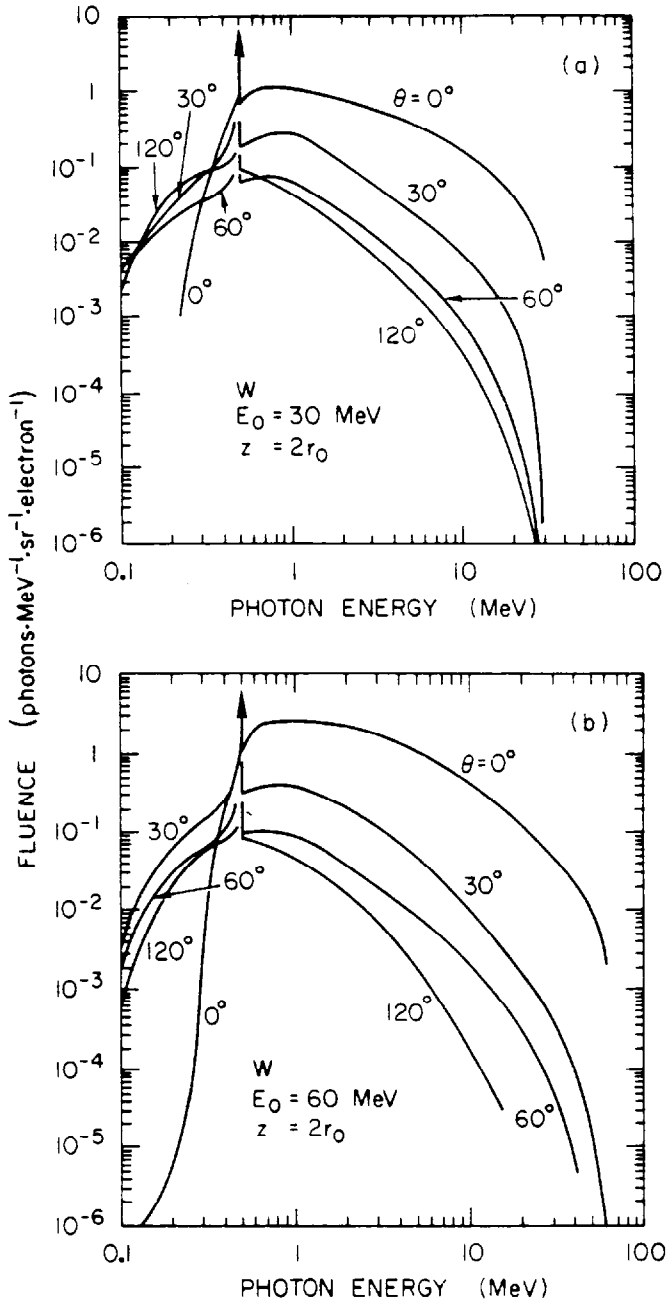

Fig. 1.14 Spectra of bremsstrahlung photons emerging in various directions from thick tungsten targets irradiated by monoenergetic electron beams, normally incident. The target thickness in both cases is 2 r_o, or twice the mean electron range. The arrows indicate positron annihilation radiation at 0.511 MeV. (a) Kinetic energy 30 MeV, thickness z = 24 g cm^{-2} (3.6X_o); (b) 60 MeV, z = 33 g cm^{-2} (4.9X_o). [Reproduced from (Sw79).]

At higher energies (E_o > approximately 100 MeV), the electromagnetic cascade development in accelerator components is very important and can result in a forward "spike" of photons with a characteristic angle of $\theta_c = 29.28/E_o$ (degrees, if E_o is in MeV). This phenomena could be important at electron storage rings and colliders.

Synchrotron radiation

Reference (Sw90) presents a summary discussion of this important phenomenon. The movement of electrons in a circular orbit results in their centripetal acceleration. This gives rise to emission of photons and has been treated in much more detail and completeness by others.

At nonrelativistic energies, this radiation is largely isotropic. However, at relativistic energies, the photons emerge in a tight bundle along a tangent to any point on a circular orbit. Figure 1.15 taken from (Sw90) shows this bundle:

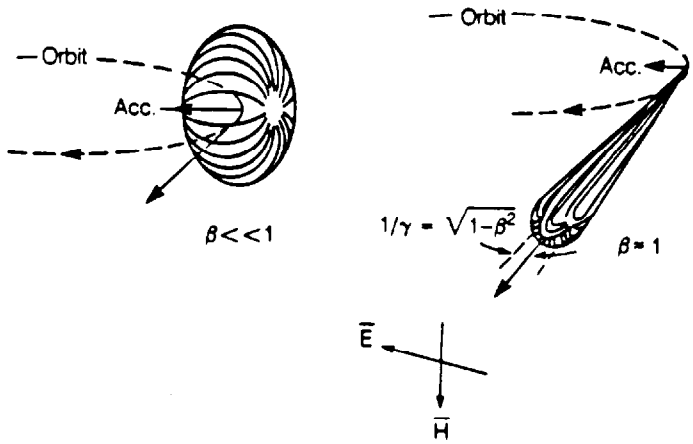

Fig. 1.15 Synchrotron radiation angular distribution for slow and relativistic particles showing direction of polarization. [Reproduced from (Sw83).]

The characteristic angle (i.e., the angle of 1/e of the zero degree intensity) of this "lobe" is

$$\theta_c = \frac{1}{\gamma} = \sqrt{1-\beta^2} \text{ radians.} \qquad (1.29)$$

The median energy of the power spectrum, ε_c, is given in terms of the total energy, W (GeV) [$\gamma m_0 c^2$], and bending radius, ρ (meters) by (Sw90):

$$\varepsilon_c = 2.218 W^3/\rho \quad \text{(keV). [For protons, multiply by } (m_e/m_p)^3.] \qquad (1.30)$$

From (Sw90), the radiated power, P (watts) for a circulating electron current, I (milliamperes) is

$$P = 88.46\, W^4 I/\rho \text{ . [For protons, multiply by } (m_e/m_p)^4.] \qquad (1.31)$$

Figs. 1.16 and 1.17 taken from (Sw90) (and citations therein) give the universal radiation spectrum and calculations for high energies. These calculations were done in the course of the development of the LEP (Large Electron Positron) collider at CERN.

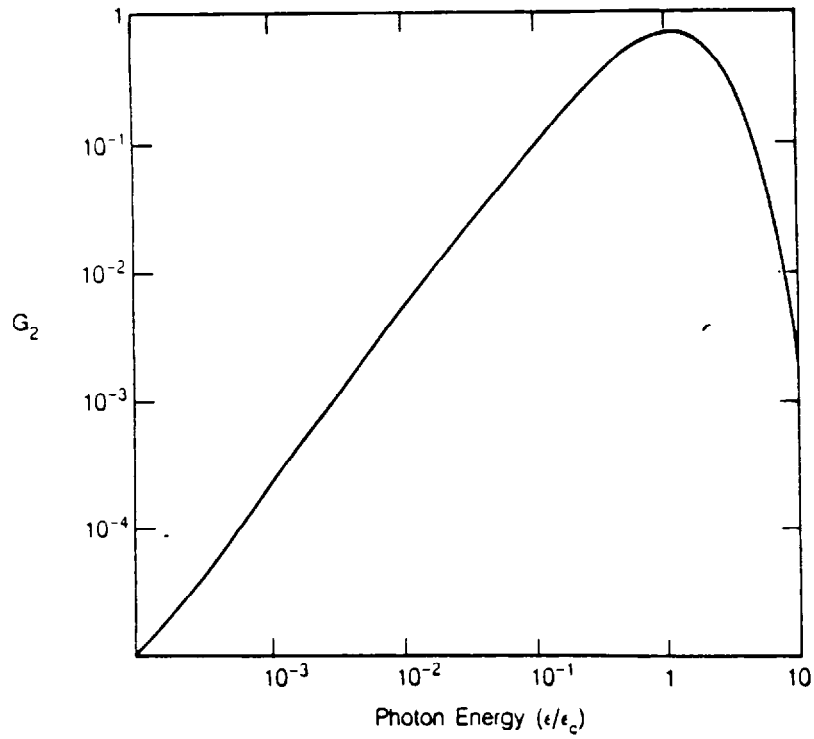

Fig. 1.16 Universal synchrotron radiation spectrum. The dimensionless quantity G_2 gives the relative power as a function of photon energy in units of characteristic energy, ε_c. [Reproduced from (Sw83).]

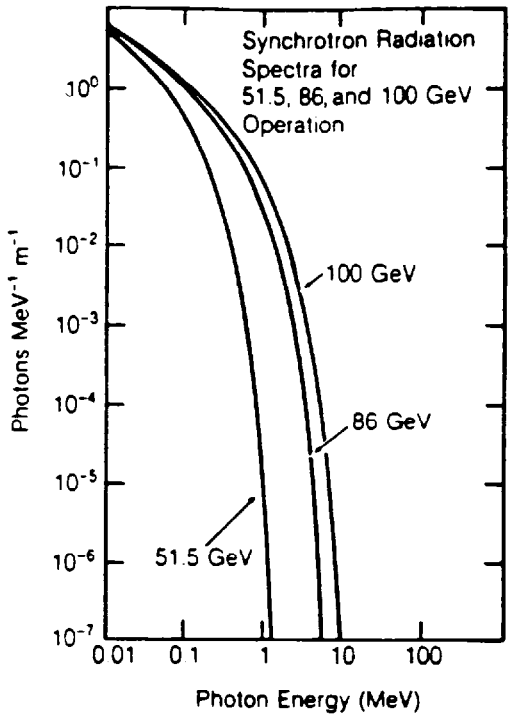

Fig. 1.17 Primary synchrotron radiation spectrum at three high energies. [Reproduced from (Sw83).]

Neutrons

Several basic physical mechanisms have been described in (Sw79). The dominant one at electron machines, especially for kinetic energies $E_0 < 150$ MeV is that of photonuclear reactions; that is reactions in which a photon absorbed by a nucleus creates an excited nuclear state which subsequently decays be emitting a neutron. [A (γ, n) nuclear reaction as written in the scheme of notation in which the first symbol in the parentheses represents the incoming particle in a reaction while the second represents the outgoing particle.]

The total neutron yields and neutron energy spectra are typified by Figs. 1.18 and 1.19 taken from (Sw79). Note that saturation (normalized to beam power!) tends to occur at $E_0 \approx 100$ MeV. (Sw79) and (Sc90) contain more details about such scaling.

Because of the nature of the (γ,n) reaction, these neutron fields are nearly isotropic and the inverse square law may be used to estimate the flux density at any given distance, r. There is actually a slight enhancement at $\theta = 90^o$ of about a factor of 1.5. The production of these neutrons chiefly is influenced by giant resonances in the target nuclei. These resonances are nuclear excited states having very broad widths in energy. These states are excited by the photons and some finite time later decay by emitting neutrons. The yields of neutrons are approximately proportional to the beam power loss (and hence independent of energy) at high energies and isotropically distributed. Photoneutron energy spectra, dN/dE_n fall rapidly as a function of neutron energy, typically as

$$\frac{dN}{dE_n} = E_n^{-\alpha} \text{ where, approximately, } 1.7 < \alpha < 3.6. \qquad (1.32)$$

The slope becomes steeper as E_0, the kinetic energy of the incident electron, is approached.

Table 1.3 taken from (Sc90) displays the following table of values for yields of giant resonance neutrons per watt of beam power ($s^{-1}W^{-1}$), the yield per GeV per sr (Y_n GeV^{-1} sr^{-1}) [measured and calculated], and a recommended dose equivalent source term (Sv cm^2 GeV^{-1}). The last column would be used in the following equation:

$$H = \frac{S_n}{r^2} E_0 I \ , \qquad (1.33)$$

where H is the dose equivalent in Sieverts, r is the radial distance from the target in cm, E_0 is in GeV, and I is the total beam particles incident (e.g., in some time interval).

For $E_0 > 150$ MeV other, more complicated mechanisms come into play such as the quasi-deuteron effect (important in $30 < E_0 < 300$ MeV) and photopion reactions ($E_0 > 300$ MeV). The quasi-deuteron effect is so-named because for $E_0 > 30$ MeV the photon wavelength is in resonance with the average inter-nucleon distance so that the photon interactions tend to occur with "pairs" of nucleons. Only neutron-proton pairs have a nonzero electric dipole moment, which makes interactions of photons with such pairs (pseudo-deuterons) favorable.

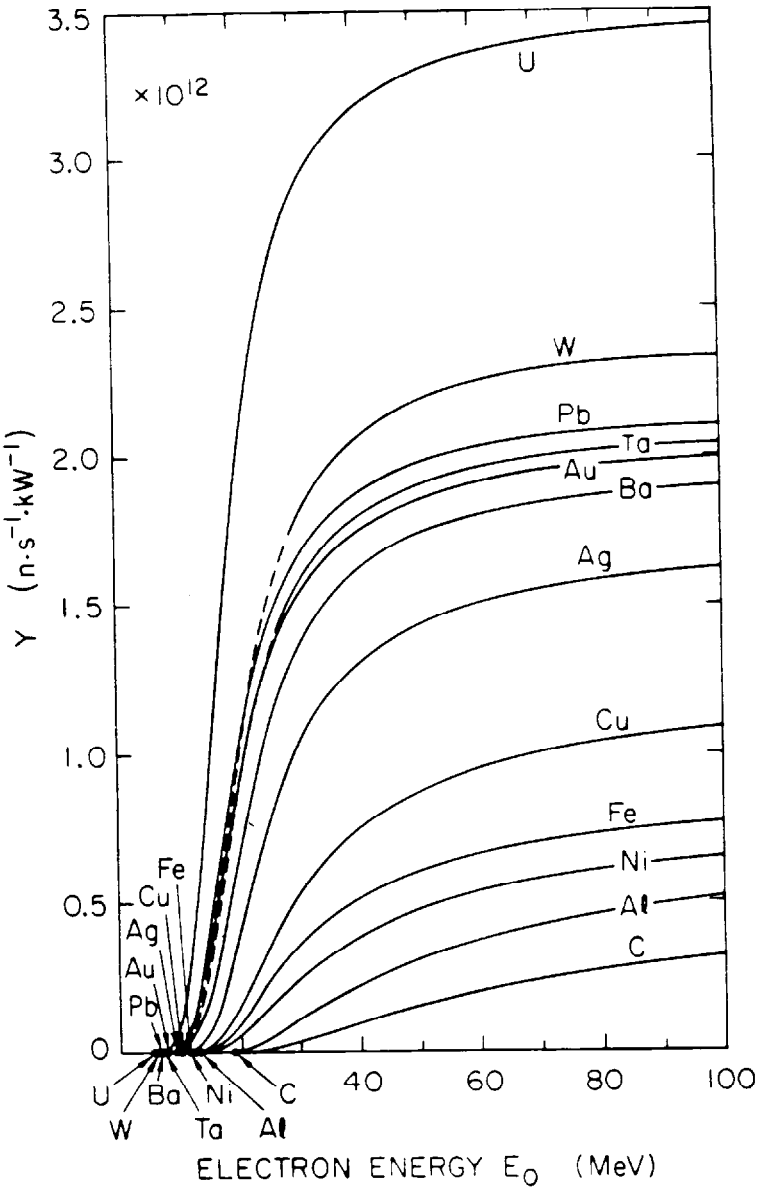

Fig. 1.18 Neutron yields from infinitely thick targets per kW of electron beam power as a function of electron beam energy E_o, disregarding target self-shielding. [Reproduced from (SW79).]

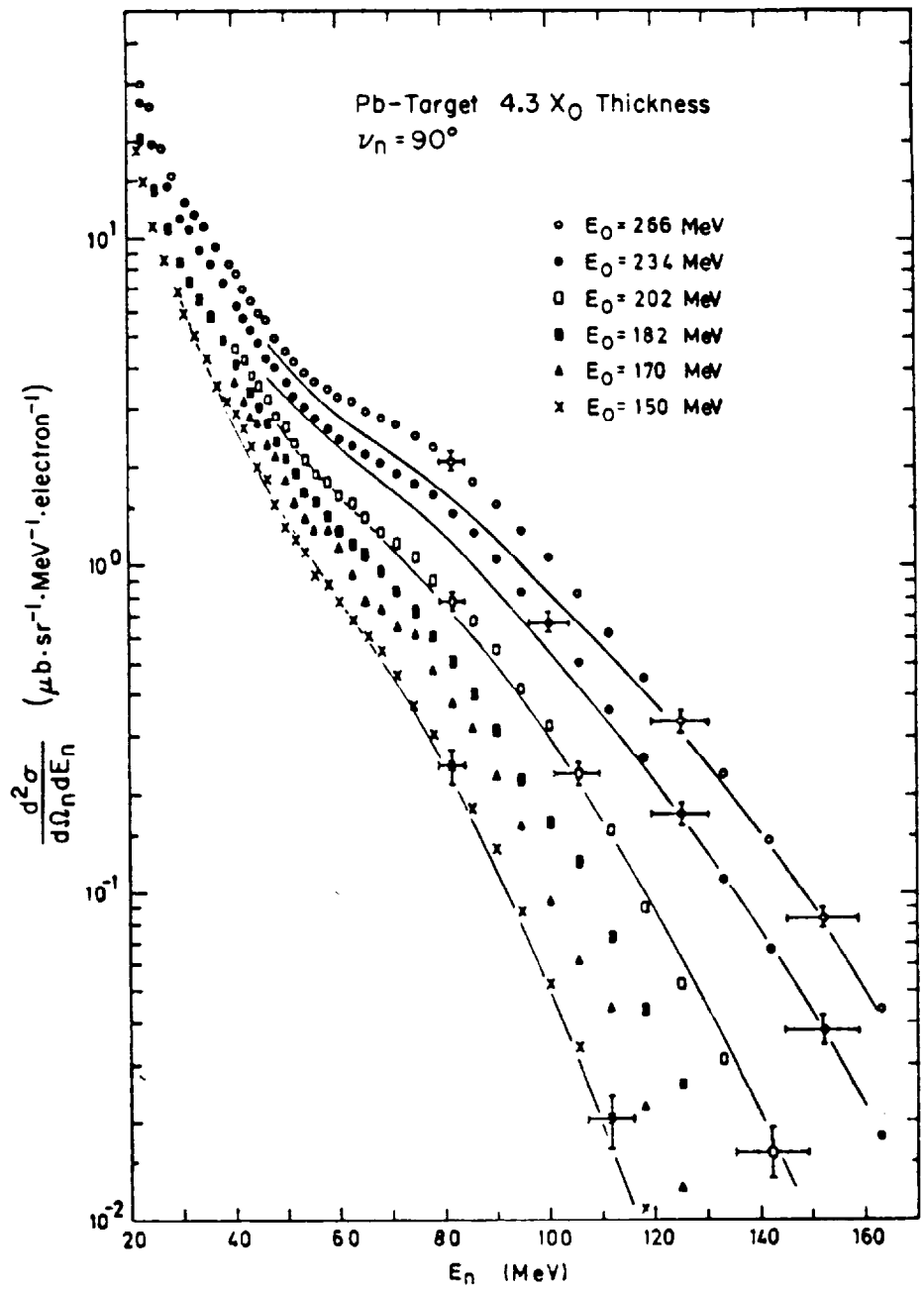

Fig. 1.19 Photoneutron spectra produced at $\theta = 90°$ by electrons of energy E_0 = 150, 170, 182, 202, 235, and 266 MeV, incident on a thick lead target (4.3 X_0). The solid lines are predictions of a quasi-deuteron model. [Reproduced from (Sw79). See references cited therein.]

Table 1.3 Yields and source terms of giant resonance neutrons in an optimum target geometry. [Reproduced from (Sc90) as adapted from references cited therein.]

Material	Calculations [Swa 79b]		Measurements of neutrons	Recommended source terms *) S_n
	Total neutron production $s^{-1} W^{-1}$	Yield per GeV, steradian and electron Y_n $GeV^{-1} sr^{-1}$	Yield per GeV, steradian and electron Y_n $GeV^{-1} sr^{-1}$	$Sv\ cm^2\ GeV^{-1}$
C	4.40E8	5.61E−3	1.4E−2 [Bat 67b]	4.3E−12
Al	6.20E8	7.90E−3		6.0E−12**)
Fe	8.18E8	1.04E−2		7.7E−12
Ni	7.36E8	9.38E−3		6.9E−12
Cu	1.18E9	1.50E−2	2.4E−2 [Bat 67b] 1.5E−2 [DeS 68] 2.7-3.6E−2 [Ste 83]	1.1E−11
Ag	1.68E9	2.14E−2		1.5E−11
Ba	1.94E9	2.47E−2		1.8E−11
Ta	2.08E9	2.65E−2	2.7E−2 [Han 75]	1.8E−11
W	2.36E9	3.01E−2		2.0E−11
Au	2.02E9	2.58E−2		1.8E−11
Pb	2.14E9	2.73E−2	3.3E−2 [Bat 67b] 2.9E−2 [Als 73]	1.9E−11
U	3.48E9	4.44E−2		3.0E−11

[Swa 79b] All calculations at electron energies of 500 MeV or 1 GeV.
[Bat 67b] Measurements at 6.3 GeV with indium in a moderator. In the case of copper the source term for neutrons up to 25 MeV is 2.8E−2 $GeV^{-1} sr^{-1}$.
[DeS 68] Measurement at 7 GeV with indium in a moderator.
[Han 75] Electrons on tantalum and lead targets at 100 MeV.
[Als 73] Calculation at 400 MeV.
[Ste 83] Long-counter measurements: 2.7E−2 at 50 GeV, 3.2E−2 at 80 GeV and 3.6E−2 at 100 GeV.

*) In order to obtain source terms in $Sv\ cm^2\ h^{-1}\ kW^{-1}$ the values have to be multiplied by 2.25E16.
**) The value for aluminium is recommended also for concrete.

Interactions in which the production of other elementary particles, perhaps best typified by pions, becomes energetically possible at still higher energies. These pions can then produce neutrons through secondary interactions as will be discussed in Chapter 3. The literature has very little on the yield values for such particles tailored to the needs of radiation dosimetry. H. DeStaebler of SLAC (De65) has parameterized the yield of high energy particles per GeV, steradian, and electron (taking experimental results into account):

$$Y_n = \frac{7.5 \text{ X } 10^{-4}}{(1 - 0.75 \cos\theta)^2 A^{0.4}} \qquad (1.34)$$

where A is the atomic mass (g/mol) of the target material. It is reasonable to use a dose equivalent conversion factor of $\approx 1 \text{ X } 10^{-13}$ Sv m^2 for these neutrons.

Muons

With electron beams, muons become significant above an electron energy of approximately 211 MeV (the "di-muon" rest mass) by the pair production process in which a μ^+, μ^- pair results. They can, at much smaller fluxes, be produced by the decay of $\pi^\pm$ and $K^\pm$ which are, in turn, due to secondary production processes. Such decay muons will be discussed in more detail later. [The muon rest energy is 105.7 MeV, its meanlife $\tau = 2.19 \text{ X } 10^{-6}$ s and $c\tau = 658.6$ m.] These particles are highly forward peaked. Figures 1.20 and 1.21[2] taken from (Sw79) give the muon flux densities as a function of energy and at various energies and angles as well as the peak flux density at $\theta = 0^o$. The reasonableness of scaling with energy to larger values of E_o is well-demonstrated.

The flux density to dose equivalent conversion factor has been found by Stevenson [(St73), quoted in (Sw90)] to be 40 fSv m^2 (25000 muons cm^{-2} per mrem) for 100 MeV $< E_\mu <$ 200 GeV. [At lower energies range-out of muons in the body with consequential higher energy deposition gives a conversion factor of 260 fSv m^2 (3850 muons cm^{-2} per mrem)] .

A detailed theoretical treatment of muon production by incident electrons from a dosimetric perspective is given in (Ne68) and (Ne74).

Muons have very long mean ranges as shown in Fig. 1.22 taken from (Sw90). At high energies (> 100 GeV), range straggling becomes severe (Va87). Also, above a critical energy for muons of several hundred GeV (in, say, iron), radiative losses begin to dominate such that:

$$-\frac{dE}{dx} = a(E) + b(E)\,E \qquad (1.35)$$

where a(E) is the collisional dE/dx and E is in GeV. Obviously, the range-energy relation of muons and considerations related to their energy loss mechanisms is relevant to shielding against muons regardless of the origin of the muons. The results presented here will thus be relevant to further discussion in this chapter and in Chapter 3.

[2]The handwritten factor of $1 \text{ X } 10^5$ is applied to the left-hand axis of Fig. 1.21 to correct a longstanding error that has been propagated through several publications. This correction was verified by a private communication between the author and W. R. Nelson.

For this equation, $a(E) \approx 0.002$ GeV/gm cm^{-2} and b(E) is the radiative coefficient for E in GeV in Fig. 1.23 taken from (Sw90). The total dE/dx is also given in Fig. 1.24 taken from (PR92). The mean range is approximated by

$$x_0 \approx (1/b)\ln(a + bE_0), \tag{1.36}$$

where E_0 is the kinetic energy of the muon, not the incident electron.

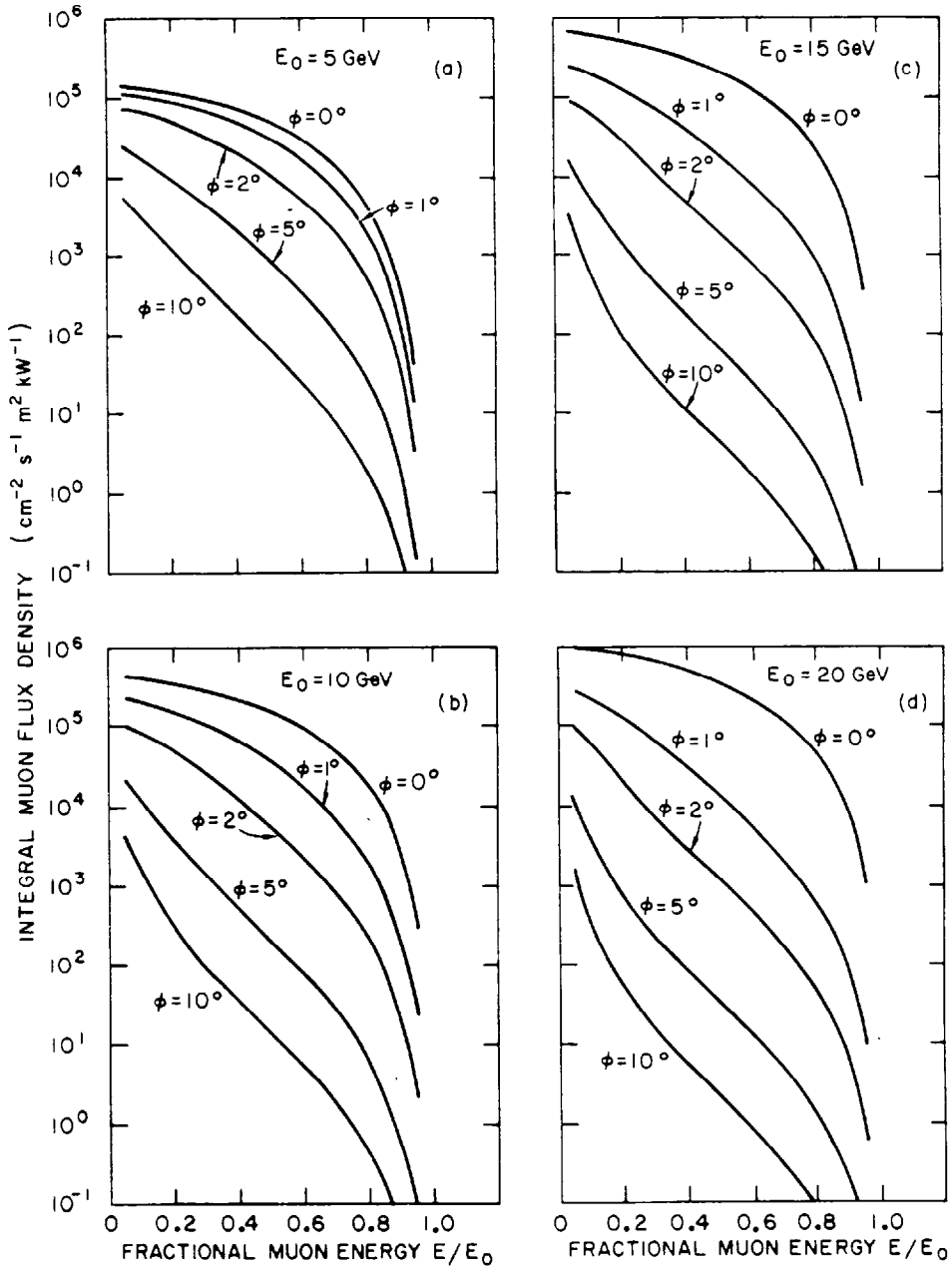

Fig. 1.20 Integral muon flux density at 1 meter per unit electron beam power, versus fractional muon energy, E/E_0, for electron energies E_0 incident on a thick iron target. These data are normalized to 1 kW beam power, 1 meter from the target. [Reproduced from (Sw79), adapted from (Ne68).]

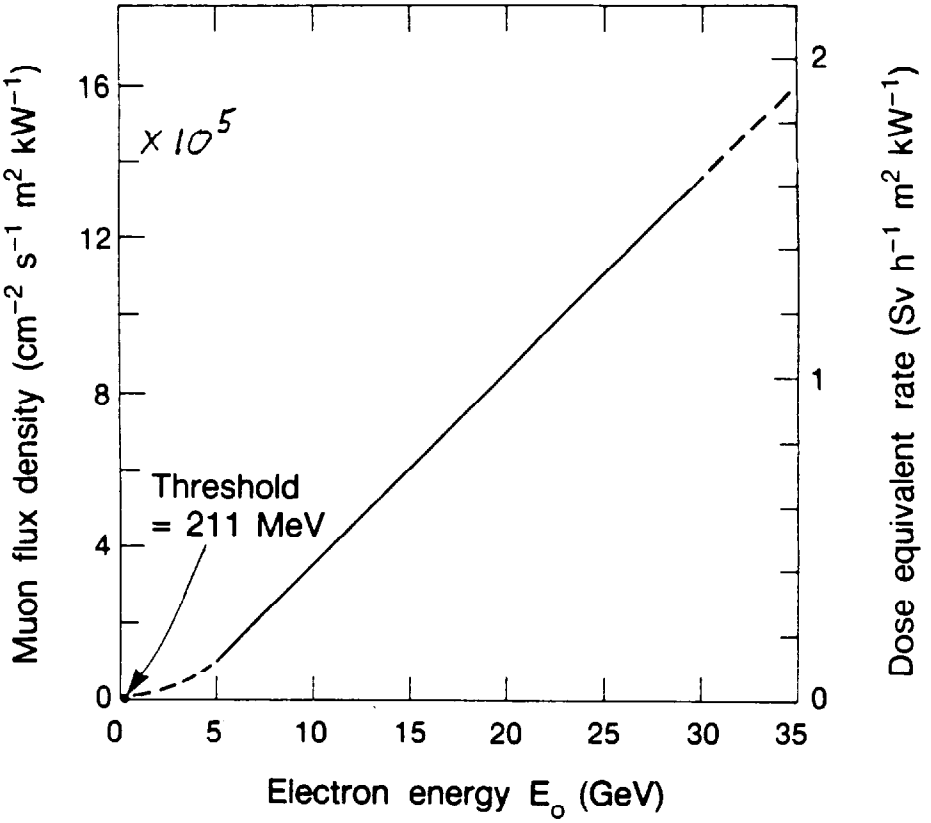

Fig. 1.21 Muon production at $\theta = 0^o$ from an unshielded thick iron target, as a function of electron energy, E_o. Left-hand scale: muon flux density at 1 meter per unit electron beam power ((cm $^{-2}$ s^{-1}) (kW m^{-2})$^{-1}$). Right hand scale: unshielded dose-equivalent rate normalized to 1 meter per unit electron beam power ((rem h^{-1})(kW m^{-2})$^{-1}$) [Reproduced from (Sw79), adapted from (Ne68).]

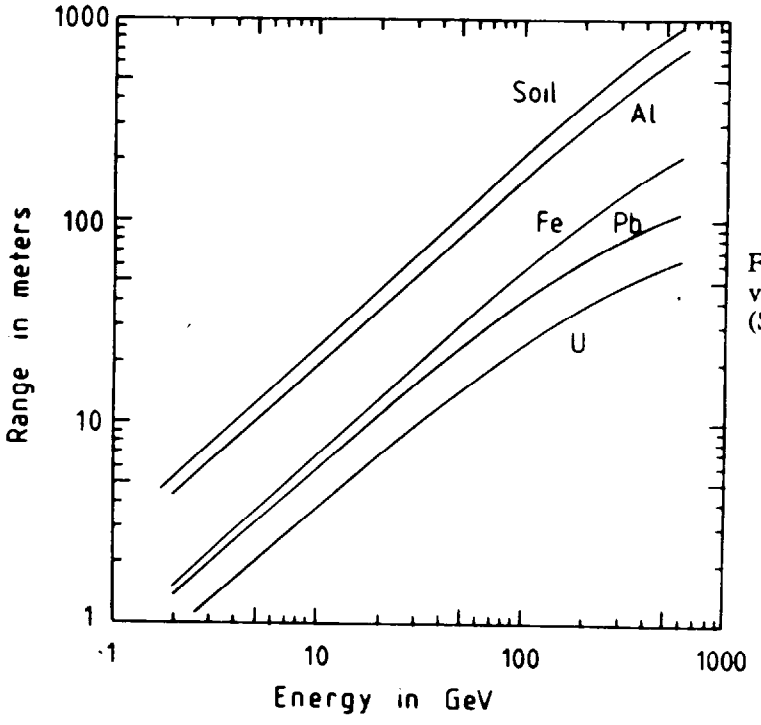

Fig. 1.22 Range-energy curves for muons in various materials. [Reproduced from (Sw83).]

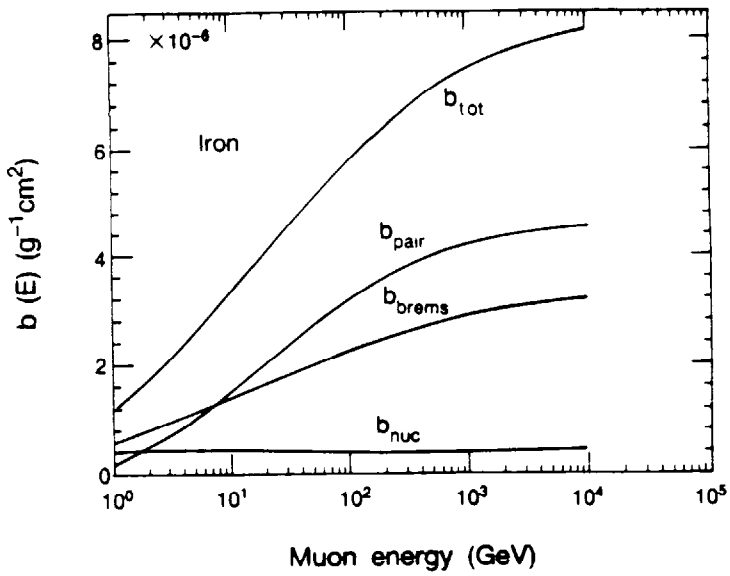

Fig. 1.23 Contributions to the fractional energy loss by muons in iron due to e^+e^- pair production, bremsstrahlung, and photonuclear interactions. [Reproduced from (PR92), adapted from references cited therein.]

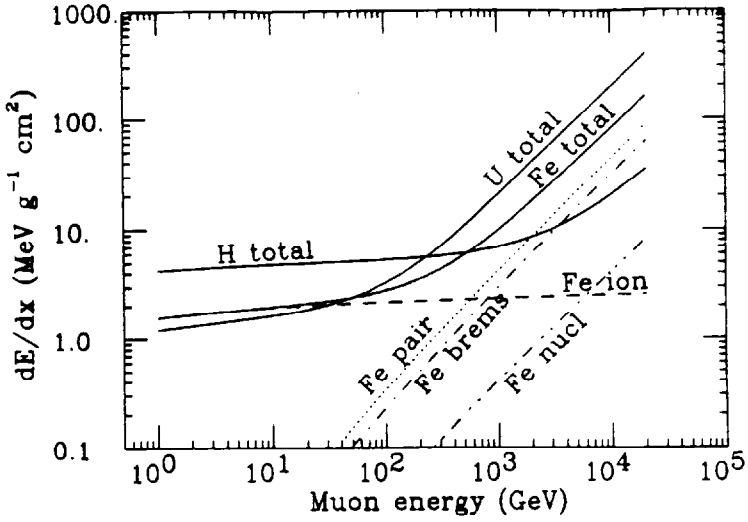

Fig. 1.24 The average energy loss of a muon in hydrogen, iron, and uranium as a function of muon energy. Contributions to dE/dx in iron from ionization and the processes shown in Fig. 1.23 are also shown. [Reproduced from (PR92), adapted from references cited therein.]

Muon range straggling (Va87) is chiefly due to the fact that, above 100 GeV, electron-positron pair production, bremsstrahlung, and deep inelastic nuclear reactions become the dominant energy loss mechanisms. The cross sections for the latter two mechanisms are such that only a few interactions can be expected. Although these processes have low probability, when they do occur they involve large energy losses and thus have quite significant effects.

Tables 1.4 and 1.5 below give fractional energy loss and comparisons of muon ranges at high energies, as taken from (Sc90) and derived from (Va87).The results of (Va87) illustrated in Fig. 1.25 taken from (Sc90) show this phenonema for muons incident on a soil shield having a density of 2.24 g cm^{-3}. At the higher energies the effect is very important since shielding calculations based upon using the mean range values can lead to significant underestimates of the number of muons which can penetrate the shield.

Table 1.4 Fractional enegy loss of muons [(Sc90) adapted from (Va87)] in soil (ρ = 2.0 g cm^{-3}). The fractions of the total energy loss due to the four dominant energy loss mechanisms are given.

E GeV	Ionization	Brems-strahlung	Pair production	Deep inelastic nuclear interactions
10	0.972	0.037	8.8E−04	9.7E−04
100	0.888	0.086	0.020	0.0093
1000	0.580	0.193	0.168	0.055
10000	0.167	0.335	0.388	0.110

Table 1.5 Comparison of muon ranges (meters) in heavy soil (ρ = 2.24 g cm^3) [(Sc90) adapted from (Va87)]

Energy	Calculations of Van Ginneken [Van 87]		Mean Ranges calculated from dE/dx		
	Mean Range	standard deviation	All processes	Coulomb losses only	Coulomb plus pair production losses
10 GeV	22.8	1.6	21.4	21.5	21.5
30 GeV	63.0	5.6	60.3	61.1	60.8
100 GeV	188	23	183	193	188
300 GeV	481	78	474	558	574
1 TeV	1140	250	1140	1790	1390
3 TeV	1970	550	2060	5170	2930
10 TeV	3080	890	3240	16700	5340
20 TeV	3730	1070			

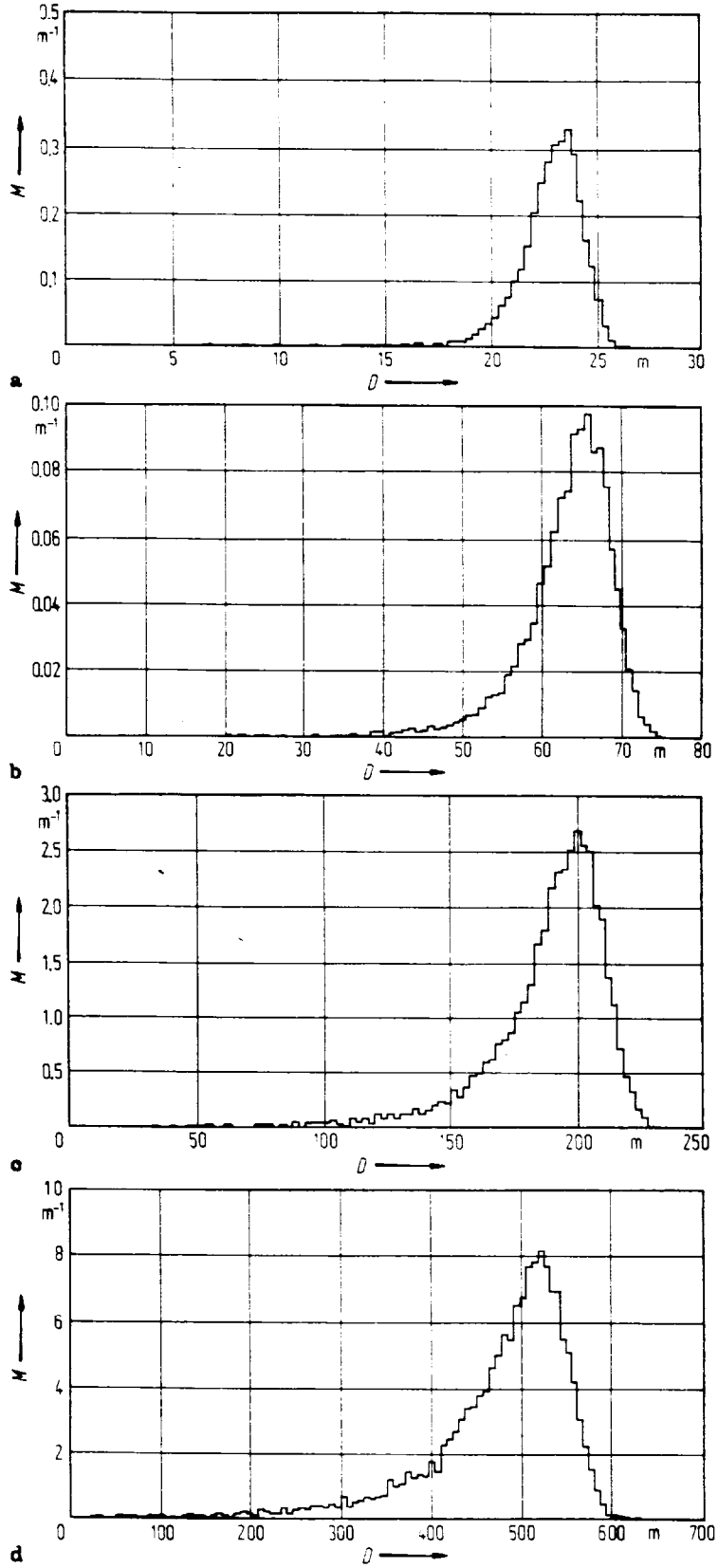

Fig. 1.25 Longitudinal distribution of monoenergetic muons stopping in heavy soil (2.24 g cm^{-3}). M is the muon density (m^{-1}), D is the depth of penetration (meters). [Reproduced (Sc90), adapted from (Va87).] a) E_o = 10 GeV, b) E_o = 30 GeV, c) E_o = 100 GeV, d) E_o = 300 GeV.

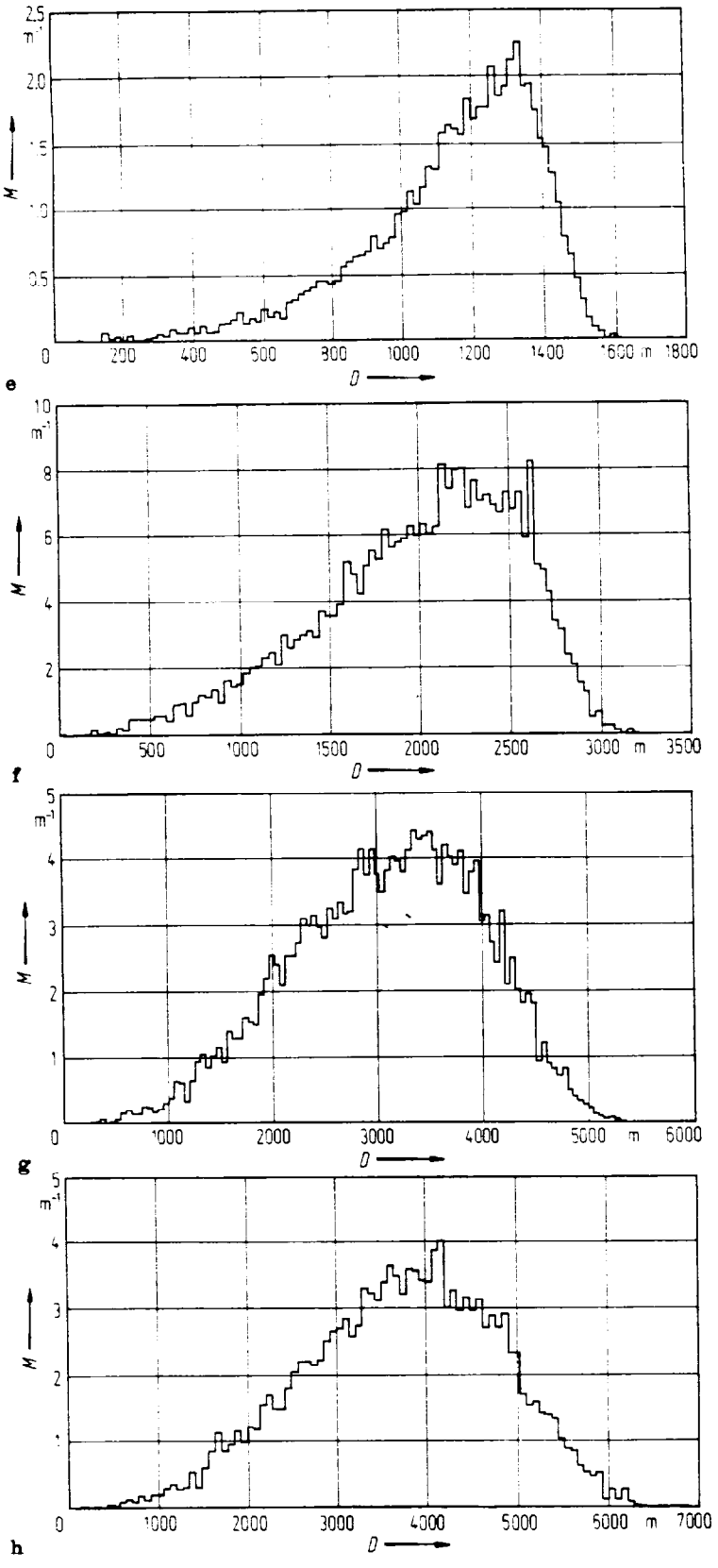

Fig. 1.25 -Continued e)E_o = 1 TeV, f) E_o = 3 TeV, g) E_o = 1 0TeV, h)E_o = 20 TeV.

Summary

In (Sw79), Swanson provided the content of Fig. 1.26 which illustrates the broad features of the radiation field due to the interactions of electrons with no shielding. This figure is useful for making crude estimates of the resultant radiation field. As one can see, at all angles, from the standpoint of dose equivalent, the unshielded field is always dominated by photons. At small angles, the field is dominated by photons with muons as the next most important ingredient at TeV energies.

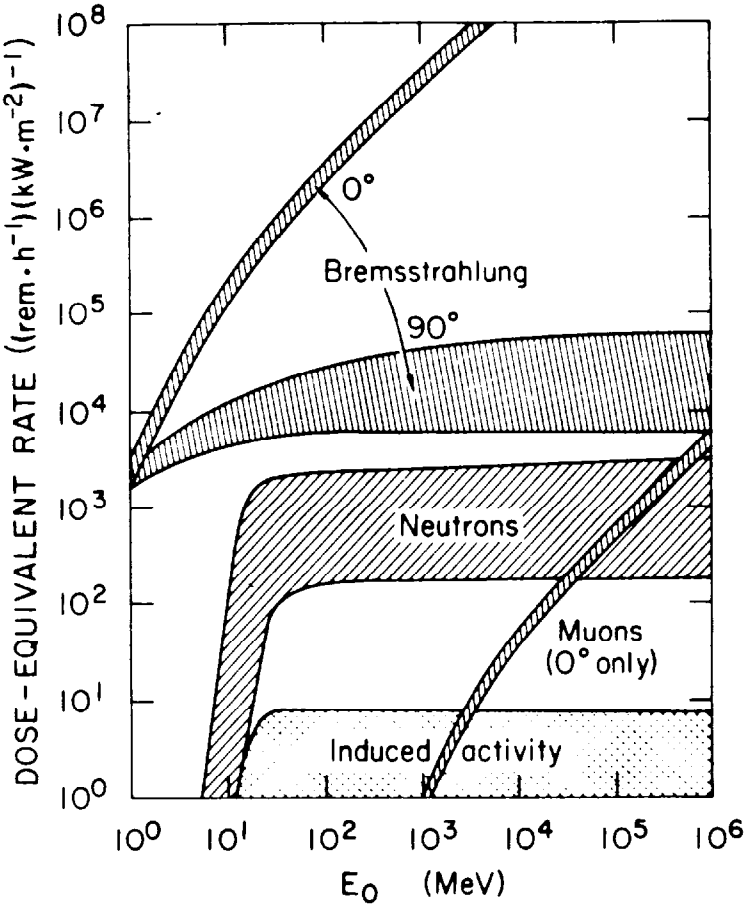

Fig. 1.26 Dose-equivalent rates per unit primary beam power, produced by various types of "secondary" radiations from a high-Z target as a function of primary beam energy, if no shielding were present (qualitative). The width of the bands suggests the degree of variation found, depending on such factors as target material and thickness. [Reproduced from (Sw79).]

V. Radiation Production by Proton Accelerators *(Much of the material in this section is taken from (NC96) and the work referenced therein.)*

The Direct Beam

Direct beams at proton accelerators, from the dosimetric standpoint, nearly always dominate over any type of secondary phenomena since the beam current is generally concentrated into small dimensions. Figure 1.7 gives the fluence to dose equivalent conversion factor as a function of proton energy. The physical reason that the conversation factor shows such a prominent transition at about 200 MeV is that below that energy the proton range is less than the thickness of the human body. Hence as the energy is increased above 200 MeV, the energy largely escapes from the body so that it requires a far larger fluence of protons to deliver the same dose equivalent.

As the energy of a proton beam increases, the range of the protons increases to where the probability of the proton interacting before it has lost all of its energy due to ionization in a target gradually becomes significant. Klaus Tesch of HERA/DESY has illustrated this point in Fig. 1.27 taken from (Te85) for various materials and energies.

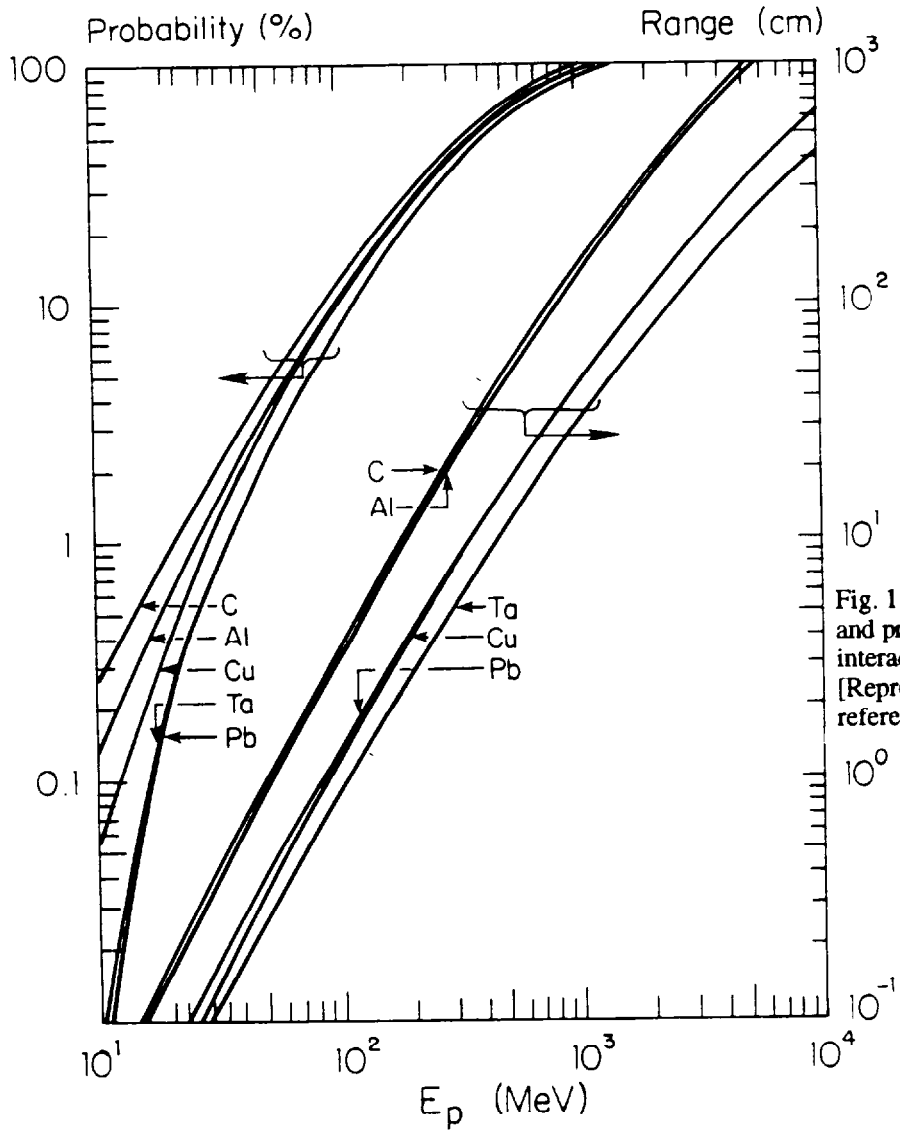

Fig. 1.27 Range of protons (right hand scale) and probability of inelastic nuclear interaction within the range (left hand scale) [Reproduced from (Te85), adapted from references cited therein.]

Neutrons (and other hadrons at high energies)

E_o < 10 MeV:

For nuclear reactions, the **Q-value**, Q_v, is defined in terms of the masses, m_i,

$$Q_v \equiv [(m_1 + m_2) - (m_3 + m_4)]c^2 \tag{1.37}$$

for nuclear reaction $m_1 + m_2 \rightarrow m_3 + m_4$. [In general such reactions are denoted $m_2(m_1,m_3)m_4$.] $Q_v > 0$ implies an **exothermic** nuclear reaction. **Endothermic** ($Q_v \leq 0$) reactions are characterized by a **threshold energy**, E_{th}, given by:

$$E_{th} = \frac{m_1 + m_2}{m_2}|Q_v|. \tag{1.38}$$

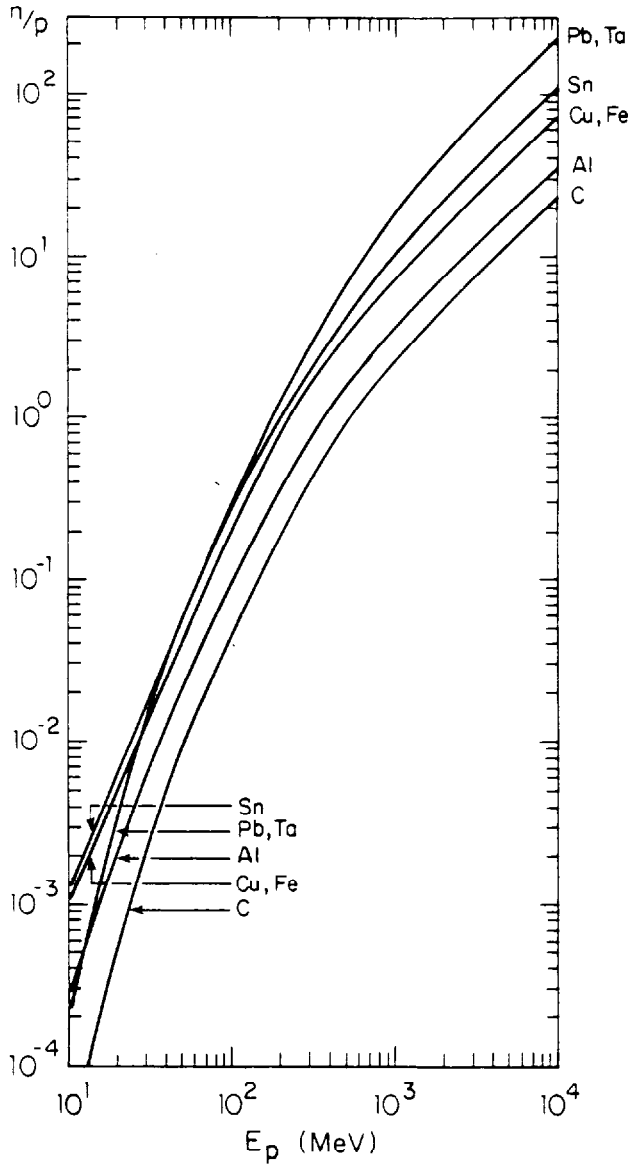

Fig. 1.28 Total neutron yield per proton for different target materials. [Reproduced from (Te85).]

Below 10 MeV, (p,n) reactions are important for some materials because these reactions commonly have very low thresholds (< 5 MeV) . Many features are highly dependent upon the details of the structure of the target nuclei and are often highly dependent upon the target element, angle, and energy. For example, $^{7}Li(p,n)^{7}Be$ has a threshold of 1.9 MeV and the total cross section, σ, quickly rises to a value of 300 mb.

For protons having kinetic energies, E_o, ranging from approximately 10 MeV up to the very highest energies, neutrons are usually the dominant feature of the radiation field that results from their interactions. At these energies, the yields are smoother functions of energy due to the lack of resonances, but are also more forward-peaked. Tesch (Te85) has summarized the total yields per incident proton for different materials as a function of energy in Fig. 1.28 taken from (Te85). In this figure these curves agree with the original primary data to within about a factor of two. An important feature is that for $50 < E_o < 500$ MeV, $Y \propto E_o^2$ while for $E_o > 1$ GeV, $Y \propto E_o$.

$10 < E_o < 200$ MeV

In this region there are extensive angular distribution data as a result of nuclear physics research. The general features is that the distributions are forward-peaked. Representative examples are given in Figs. 1.29 and 1.30 taken from Nakamura (Na78) for 52 MeV protons and from Alsmiller (Al75) and Hagan (Ha88) for 200 MeV protons, respectively. The fluence above a 5 MeV threshold is plotted in Fig. 1.29 while yields are plotted in Fig. 1.30.

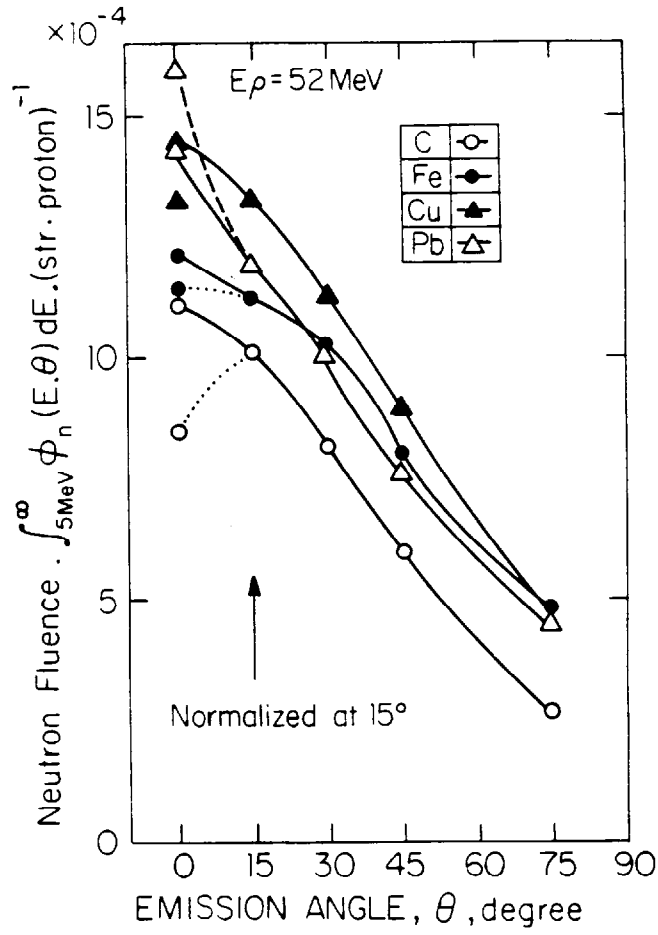

Fig. 1.29 Angular distributions of total neutron yield above 5 MeV for carbon, iron, copper, and lead bombarded by 52 MeV protons [Reproduced from (Na78).]

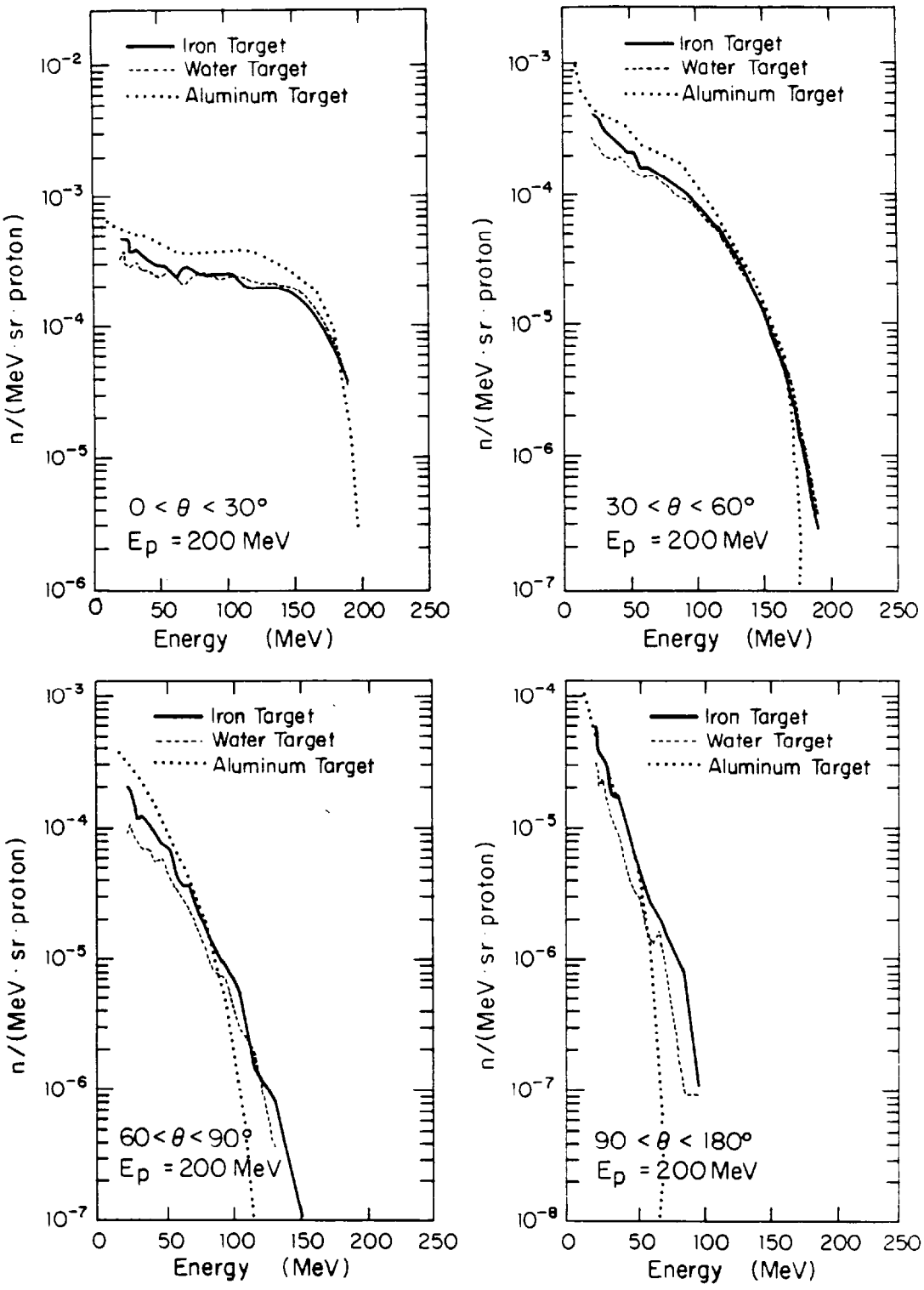

Fig. 1.30 Calculated energy spectra of neutrons emitted by water, iron, and aluminum targets bombarded by 200 MeV protons for four ranges in θ. The iron and water calculations are from (Ha88) while the aluminum results are from

200 MeV < E_o < 1 GeV ; ("intermediate" energy):

In this region, many more reaction channels become open and the number of protons emitted gradually becomes approximately equal to the number of neutrons. In fact, at the highest energies for such unshielded conditions, the radiation effects of protons and neutrons are essentially identical and both must be taken into account. Thus reliance on the Tesch yield curve in Fig. 1.28 could underestimate radiation effects by as much as a factor of two.

E_o > 1 GeV ("high" energy region):

In this region, both the calculations and measurements become much more difficult. Often, "threshold" detectors are used to detect neutrons above some reaction threshold energy. Figures 1.31 (Gi68), 1.32 (Gi68), 1.33 (Ra72), and 1.34 (St85) show representative data at 14, 26, 22, and 225 GeV, respectively. In Figs. 1.31 and 1.32, the parameter $g(\theta)$ is the integral of $d^2Y/d\Omega dE$ above such a designated threshold energy. These should be regarded as thin target values. "Thin" target in this context means a target shorter than the removal mean free path for high energy protons. Table 1.6 summarizes common removal mean free paths.

Table 1.6 Summary of removal mean free paths for protons

MATERIAL	DENSITY (grams/cm^3)	REMOVAL MEAN FREE PATH (grams/cm^2)	REMOVAL MEAN FREE PATH (cm)
hydrogen gas	9.00×10^{-5}	43.3	4.81×10^5
beryllium	1.85	55.5	30.03
carbon	2.27	60.2	26.58
aluminum	2.70	70.6	26.15
iron	7.87	82.8	10.52
copper	8.96	85.6	9.55
lead	11.35	116.2	10.24
uranium	18.95	117.0	6.17
air	1.29×10^{-3}	62.0	4.81×10^4
water	1.00	60.1	60.10
concrete(typical)	2.50	67.4	26.96
silicon dioxide (quartz)	2.64	67.0	25.38
plastics (polyethylene)	0.93	56.9	61.51

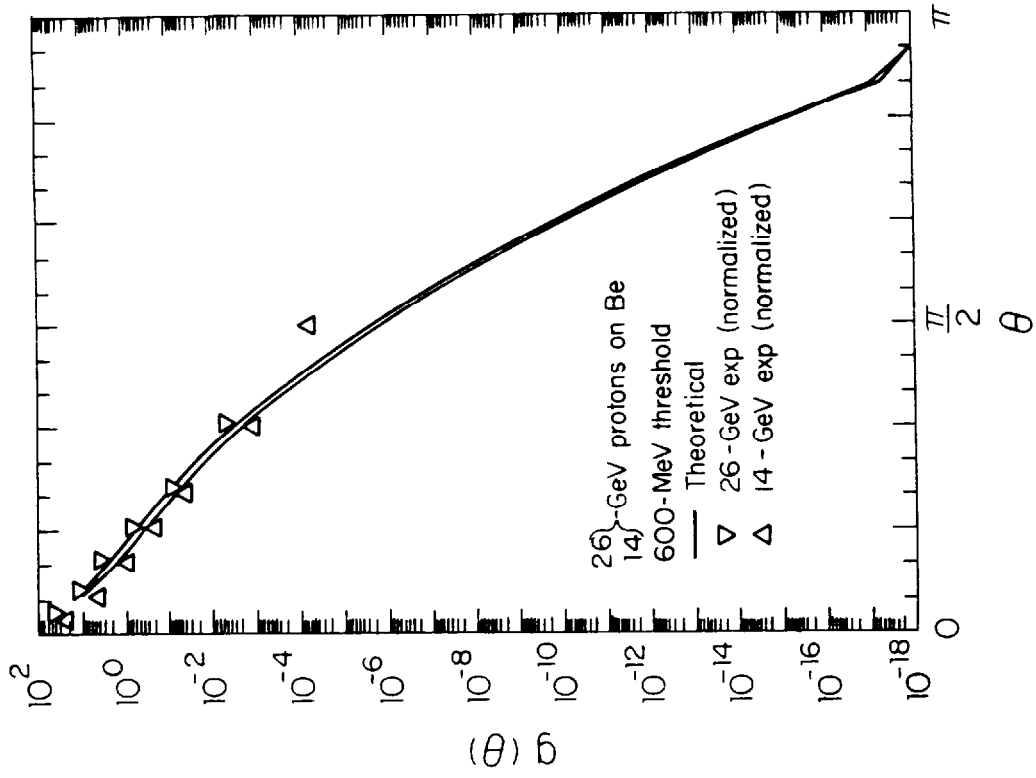

Fig. 1.32 The angular distribution $g(\theta) = dY/d\Omega$ of neutrons above 600 MeV produced by 14 and 26 GeV protons on a thin beryllium target. [Reproduced from (Gi68).]

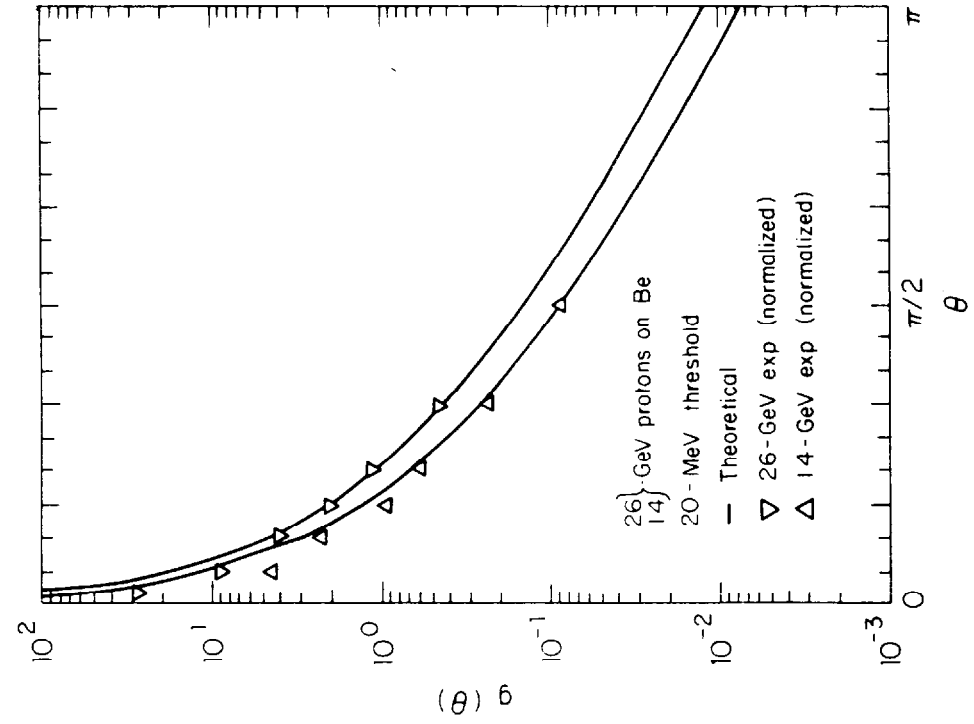

Fig. 1.31 The angular distribution $g(\theta) = dY/d\Omega$ of neutrons above 20 MeV produced by 14 and 26 GeV protons on a thin beryllium target. [Reproduced from (Gi68).]

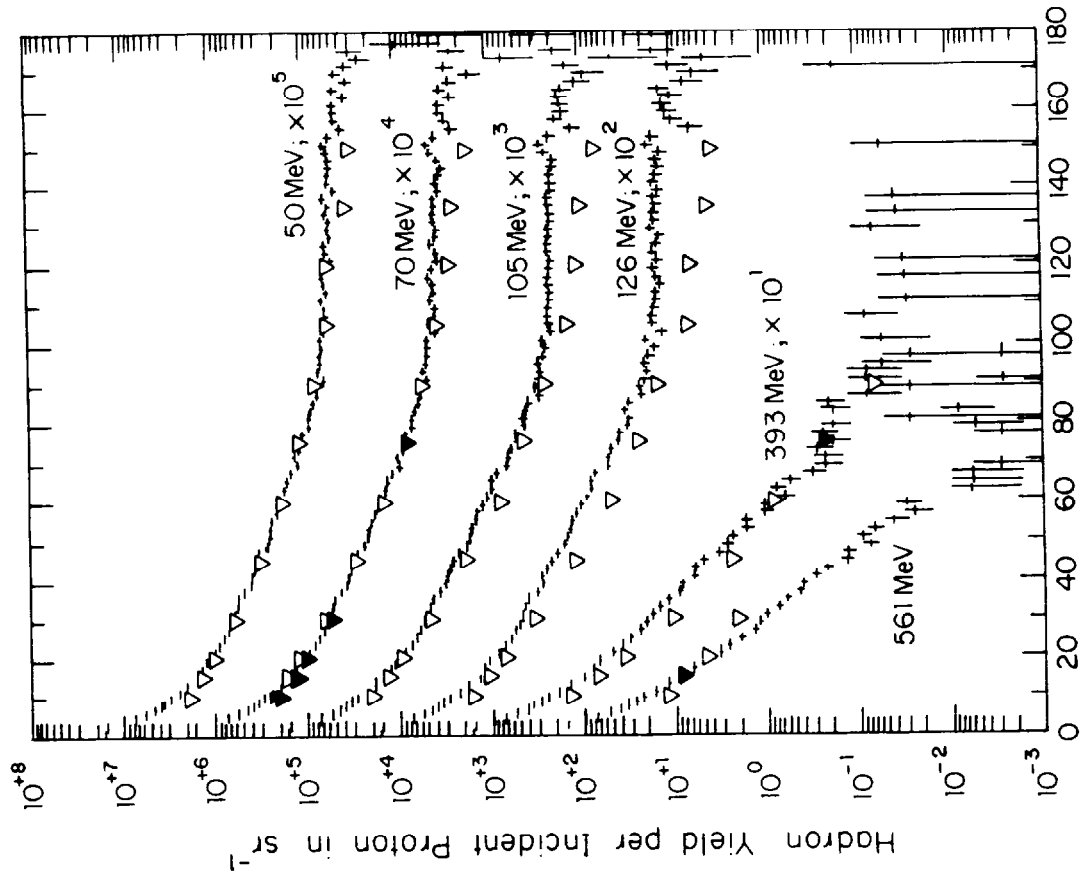

Fig. 1.33 Comparison of calculated and measured angular distributions of hadron fluxes (particles cm^{-2}) at 100 cm from a copper target bombarded by 22 GeV protons. Several choices of hadron energy thresholds are shown. [Reproduced from (Ra72).]

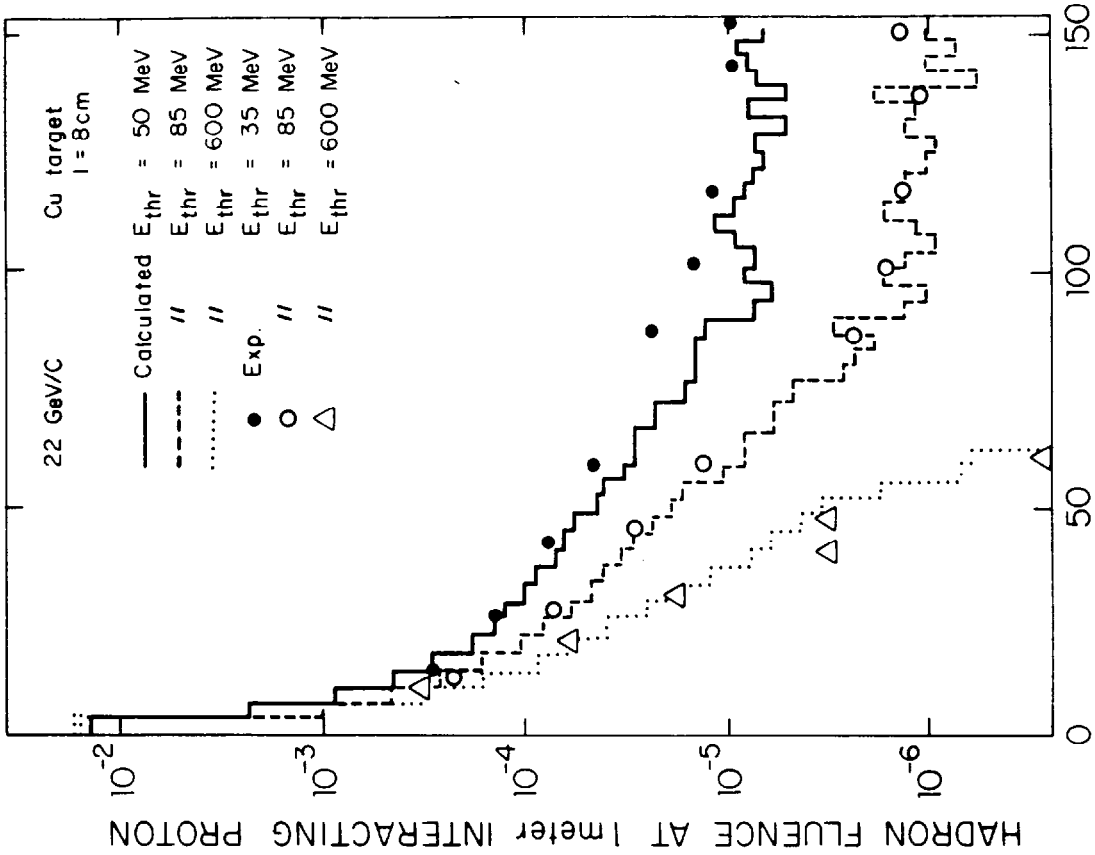

Fig. 1.34 Comparison of the experimental (open symbols) and calculated (+) hadron fluences above different energy thresholds as a function of polar angle θ around a 15 cm long copper target bombarded by 225 GeV protons. The data have been multiplied by the indicated factors prior to plotting and represent hadrons/(incident proton steradian). [Reproduced from (St85).]

Anthony Sullivan of CERN (Su89) has developed a simple formula for the angular distribution of fluence, Φ (θ) (cm^{-2}), of hadrons with $E_o > 40$ MeV at one meter from a copper target struck by protons in the energy region $5 < E_o < 500$ GeV per interacting proton:

$$\Phi(\theta) = \frac{1}{2\left[\theta + \left(35/\sqrt{E_o}\right)\right]^2} \qquad (1.39)$$

where E_o is in GeV and θ is in degrees.

This formula also adequately accounts for the distributions of neutrons per incident proton produced by protons in the region of incident proton energy $0.025 < E_o < 1$ GeV if it is multiplied by, approximately, a factor of two. This equation can be plotted as in Fig. 1.35, taken from the preprint of (Su89), in the "lateral" ($\theta \approx 90^o$) and "forward" ($\theta \approx 0^o$) directions.

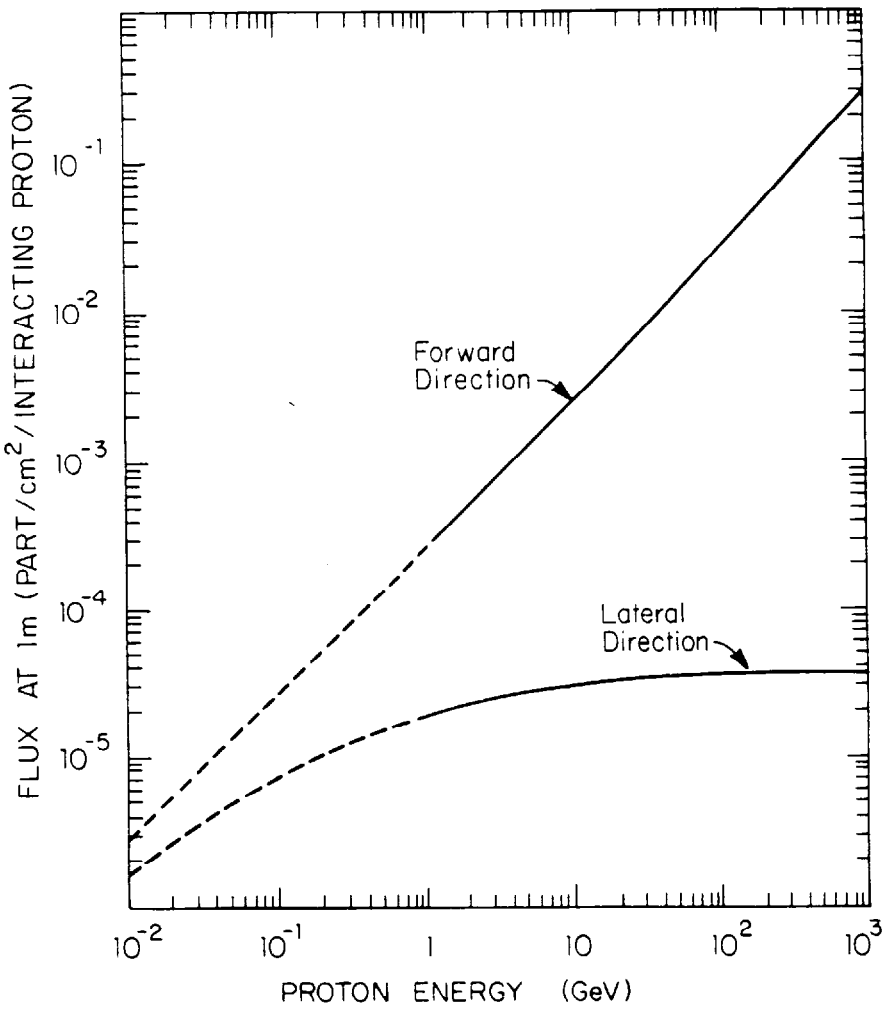

Fig. 1.35 Flux of hadrons exceeding 40 MeV in energy, per interaction, at 1 meter from the target in both the forward ($\theta = 0^o$) and sideways ($\theta = 90^o$) direction as a function of the interacting proton. The proton is interacting in a copper target. [Reproduced from the preprint of (Su89).]

Of course, the dose equivalent is often more important to know than is the "raw" fluence. In principal, the dose equivalent can be obtained by integrating thus;

$$H = \int_0^{E_{max}} P(E)\Phi(E)dE, \tag{1.40}$$

or by summation, taking into account the "coarseness" of available data and/or calculations:

$$H = \sum_{j=1}^{m} P_j(E)\Phi_j(E)(\Delta E)_j. \tag{1.41}$$

Tesch (Te85) has done this to obtain the dose equivalent at 1 meter from a copper target (θ = 90°) bombarded by protons of various energies. The result is plotted in Fig. 1.36 taken from (Te85).

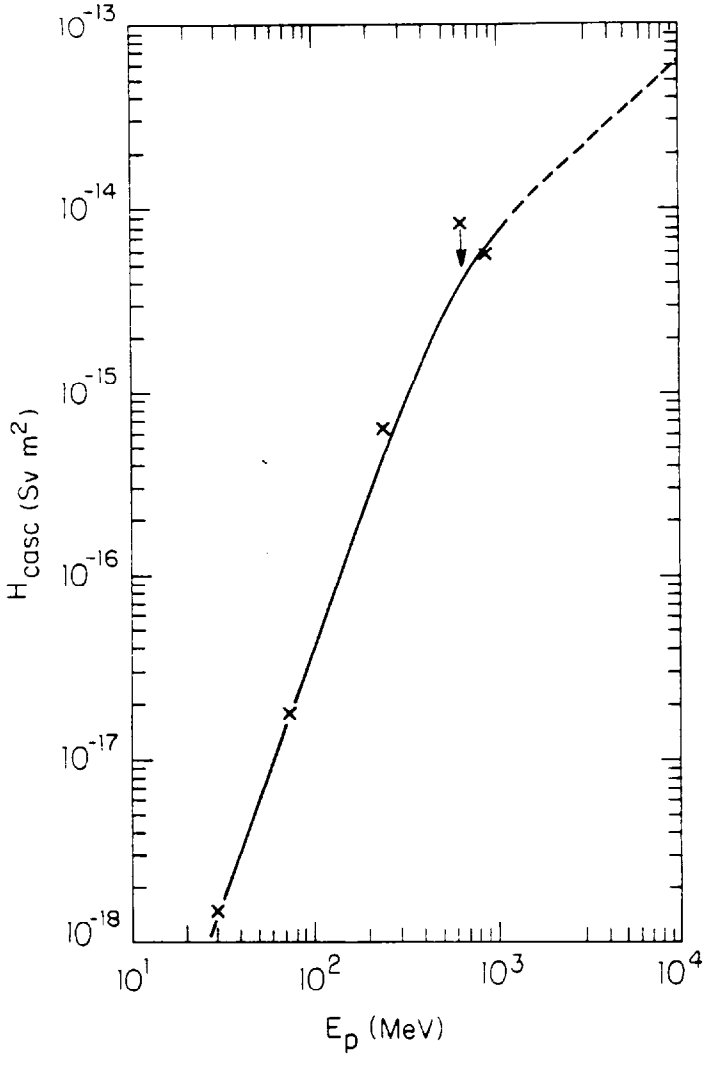

Fig. 1.36 Dose equivalent per proton due to neutrons at θ = 90° with energies higher than 8 MeV at a distance of 1 meter from a copper target. [Reproduced from (Te85).]

Levine (Le72) has obtained experimental data on the angular distribution of absorbed dose for 8 and 24 GeV/c protons incident on a Cu target. These are given in Fig. 1.37. The results are normalized to the number of interacting protons which represent about 28 % of those incident.

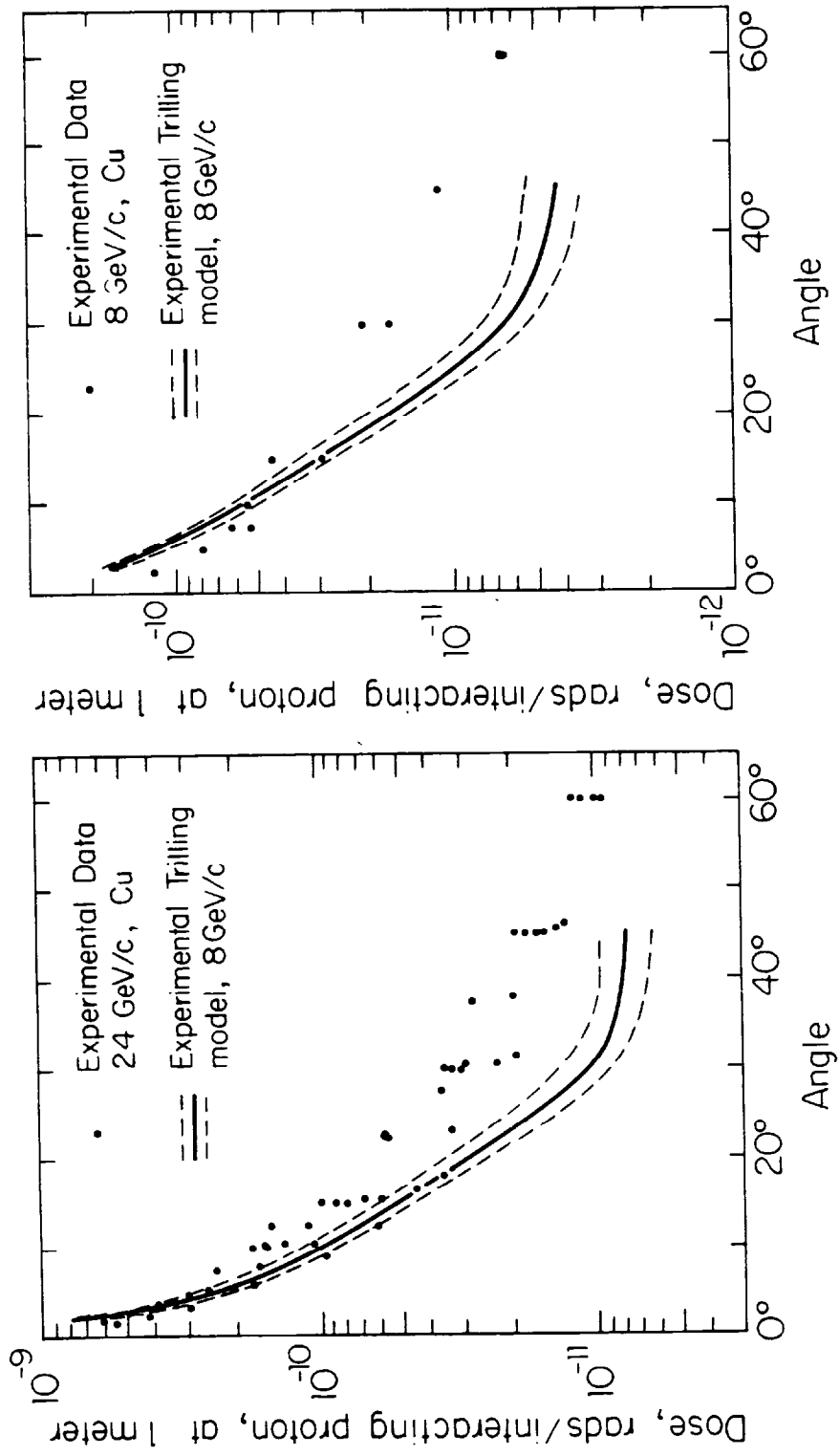

Fig. 1.37 Plots of absorbed dose per interacting proton at a distance of one meter from a 5 cm long copper target bombarded by 24 GeV (left) and 8 GeV (right) protons taken from (Le72). The filled symbols are measurements while the curve is a theoretical prediction. Multiply the plotted values by 0.28 for the approximate results per incident proton.

Muons

Muons at proton accelerators arise from two principal mechanisms. Production by pion and kaon decay are outlined as follows where mass of the parent particles, the branching ratio (the percentage of time the parent particle decays by the reaction given), the meanlife, and the value of $c\tau$ (PR92) are also given.

$\pi^{\pm} \rightarrow \mu^{\pm} + \nu_{\mu}$; m_{π} = 139.6 MeV, $\tau = 2.6 \times 10^{-8}$ s, (99.99 % branch), ($c\tau$ = 7.804 m)

$K^{\pm} \rightarrow \mu^{\pm} + \nu_{\mu}$; m_K = 493.6 MeV $\tau = 1.2 \times 10^{-8}$ s, (63.51 % branch), ($c\tau$ = 3.709 m)

The other important muon production mechanism associated with incident protons is the so-called "direct" muon production. These will discussed in more detail in Chapter 3.

At proton and ion accelerators, thus, the production of muons is usually dominated by a tertiary effect due to the decay of secondary particles. Muon fields are forward-peaked and, normally, dominated by those from pion decay (except, perhaps at the highest energies). Usually, Monte-Carlo techniques are needed to accurately estimate muon intensities. This is because of the need to:

A. calculate the production of pions from the proton interactions
B. follow the pions until they decay or interact
C. adequately account for the range-energy relation and range straggling
D. track the muons to the point of interest.

A full discussion of muon production and shielding must await Chapter 3.

VI. Primary Radiation Fields at Ion Accelerators

Because the ionization range for ions of a given kinetic energy decreases as a function of ion mass, targets become effectively "thicker" as the ion mass increases.

light ions (ion mass number, $A \leq 5$)

For such ions there are "special case" exothermic reactions to be concerned with. Noteworthy examples (followed by their reaction Q-values, Q_v, in parentheses) are:

$D(d,n)^3He$ ($Q_v = 3.266$ MeV)
$^9Be(\alpha,n)^{12}C$ ($Q_v = 5.708$ MeV)
$^3H(d,n)^4He$ ($Q_v = 17.586$ MeV).

In some cases monoenergetic beams of neutrons are possible using these or the following slightly endothermic reactions:

$^{12}C(d,n)^{13}N$ ($Q_v = -0.281$ MeV)
$T(p,n)^3He$ ($Q_v = -0.764$ MeV)
$^7Li(p,n)^7Be$ ($Q_v = -1.646$ MeV).

The energies of such neutrons can range from 0 to 27 MeV for bombarding energies up to 10 MeV.

In general, deuteron stripping reactions [(d,n)] have the highest yields because the binding energy of the deuteron is only 2.225 MeV. (One gets an extra neutron "for free"!). This phenomena is especially pronounced at the lower energies. In the low energy region, and especially with light ions, one should carefully consider all possible reactions given the materials present in conjunction with the ions that are being accelerated.

Figure 1.38 taken from (Pa73) gives examples of typical light ion yield results.

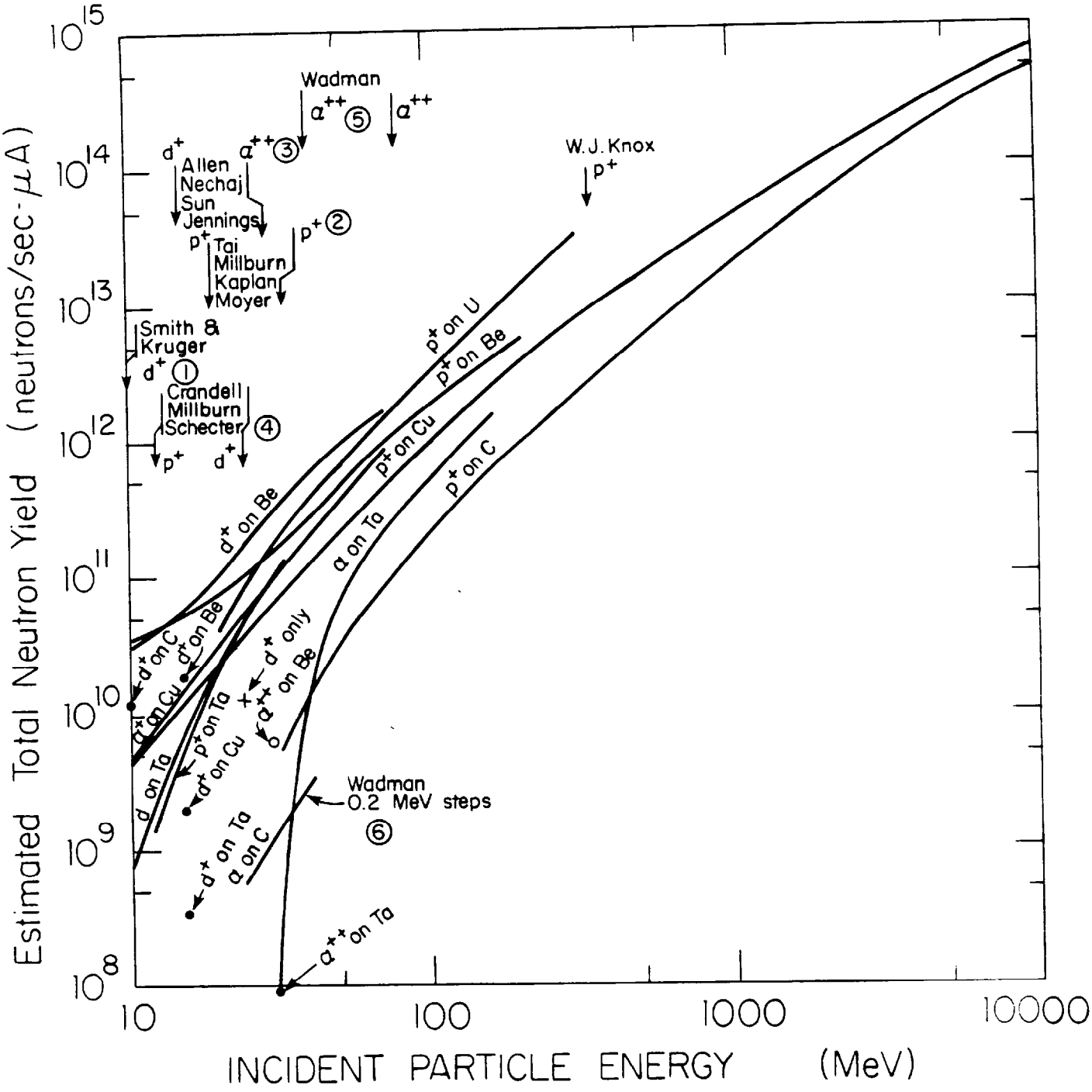

Fig. 1.38 Plots of total neutron yields for various light ions on a number of materials. One sec-μA (1 micro-Coulomb of electric charge) corresponds to 6.25×10^{12} incident protons, 3.125×10^{12} incident α^{++} ions, etc. [Reproduced in (Pa73), adapted from references cited therein.]

heavier ions (ions with A > 4)

At higher energies and especially at higher masses, neutron yield and dose equivalent data and calculations are very sparse. The data often is normalized in terms of kinetic energy per atomic mass unit (**specific energy**, usually expressed in units of MeV/amu), or kinetic energy per nucleon because reaction parameters generally scale to that parameter. In the literature the technical distinction between energy/amu and energy/nucleon is often ignored. In the range up to 20 MeV/amu, this is illustrated by the Figs. 1.39 and 1.40 taken from (NC96) [adapted from (Hu60) & Oh80)] for both yield and dose equivalent for targets slightly thicker than the particle range:

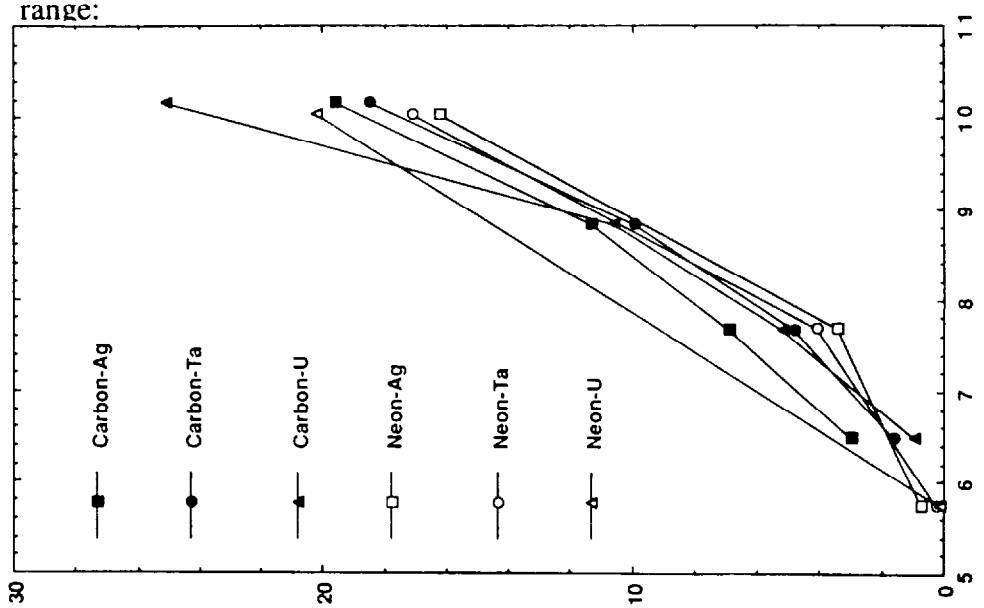

Fig. 1.40 Plots of total neutron yield for incident ^{12}C and ^{20}Ne ions incident on heavy targets with specific energies ranging from 6 to 10 MeV/amu. [Adapted from (Hu60) and (Pa73).]

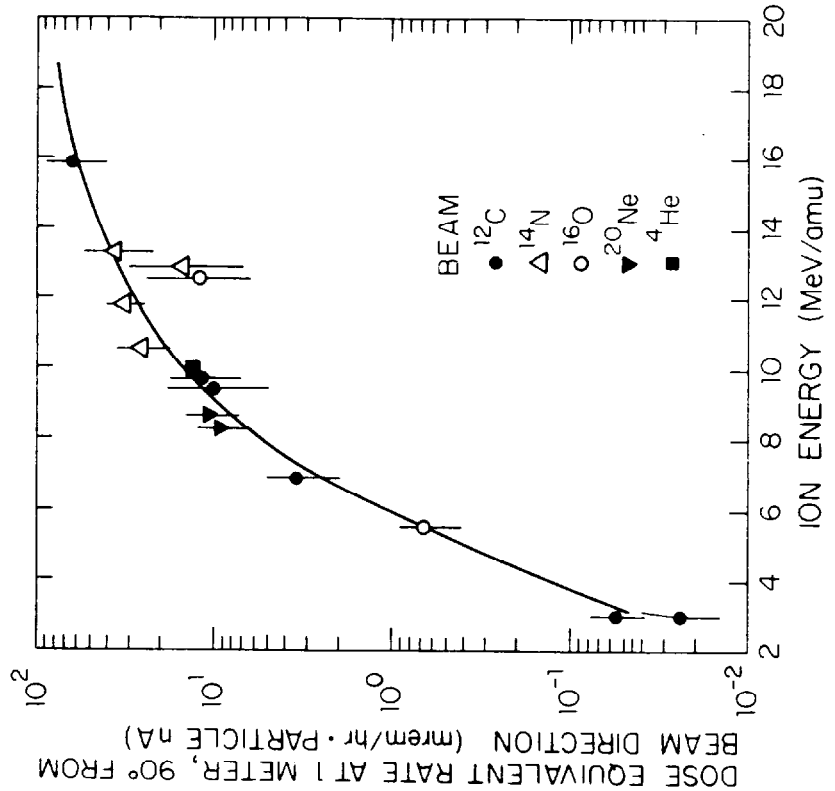

Fig. 1.39 Fast neutron dose equivalent rates at 1 meter from thick targets of iron, nickel, or copper and at θ = 90°. The ^{16}O and ^{14}N points near 13 MeV/amu were ignored in drawing the smooth curves. one "particle nanoAmpere" is 6.25 X 10^9 particles per sec. One mrem/hr per particle nanoAmpere is equivalent to 4.44 X 10^{-19} Sv per incident ion [Reproduced from (Oh80).]

Tuyn et. al [(Tu84), also reported in (NC96)] reports studies done with 86 MeV/amu ^{12}C ions incident on Fe targets slightly thicker than one range. These were compared with theoretical calculations. The data measured are shown in Figs. 1.41 and 1.42 taken from (Tu84).

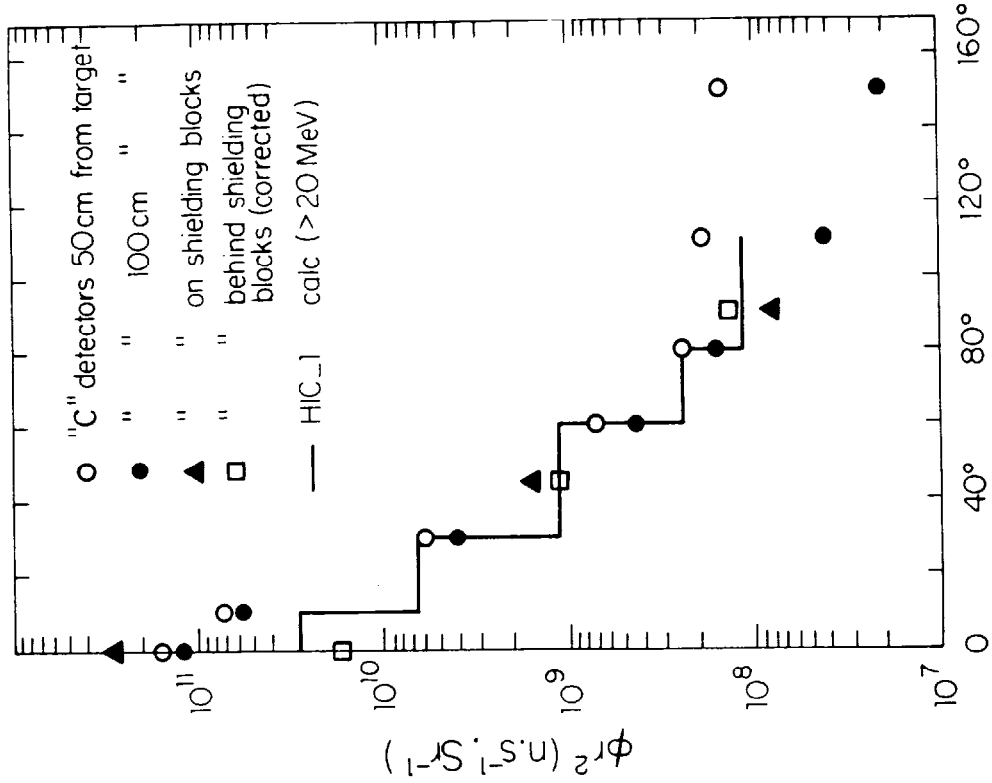

Fig. 1.42 Comparison between measured and calculated yields per 10^{11} ions s^{-1} at 86 MeV/amu 12C ions incident on an iron target for neutron energies above 20 MeV using the $^{12}C(n,2n)^{11}C$ reaction. Measurements were made at the indicated radial distances [Reproduced from (Tu84).]

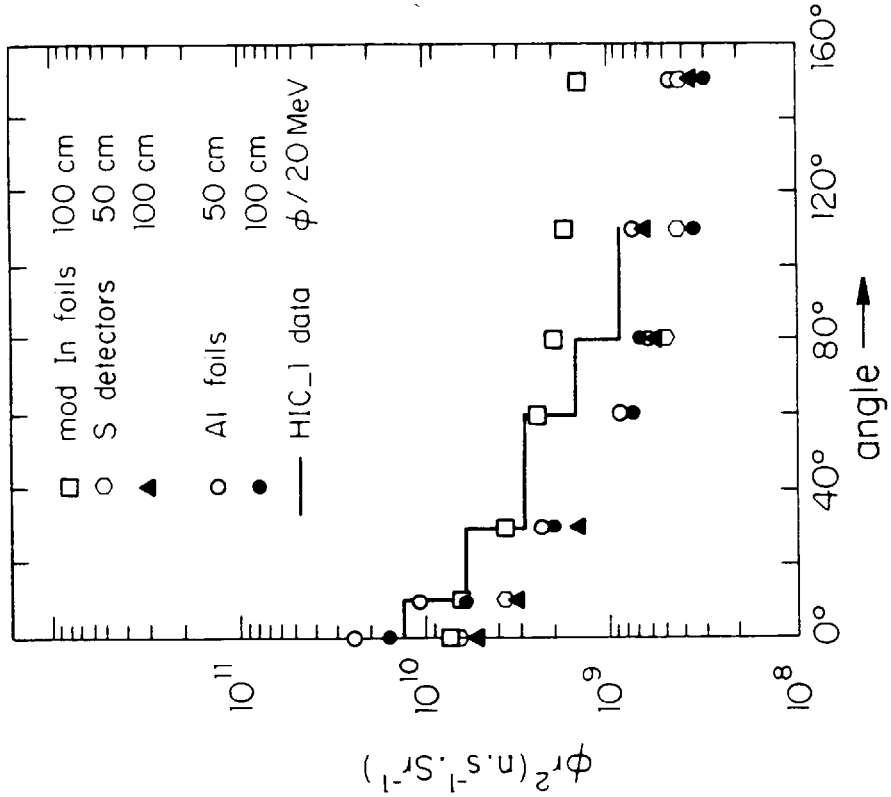

Fig. 1.41 Comparison between measured and calculated yields per 10^{11} ions s^{-1} at 86 MeV/amu ^{12}C ions incident on an iron target for neutron energies below 20 MeV. Activation detectors with the following sensitive regions in neutron energy, E_n, were used: moderated In foils ($0.4 < E_n < 107$ eV), $^{33}S(n,p)^{32}P$ ($E_n > 3$ MeV), $^{27}Al(n,\alpha)^{24}Na$ ($E_n > 7$ MeV). Measurements were made at the various radial distances. [Reproduced from (Tu84).]

Clapier and Zaidins (Cl83) have surveyed the existing data from 3 to 86 MeV/amu and have been able to parameterize it. They found that the following fits the angular distribution of flux density:

$$\phi(\theta,\xi) = \frac{1}{4\pi}\left\{\frac{1}{\log[1 + 1/\xi]}\right\}\left\{\frac{1}{\xi + \sin^2(\theta/2)}\right\} \qquad (1.42)$$

where θ is in degrees and the fitting parameter ξ is determined by

$$\xi = \frac{\phi(90^o)}{\phi(0^o) - \phi(90^o)} = \frac{1}{\phi(0^o)/\phi(90^o) - 1} \qquad (1.43)$$

and where $\phi(\theta)$ is the value of the fluence or dose equivalent at θ.

These same authors have found that the total yield, Y (neutrons/ion) can be approximately fit as a function of the target atomic number, Z, and the specific energy, W (MeV/amu). [Again, note the lack of dependence on projectile atomic number!]

The expressions which result are:

$$Y(W,Z) = C(Z)W^{\eta(Z)} \qquad \text{with} \qquad (1.44)$$

$$\eta(Z) = 1.22\sqrt{Z} \qquad \text{and} \qquad (1.45)$$

$$C(Z) = \frac{1.95 \times 10^{-4}}{Z^{2.75}}\exp[-0.475\,(\ln Z)^2]. \qquad (1.46)$$

These authors have tabulated the values of the parameters C(Z) and $\eta(Z)$ in Table. 1.7.

Table 1.7 Values of the parameters η (Z) and C(Z) as expressed in (Cl83).

Atomic Number	(element)	η (Z)	C(Z)
1	(hydrogen)	1.5	1.7×10^{-4}
2	(helium)	2.6	3.9×10^{-6}
6	(carbon)	2.7	2.5×10^{-6}
8	(oxygen)	3.6	3.6×10^{-7}
10	(neon)	7.0	2.7×10^{-10}
18	(argon)	7.0	5.1×10^{-11}
36	(krypton)	7.9	6.0×10^{-12}
82	(lead)	11.0	1.7×10^{-13}

They also give a few examples of the parameter, ξ, in the expression for fitting the angular distribution. They report values of 0.07 for uranium incident on uranium at 9 MeV/amu, 0.025 for neutrons of energy < 20 MeV produced by 86 MeV/amu ^{12}C incident on iron, and 3 X 10^{-4} for neutrons of energy > 20 MeV produced by 86 MeV/amu ^{12}C incident on iron. Fig. 1.43 gives the results found. One could use values given in Table 1.7 taken from (Cl83) or the direct calculation and obtain some idea of the uncertainties inherent in this fit to such a broad range of data.

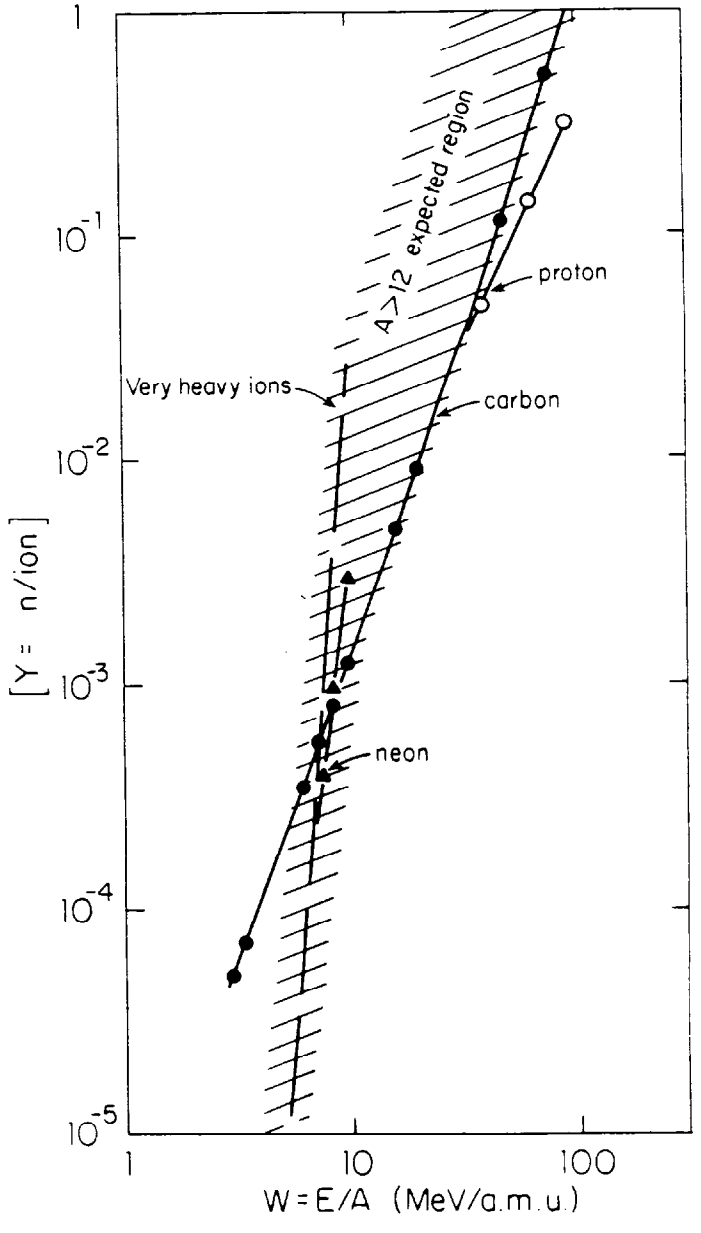

Fig. 1.43 Total neutron yields as a function of specific energy for a variety of ions. The shaded region is representative of the uncertainties in the associated parametric fit to the available data. [Reproduced from (Cl83).]

McCaslin, et al (McC85) measured the angular distribution of yields of 670 MeV/amu Ne and Si ions and obtained the following results:

For incident 670 MeV/amu ^{20}Ne ions including all neutrons above 6.5 MeV at a radius of 1 meter, McCaslin found:

$$\phi(\theta) = 372\ \theta^{-1}\ \text{neutrons m}^{-2}\text{/ion} \quad (\text{for } 2^\circ < \theta < 180^\circ,\ \theta \text{ in degrees}) \tag{1.47}$$

For incident 670 MeV/amu ^{20}Ne ions including all neutrons above 20 MeV;

$$\phi(\theta) = 248\ e^{-0.2\theta}\ \text{neutrons m}^{-2}\text{/ion} \quad (\text{for } 0^\circ < \theta < 20^\circ,\ \theta \text{ in degrees}) \tag{1.48}$$

and

$$\phi(\theta) = 10\ e^{-0.038\theta}\ \text{neutrons m}^{-2}\text{/ion} \quad (\text{for } 20^\circ < \theta < 120^\circ,\ \theta \text{ in degrees}). \tag{1.49}$$

The neutron yields at this high specific energy for heavy ions turn out to be quite large.

References

(Al75) R. G. Alsmiller, R. T. Santoro,, and J. Barish, "Shielding calculations for a 200 MeV proton accelerator and comparisons with experimental data", Particle Accelerators 7 (1975) 1-7.

(Cl83) F. Clapier and C. S. Zaidins, "Neutron dose equivalent rates due to heavy ion beams", Nucl. Instr. and Meth. 217 (1983) 489.

(De65) H. DeStaebler, "Similarity of shielding problems at electron and proton accelerators", Stanford Linear Accelerator Center report SLAC Pub 179 (1965). [Result also quoted in (Sc90)].

(Gi68) W. S. Gilbert, et. al, "1966 CERN-LRL-RHEL shielding experiment at the CERN Proton Synchrotron", UCRL-17941 (1968). [Much of this material is summarized in (PA73))

(Ha88) W. K. Hagan, B. L. Colborn, T. W. Armstrong, and M. Allen, "Radiation shielding calculations for a 70-250 MeV proton therapy facility", Nuclear Science and Engineering, 98,(1988)272-278.

(Hu60) E. L. Hubbard, R. M. Main, and R. V. Pyle, "Neutron production by heavy-ion bombardments", Phys. Rev. 188 (1960) 507.

(IC73) Data for protection against ionizing radiation from external sources, Supplement to ICRP 15, ICRP Report #21 (1973)

(IC78) ICRU, "Basis aspects of high-Energy particle interactions and radiation dosimetry", Report No. 28, Washington, DC, 1978.

(Le72) G. S. Levine, D. M. Squier, G. B. Stapleton, G. R. Stevenson, K. Goebel, and J. Ranft, "The angular dependence of dose and hadron yields from targets in 8 GeV/c and 24 GeV/c extracted beams", Particle Accelerators 3 (1972) 91-101.

(McC85) J. B. McCaslin, P. R. LaPlant, A. R. Smith, W. P. Swanson, and R. H. Thomas, "Neutron production by Ne and Si ions on a thick Cu target at 670 MeV/A with application to radiation protection," IEEE Trans. on Nucl. Sci. NS-32, No. 5 (1985) 3104.

(Na78) T. Nakamura, M. Yoshida, and T. Shin, "Spectra measurements of neutrons and photons from thick targets of C, Fe, Cu, and Pb by 52 MeV protons", Nucl. Instr. and Meth. 151 (1978) 493-503.

(NC96) R. H. Thomas (chair), W. R. Casey, N. Rohrig, J. D. Cossairt, L. A. Slaback, K. O'Brien, G. B. Stapleton, and W. P. Swanson, National Council on Radiation Protection and Measurements (NCRP), NCRP Report 51 (Revised)--in preparation.

(Ne68) W. R. Nelson, "The shielding of muons around high energy electron accelerators", Nucl. Instr. and Meth. 66 (1968) 293.

(Ne74) W.R. Nelson and K. R. Kase, "Muon shielding around high-energy electron accelerators, Part I, Theory, Nucl. Instr. and Meth., 120 (1974) 401, and W.R. Nelson, K. R. Kase, and G. K. Svensson, "Muon shielding around high-energy electron accelerators, Part II, Experimental Investigation, Nucl. Instr. and Meth., 120 (1974) 413.

(Oh80) W. F. Ohnesorge, H. M. Butler, C. B. Fulmer, and S. W. Mosko, "Heavy ion target area fast neutron dose equivalent rates", Health Physics 39 (1980) 633.

(Pa73) H. W. Patterson and R. H. Thomas, *Accelerator Health Physics,* Academic Press, new York, 1973.

(PR92) *Review of Particle Properties,* Physical Review D45 Part 2 (June, 1992).

(Ra72) J. Ranft and J. T. Routti, "Hadronic cascade calculations of angular distributions of integrated secondary particle fluxes from external targets and new empirical formulae describing particle production in proton-nucleus collisions", Part. Acc. 4 (1972) 101.

(Sc90) H. Schopper (editor), A. Fassò, K. Goebel, M. Höfert, J, Ranft, and G. Stevenson, *Landolt-Börnstein Numerical Data and Functional Relationships in Science and Technology New Series; Group I: Nuclear and Particle Physics Volume II: Shielding Against High Energy Radiation* (O. Madelung, Editor in Chief, Springer-Verlag, Berlin, Heidelberg, 1990).

(St83) G. R. Stevenson, "Dose and dose equivalent from muons", Rep. TIS-RP/099, CERN, Geneva Switzerland (1983). Important conclusions from this work are presented in (Sc90).

(St85) G. R. Stevenson, P. A. Aarnio, A. Fassò, J. Ranft, J. V. Sandberg, and P. Sievers, "Comparison of measurements of angular hadron energy spectra, induced activity, and dose with FLUKA82 calculations", Nucl. Instr. and Meth. A245 (1985) 323-237.

(Su89) A. H. Sullivan, "The intensity distribution of secondary particles produced in high energy proton interactions", Rad. Prot. Dos. 27 (1989) 189-192. [Fig 1.35 was obtained from the preprint to this paper, CERN Report TIS-RP/209/PP (1988).

(Su92) A. H. Sullivan, *A Guide to Radiation and Radioactivity Levels Near High Energy Proton Accelerators,* (Nuclear Technology Publishing, Ashford, Kent, TN23 1JW, England, 1992.)

(Sw79) W. P. Swanson, "Radiological Safety aspects of the operation of electron linear accelerators," Technical Report No. 188, Vienna, 1979.

(Sw90) W. P. Swanson and R. H. Thomas, "Dosimetry for radiological protection at high energy particle accelerators", Chapter 1 in *The Dosimetry of Ionizing Radiation,* Volume III (Academic Press, 1990) [Figure taken from W.R. Nelson, et. al., CERN Report CERN-TIS-RP/100/PP (1983)].

(Te85) K. Tesch, "A simple estimation of the lateral shielding for proton accelerators in the energy range from 50 to 1000 MeV," Rad. Prot. Dos. 11 (1985) 165-172.

(Th88) R. H. Thomas and G. R. Stevenson, "Radiological safety aspects of the operation of proton accelerators", Technical Report No. 283, IAEA, Vienna, 1988.

(Tu84) J. W. N. Tuyn, R. Deltenre, C. Lamberet, and G. Roubaud, "Some radiation aspects of heavy ion acceleration," Proc. 6th Int. Cong. IRPA, Berlin (1984) 673.

(Va87) A. Van Ginneken, P. Yurista, and C. Yamaguchi, "Shielding calculations for multi-TeV hadron colliders, Fermilab Report FN-447 (1987).

1. a) To how many GeV/s does 1 kW of beam power correspond?

   b) To how many singly charged particles per second does 1 ampere of beam current correspond?

   c) To how many GeV/kg of energy deposition does an absorbed dose of 1 Gy correspond?

2. Which has the higher quality factor, a 10 MeV (kinetic energy) α-particle or a 1 MeV neutron? Write down the quality factors for each particle.

3. Calculate the number of ^{12}C and ^{238}U atoms per cm^3 of solid material.

4. Calculate the velocity and momenta of a 200 MeV electron, proton, iron ion, π^+, and μ^+. The 200 MeV is kinetic energy and the answers should be expressed in units of the speed of light (velocity) and MeV/c (momenta). Iron ions have an isotope-averaged mass of 52021 MeV (A = 55.847 X 931.5 MeV/amu). The π^+ mass is 140 MeV and the μ^+ mass = 106 MeV . Do the same calculation for 20 GeV protons, iron ions, and muons. It is suggested that these results be presented in tabular form. Make general comments on the velocity and momenta of the particles at the two energies. (The table may help you notice any algebraic errors that you have made.)

5. Calculate the mass stopping power of a 20 MeV electron (ionization only) and a 200 MeV proton in ^{28}Si.

6. An electron accelerator has a beam profile in the form of a 2 mm diameter circle uniformly illuminated by the beam. Make a crude plot of the value of the dose equivalent rate in the beam as the energy increases from 1 MeV to 10 GeV. The average beam current is 1 microamp (1 μA). Assume the beam profile is unchanged during acceleration. Compare with Swanson's simple formula ("conservative" value) . Is his formula "conservative" above 100 MeV? (Hint: use Fig. 1.9)

7. Calculate the critical energy and length of material that corresponds to the radiation length for carbon and for lead. What does this say about the effectiveness of low-Z versus high-Z shielding materials for electrons?

8. A 100 MeV electron accelerator produces a 1.0 μA beam incident on a high-Z (thick) target. Estimate the bremsstrahlung absorbed dose rates at $\theta = 0^o$ and 90^o at r = 2 m from the target using Swanson's rules of thumb. Compare the 0^o result with the "in the beam dose equivalent rate" found in problem 6. How do the bremsstrahlung and in-beam dose rates compare?

9. Suppose the Tevatron enclosure at Fermilab is converted into an enclosure for an electron synchrotron. The radius of the synchrotron is 1000 m. If the circulated beam is 10^{12} electron, calculate the median energy of the synchrotron radiation photons for E_0 = 100 GeV. Also find θ_c of the "lobe."

10. For the accelerator of problem 8, calculate the neutron flux density at r = 2 m at large angles using the values in Table 1.3 for a high-Z (tungsten) target. Also use Table 1.3 to estimate the dose equivalent r = 2 m. Check this result by "guessing" the average neutron energy is 1-10 MeV and use the curve in Fig. 1.6. Compare this neutron dose with the Bremsstrahlung dose at larrge angles obtained in problem 8.

11. Fig. 1.21 gives both muon flux density and muon dose equivalent rate at one meter at $\theta = 0^o$ as a function of electron beam energy. From the figure determine the fluence-to-dose equivalent factor used to obtain the dose equivalent rate from the primary calculation of muon flux density. Compare with Stevenson's result.

12. Calculate the muon fluence necessary to produce a dose equivalent of 1 mrem assuming a quality factor = 1 and that tissue is equivalent to water for minimum ionizing muons. (Hint: use Table 1.2) Could this explain the slight discrepancy noted in this conversion factor found in problem 11? How?

13. For a 20 GeV electron accelerator, the electron beam strikes a beam stop made of aluminum or iron. How long (in Z) does the beam stop have to be to range out the muon having the average energy (for both Al & Fe)? (Hint: use curves from Fig. 1.20 to calculate the average energy by looking at flux versus energy.) What will the relative dose rates be at the immediate downstream ends of each material? Assume multiple scattering is not important. Compare the dose rates at the immediate downstream ends of each material. (Assume the production of muons from Fe is apprxoimately equal to that from Al. Recall the inverse square law.)

14. One can use measurement results to check Sullivan's formula for hadron fluence above 40 MeV for high-energy proton interactions. Check the agreement for the 22 and 225 GeV/c data in Figs. 1.33 and 1.34 for 3 representative angles at one meter. (Ignore the fact that the formula is for hadrons > 40 MeV while the only data provided is for hadrons >35 MeV and 50 MeV but do not ignore the difference between normalizing to incident versus interacting protons.) (It is valid to make the comparison on yield per interacting proton since the results in Fig. 1.34 is for targets approximately 1 interaction length long.) Comment on the quality of the agreement.

15. Calculations can also be used to check the Tesch curve for dose equivalent at $\theta = 90^o$ (Fig. 1.36). Use the 200 MeV calculations in Fig. 1.30 to do this by crudely numerically integrating the $60^o < \theta < 90^o$ yields to determine the average energy of the neutrons and the total fluence at $\theta = 90^o$ and at 1 meter. Use the results along with fluence-to-dose equivalent rate curves (Fig. 1.6) to obtain the dose equivalent per proton to compare with Tesch's result. (Iron is considered equivalent to copper for this problem.)

16. Use Tesch's curve in Fig. 1.36 to calculate the dose equivalent rate at 2 m and $\theta = 90^o$ from a target struck by 1 μA of 100 MeV protons. Compare with the neutron dose rate calculated in problem 10 for an electron accelerator having the same intensity and beam energy and discuss. (Scale the relevant result of problem 10 by the appropriate yield for copper vs. Tungsten.)

17. It is often necessary to work from fragmentary data to determine other quantitites.

    a) Use McCaslin's results and appropriate fluence to dose factors to calculate the dose equivalent rate at 1 meter and at $\theta = 30^o$ for a target struck by 10^8 670 MeV/amu ^{20}Ne ions per sec. (Hint: use all available spectrum information.)

    b) Use McCaslin's results to obtain the total yield of neutrons per ion with $E_n > 6.5$ MeV. Assuming the target to be iron or copper, how does this yield correspond to that due to 700 MeV protons? Do this for both $E_n > 6.5$ MeV and $E_n > 20$ MeV to understand the overall composition.
    Hint: Integrate over the unit sphere (double integral over spherical coordinates θ & ϕ)

The following indefinite integrals are needed:

$$\int dx \frac{\sin x}{x} = x - \frac{x^3}{3 \cdot 3!} + \frac{x^5}{5 \cdot 5!} - \frac{x^7}{7 \cdot 7!}$$

$$\int dx\, e^{ax} \sin(bx) = \frac{e^{ax}[a \sin(bx) - b \cos(bx)]}{a^2 + b^2}$$

The elemental area on the sphere of radius R is $dA = r^2 \sin\theta\, d\theta d\phi$, (See figure below.)

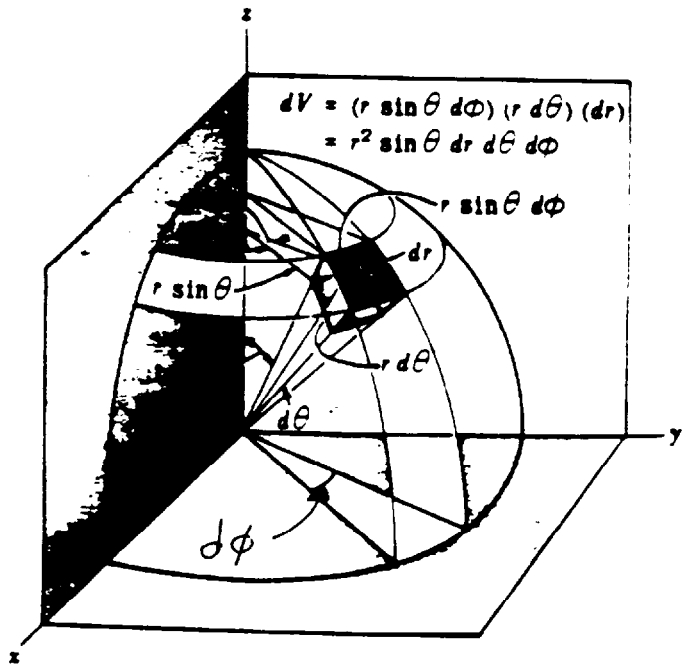

In this chapter the major features of the shielding of electrons and photons at accelerators are described. It includes extensive discussion of the electromagnetic cascade and a discussion of the shielding of photoneutrons and high energy particles that result from these interactions. The chapter concludes with a treatment of the generalized shielding problem with specific attention given to the Monte-Carlo method.

I. The Electromagnetic Cascade-Introduction

The "prime mover" in shielding design at electron accelerators is the electromagnetic cascade. This would also be true were a muon accelerator to be built.

One should recall the definitions of **radiation length**, X_o, and **critical energy**, E_c, from Chapter 1;

$$X_o = \frac{716.4\ A}{Z(Z+1)\ln(287/\sqrt{Z})}\ (\text{g cm}^{-2}) \tag{2.1}$$

and

$$E_c = 800/(Z + 1.2)\ (\text{MeV}). \tag{2.2}$$

Another parameter of importance (PR92) for describing the electromagnetic cascade is the **Molière radius**, X_m:

$$X_m = X_o E_s/E_c \tag{2.3}$$

$$\text{where } E_s = (\sqrt{4\pi/\alpha})m_e c^2 = 21.2\ \text{MeV}. \tag{2.4}$$

[α is the fine structure constant (see Table 1.1) and m_e is the mass of the electron.]

It turns out that X_m is a good characteristic length for radial distributions in electromagnetic showers. Two more scaling dimensionless variables are commonly introduced to describe electromagnetic shower behavior;

$$t = x/X_o \quad \text{(distance)} \tag{2.5}$$

$$\text{and } y = E/E_c \quad \text{(energy)}. \tag{2.6}$$

As an aside, for mixtures of n elements (PR92) states that these quantities and the stopping power dE/dx scale according to the elemental fractions by weight, f_i, as follows:

$$\frac{dE}{dx} = \sum_{i=1}^{n} f_i \left(\frac{dE}{dx}\right)_i \quad \left\{\text{all } \frac{dE}{dx} \text{ in energy/g cm}^{-2}\right\} \tag{2.7}$$

$$\frac{1}{X_o} = \sum_{i=1}^{n} \frac{f_i}{X_{oi}} \quad \{\text{all } X_{oi} \text{ in g cm}^{-2}\} \text{ and} \tag{2.8}$$

$$\frac{1}{X_m} = \frac{1}{E_s} \sum_{i=1}^{n} \frac{f_i E_{c_i}}{X_{o_i}}. \tag{2.9}$$

Another term used is that of the so-called "**Compton minimum**" which, as the term is generally used, is the energy at which the total photon cross section is at a minimum. [The use of this term is an unfortunate occurrence of technical "slang" since at the higher energies the Compton scattering cross section monotonically decreases with energy!] This value always occurs at energies less than E_c and is typically a few MeV. For high energy photons ($E_o > 1$ GeV), the total e^+e^- pair production cross section, σ_{pair}, is approximately given, for a single element, by

$$\sigma_{pair} = \frac{7}{9}\left(\frac{A}{X_o N_A}\right) \quad (cm^2), \tag{2.10}$$

where A is the atomic weight, N_A, is Avagadro's number, and X_o is the radiation length expressed in units of g/cm^2.

For energies larger than a few MeV, the pair production process dominates the total photon attenuation. The interaction length for pair production, λ_{pair}, is given by

$$\lambda_{pair} = \frac{\rho}{N\sigma} \ (g/cm^2) = \frac{\rho}{\frac{\rho N_A}{A}\frac{7}{9}\left(\frac{A}{X_o N_A}\right)} = \frac{9}{7}X_o \ , \tag{2.11}$$

where the symbols all have the same meanings as used in Chapter 1 and thus far in this chapter.

This result, along with the facts about photon production by electrons interacting in matter, leads to the most important fact about the electromagnetic cascade:

The electrons radiatively produce photons with almost the same characteristic length for which the photons produce more e^+ e^- pairs.

This is so important because as a first order approximation it means that the "size" in physical space is independent of energy. (For hadronic cascades, the result is considerably different!)

Figure 2.1 taken from (PR92) illustrates the photon cross sections for the various physical processes responsible for photon attenuation.

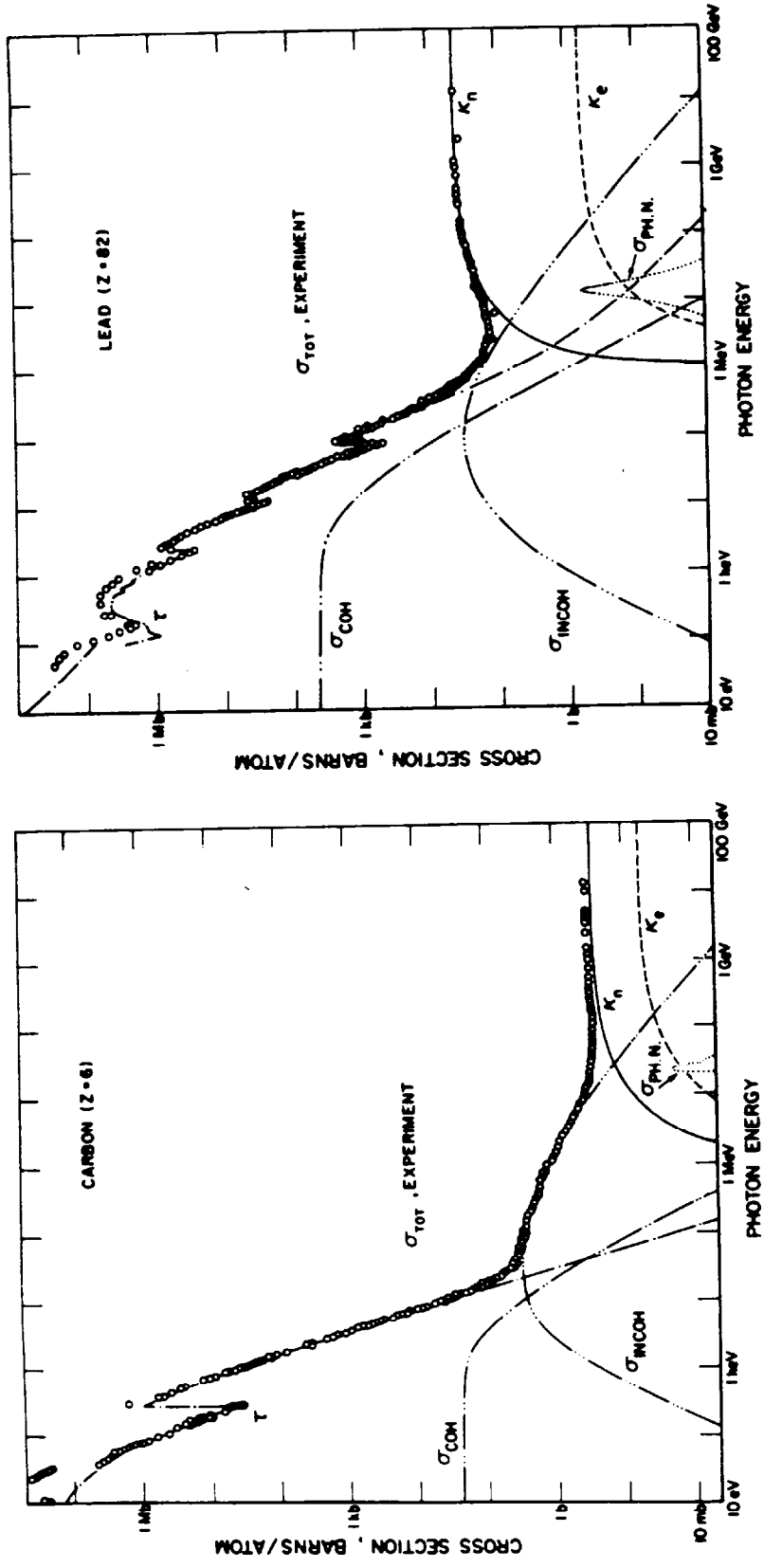

Fig. 2.1 Contributions to photon cross sections in carbon and lead. [Reproduced from (PR92) and references cited therein].

II. The Electromagnetic Cascade Process

In the most simple terms, the electromagnetic cascade at an electron accelerator proceeds qualitatively according to the following steps:

1. A high energy electron produces a high energy photon by bremsstrahlung.
2. This photon produces an $e^+ e^-$ pair after traveling, on average, a distance of X_0 (each member of the pair will have half the energy of the photon).
3. After traveling an average distance of X_0, each member of the $e^+ e^-$ pair will produce yet another bremsstrahlung photon.
4. Each electron or positron may continue on to interact again and release yet more photons before its energy is totally absorbed.

{This chain could equally well be initiated by a high energy photon from a hadron accelerator.}

Eventually, after a number of generations, the individual energies of the electrons and positrons will be degraded to values below E_c so that ionization processes then begin to dominate and terminate the shower. Likewise, the photon energies eventually are degraded so that Compton scattering and the photoelectric effect compete with the further production of $e^+ e^-$ pairs.

Figure 2.2 taken from (Sw79) shows, schematically, the electromagnetic cascade process. Of course, there are subtleties representing many different physical processes, such as the production of other particles, which must be taken into account. These are best handled by Monte-Carlo calculations. The most widely-used code incorporating the Monte-Carlo method as applied to electromagnetic cascades is that written by W. R. Nelson of SLAC called EGS (electron gamma shower, a current version is denoted EGS4) which has been described in (Ne90)[1]. Van Ginneken has also written a Monte-Carlo program which is very effective for calculating deep penetrations called AEGIS (Va78) [An appendix at the end of this discussion will briefly review the Monte-Carlo Method.] Analytical approximations have been developed and are summarized elsewhere [e.g., (Sw79)].

There are some published standard calculations from which estimates may be made which will now be introduced.

Longitudinal shower development

The dosimetric properties of the calculations of an electromagnetic cascade may be summarized in curves that give fluence, dose, or other quantities of interest as functions of shower depth or distance from the axis. Figure 2.3 taken from (Va75) shows the fraction of total energy deposited (integrated over all radii about the shower axis) versus depth from Van Ginneken and Awschalom (Va75). These authors found that a new scaling parameter, λ_ℓ, given by

$$\lambda_\ell = 325(\ln Z)^{-1.73}\ln(E_0) \ (\text{g cm}^{-2}) \quad [E_0 \text{ is in MeV}] \qquad (2.12)$$

When longitudinal lengths are expressed in units of λ_ℓ,, all curves merge approximately into this universal one.

[1]Monte-Carlo programs exist, in general, in a state of nearly continuous improvement. Thus the authors of such codes should be contacted to provide the current version.

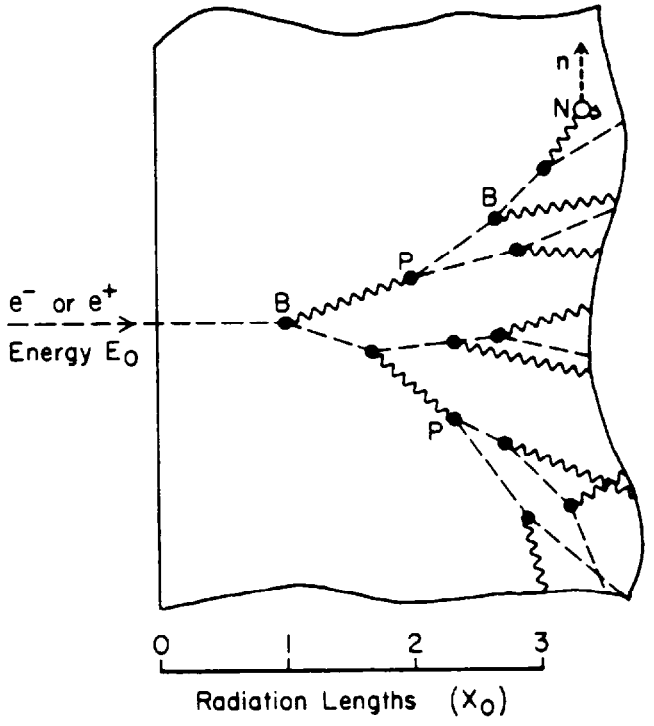

Fig. 2.2 Development of an electromagnetic cascade in a semi-infinite medium at high energy (well above the critical energy). The dashed lines represent electrons or positrons and the wavy lines represent photons. An electron or positron of energy E_0 is incident at the left (a cascade can also be initiated by a photon). The spreading in the transverse direction is greatly exaggerated for clarity. Only bremsstrahlung (B) and pair production (P) events are shown, but Compton scattering also plays a role in the dispersal of energy. Energy is deposited in the medium along the dashed lines by ionization. Photonuclear reactions, as illustrated by the (γ,n) reaction at point N, may take place along any of the wavy lines if the energy of that photon is high enough. They occur much less frequently than might be inferred from this illustration. [Reproduced from (Sw79).]

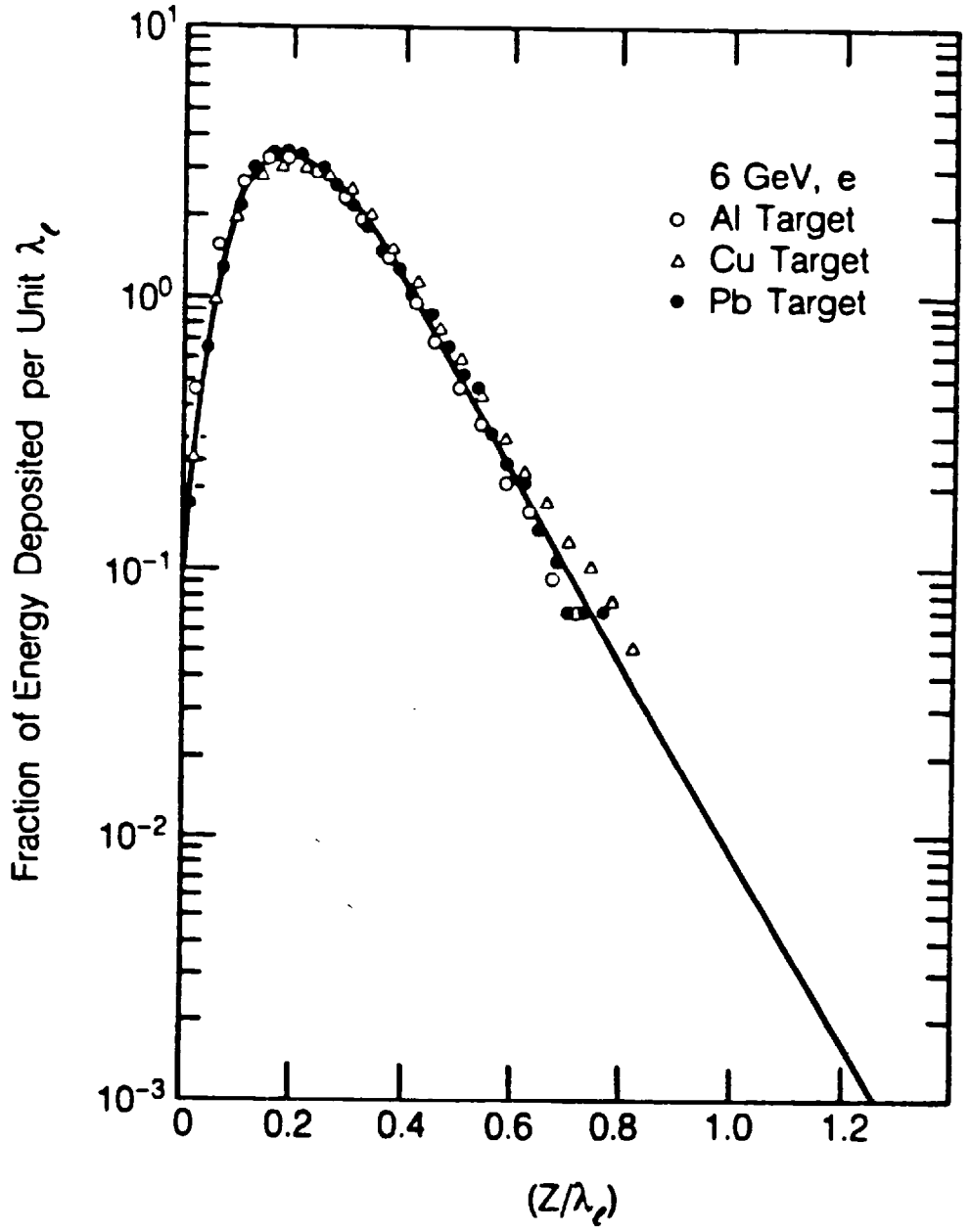

Fig. 2.3 Fraction of total energy, U, deposited by an EM cascade shower versus depth, integrated over all radii about the shower axis. [Reproduced from (Va75).]

Rossi and Griesen (Ro41), in their development of analytical shower theory, have predicted (using their so-called "Approximation B") that the total number of electrons and positrons at the shower maximum, N_{show} are proportional to the primary energy as follows:

$$N_{show} = \frac{0.31\, E_o/E_c}{[\ln(E_o/E_c) - 0.37]^{1/2}}. \qquad (2.13)$$

This makes sense intuitively; the result of the shower is to divide the energy at maximum among a number of particles with energies near E_c.

Also from this Approximation B , the location of the shower maximum X_{max}, (along the longitudinal axis usually represented by the Z coordinate) should be given by:

$$\frac{X_{max}}{X_o} = \ln\left[\frac{E_o}{E_c}\right] - C. \qquad \text{(with } C = 1\text{)} \qquad (2.14)$$

Experimentally, Bathow, Freytag, and Tesch (Ba67) found that $C = 0.77$ for Cu and 0.47 for Pb fit experimental data better. (Photon induced showers penetrate about 0.8 radiation lengths deeper. (Sc90) identifies slight differences between photon and lepton induced showers but these can normally be neglected.) The maximum energy deposited per radiation length is simply given by multiplying N_{show} by the critical energy.

(Sc90) gives the mean squared longitudinal spread, τ^2, (mean square distance lateral spread of the shower about $t \approx t_{max} = X_{max}/X_o$.):

$$\tau^2 = 1.61 \ln\left(\frac{E_o}{E_c}\right) - 0.2 \quad \text{(electron-induced shower), and} \qquad (2.15)$$

$$\tau^2 = 1.61 \ln\left(\frac{E_o}{E_c}\right) + 0.9 \qquad (2.16)$$

(photon-induced shower, for which E_o is the photon energy more conventionally denoted by k_o by some authors).

For dosimetric purposes for a shower in a given material, EGS4 results tabulated in (Sc90) have been parameterized to determine "source terms" for longitudinal dose equivalents in materials over the energy region 1 GeV < E_o < 1 TeV for dose on the Z-axis (subscripts "a"), dose averaged over a 15 cm radius about the Z-axis, (subscripts "m") and for total energy deposited (subscripts "e") . Table 2.1 taken from (Sc90) gives the various parameters for calculating dose equivalent, H_{long} (Sv per electron) at the end of a beam dump of length, L (cm) of density, ρ (g/cm^3) and gives fitted values of the various "attenuation lengths", λ_i (g/cm^2). For absorbed dose calculations, the factor C, which is the ratio of dose equivalent in tissue (Sv) to absorbed dose in the material (not tissue) (Gy), should be set to unity. The following is the formula in which these parameters from Table 2.1 are to be used:

$$H_{long} = C S_i e^{-\rho L/\lambda_i}. \qquad (2.17)$$

Table 2.1 Source terms S_a, S_m, and S_e, and corresponding recommended attenuation lengths, λ_a, λ_m, and λ_e for doses on the axis, averaged over a radius of 15 cm, and for total energy in the energy range from 1 GeV to 1 TeV in the forward direction for dumps and end-stops, respectively. Conversion factors C from absorbed dose in shielding material to dose equivalent are given. E_0 is the beam kinetic energy in GeV. [Adapted from (Sc90).]

Material	C (Sv/Gy)	S_a (Gy/electron)	λ_a (g/cm^2)	S_m (Gy/electron)	λ_m (g/cm^2)	S_e (Gy/electron)	λ_e (g/cm^2)
Water	0.95	$1.9X10^{-10}E_0^{2.0}$	58	$1.5X10^{-11}E_0^{2.0}$	59.9	$1.2X10^{-14}E_0^{1.7}$	75
Concrete	1.2	$1.9X10^{-9}E_0^{1.8}$	44	$2.2X10^{-11}E_0^{1.8}$	45.6	$9.0X10^{-14}E_0^{1.7}$	52
Aluminum	1.2	$2.3X10^{-9}E_0^{1.7}$	46	$3.4X10^{-11}E_0^{1.7}$	46.3	$1.0X10^{-13}E_0^{1.7}$	55
Iron	1.3	$2.9X10^{-8}E_0^{1.7}$	30	$1.8X10^{-10}E_0^{1.7}$	33.6	$1.1X10^{-12}E_0^{1.6}$	37
Lead	1.8	$1.9X10^{-7}E_0^{1.4}$	18	$4.6X10^{-10}E_0^{1.4}$	24.2	$4.3X10^{-12}E_0^{1.2}$	25

Lateral shower development

Figure 2.4 taken from (Ne68) shows the fraction U/E_0 of the incident energy which escapes laterally from an infinitely long cylinder as a function of cylinder radius for showers caused by electrons of various energies which bombard the front face of the cylinder. On this graph R is in units of X_m. The curve has been parameterized as:

$$\frac{U(r)}{E_o} = 0.8\exp[-3.45\,(r/X_m)] + 0.2\exp[-0.889\,(r/X_m)]. \qquad (2.18)$$

In Fig. 2.4, the universality of electromagnetic cascade curves is clear. Similar results have been obtained using EGS4 (Sc90). For large radii, a material dependent phenomenon emerges in which the photons having the largest mean free paths determined by the photon cross section at the Compton minimum will dominate the slopes. These slopes, normalized to X_m, are also shown in this figure.[2]

[2]In several publications in which Fig.2.4 has appeared, including the original one, the decimal points in the "x-axis" coordinates have been nearly invisible.!

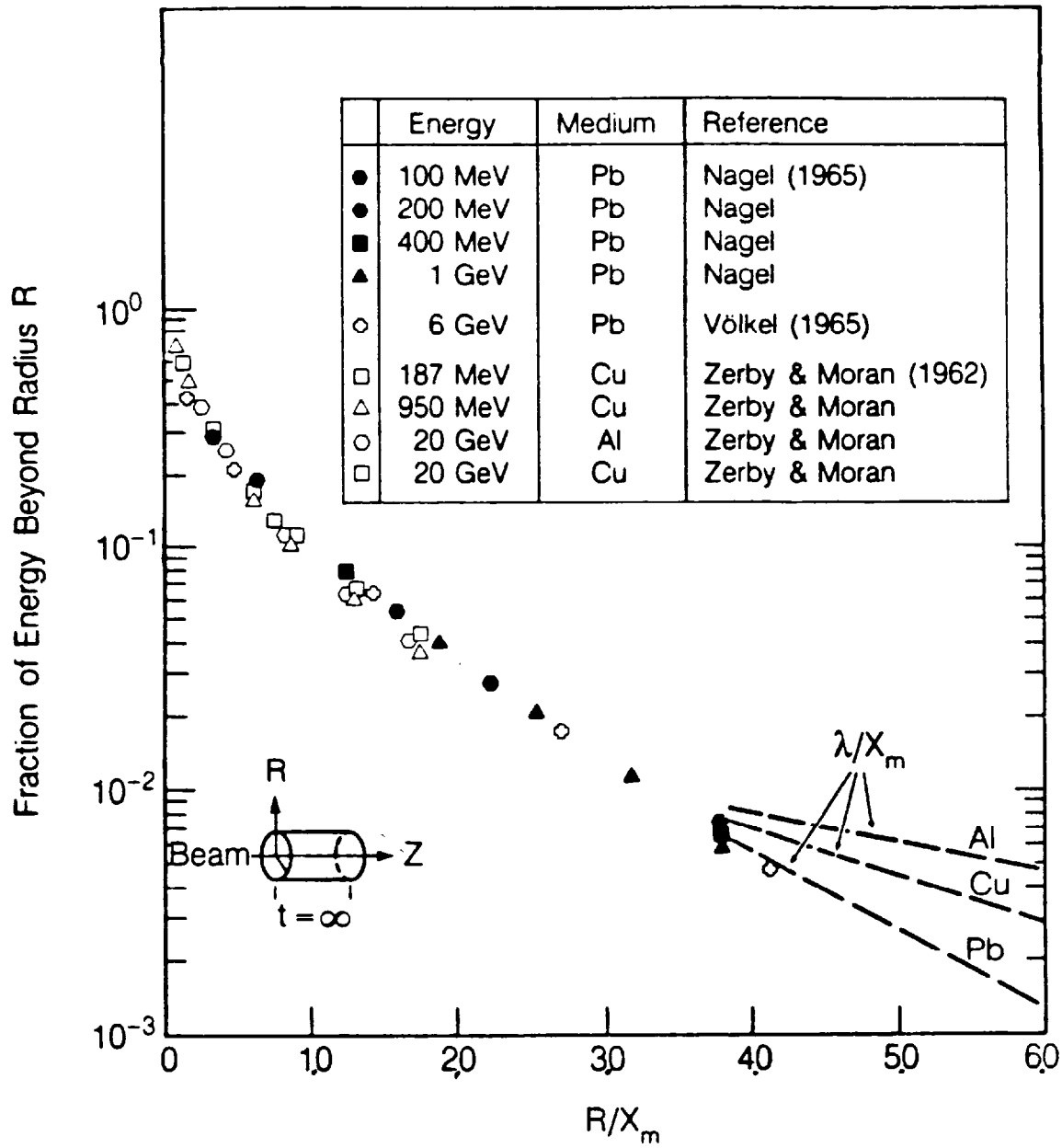

Fig. 2.4 Fraction of total energy, U, deposited beyond a cylindrical radius, R/X_m, as a function of radius for showers caused by 0.1 - 20 GeV electrons incident on various materials (Reproduced from (Ne68) and references cited therein.]

As was done for the longitudinal situation, EGS4 (Sc90) has been similarly used to give the maximum energy deposition (and by extension, the maximum absorbed dose and dose equivalent) as a function of radius R. Over the energy range 1 GeV < E_o < 1 TeV, there is direct scaling with energy in the formula for dose equivalent:

$$H_{lat} = CE_oS_1\frac{e^{-\rho R/\lambda_1}}{a^2} \quad , \tag{2.19}$$

where H_{lat} is the maximum dose equivalent laterally (Sv per electron), C is the same as before, E_o is the electron kinetic energy in GeV, S_1 is the source term from the EGS4 calculations (tabulated below), R is the lateral dimension of the shield (shield thickness) in cm, ρ is the density (g cm^{-3}), λ_1 is the attenuation length (g/cm^2), and a is the distance from the axis, in cm, where the dose equivalent is desired.

Table 2.2 taken from from (Sc90) gives the parameters needed for the above formula and Fig. 2.5 also taken from (Sc90) shows the result of the EGS4 calculations.

Table 2.2 Conversion factors C from absorbed dose in shielding material to dose equivalent, source terms S_1 for the maximum of the electromagnetic component, and recommended attenuation lengths λ_1 for the energy range 1 GeV to 1 TeV laterally for dumps or end-stops. [Adapted from (Sc90).]

Material	C (Sv/Gy)	S_1 (Gy cm^2 GeV^{-1} per electron)	λ_1 (g/cm^2)
Water	0.95	$2.5X10^{-12}$	26
Concrete	1.2	$3.6X10^{-12}$	27
Aluminum	1.2	$3.4X10^{-12}$	29
Iron	1.3	$4.7X10^{-11}$	33
Lead	1.8	$1.3X10^{-10}$	26

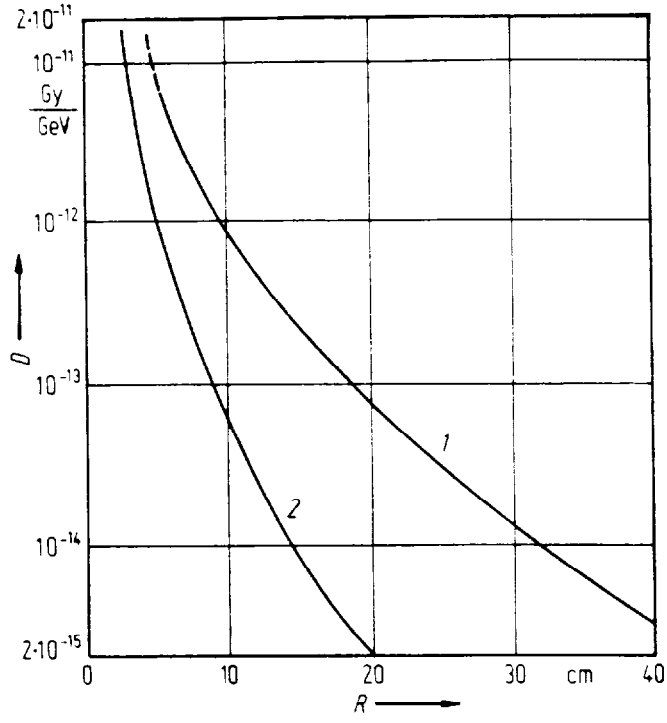

Fig. 2.5 Maximum absorbed dose D in a cylinder vs. radius R; curve 1: cylinder made of concrete of density 2.4 g/cm^3, curve 2: cylinder made of iron of density 7.2 g/cm^3. Curves calculated with EGS4 for electron beams of 1, 10, 100, and 1000 GeV and normalized per GeV become independent of energy. [Reproduced from (Sc90).]

III. Hadron Production by the Electromagnetic Cascade.

As we have seen before, neutrons are produced by high energy electrons and photons. These neutrons must be taken into account to properly shield electron accelerators. The general issues concerning the shielding of neutrons are addressed in more detail in Chapter 3. K. Tesch has summarized shielding against these neutrons in his review article (Te88). He has summarized the feature of the neutron fields with simple analytical relations for cases where "thick" targets are struck by the electron beam.

For lateral concrete shielding, the dose equivalent per electron after shield thickness, d (g/cm^2), which begins at radius r (m) from an iron target struck by electrons having primary energy E_o (GeV) is

$$H(d,r) = \frac{4.0 \times 10^{-17}}{r^2} E_o e^{-d/100} \quad (Sv). \tag{2.20}$$

This is valid for $E_o > 0.4$ GeV and $d > 200$ g cm^{-2}.

The angular variations are not severe because of the nature of the mechanisms by which the neutrons are produced at electron accelerators (namely, photoneutron production). For other target materials one can scale this equation as follows.

The neutron production is proportional to the photoproduction cross section, the track length in cm, and the number of atoms cm^{-3}. The interaction cross section is generally proportional to the atomic weight A. The track length is proportional to X_o; the production becomes proportional to the radiation length in g cm^{-2}. Thus one can, for rough estimates of dose equivalent in the environs of targets of materials other than iron, obtain results by scaling this value for iron by the factor f;

$$f = \frac{X_{o_{material}}}{X_{o_{iron}}}. \tag{2.21}$$

For shields comprised of other materials, one can simply adjust the attenuation length (g cm^{-2}) in the exponent of the above to that appropriate to the material.

(Sc90) gives a somewhat more detailed treatment separately handling the giant resonance neutrons and high energy particle components of dose equivalent and deriving "source terms" and appropriate formulas. Fig. 2.6 taken from (Sc90) illustrates the geometry for using the formulas to be given below:

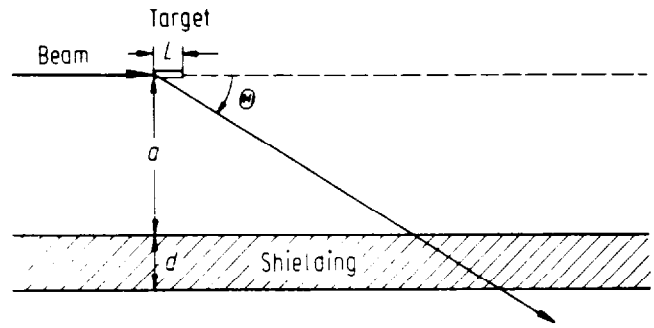

Fig. 2.6 Target and shielding geometry for the estimation of dose equivalent from bremsstrahlung, giant resonance neutrons, and high energy particles in the angular range with the beam θ from 30 to 120 degrees; a is the lateral distance between the target and the shielding and d is the shielding thickness.

The formulae given below are held to be valid for 1 GeV < E_o < 1 TeV and for 30 < θ < 120 degrees.

For the giant resonance neutrons:

$$H_n = \eta_n S_n E_o \left(\frac{\sin\theta}{a+d}\right)^2 \exp\left[-\frac{\rho d}{\lambda_n \sin(\theta)}\right] \quad \text{where } E_o \text{ is the energy (GeV),} \qquad (2.22)$$

E is the beam energy (GeV), ρ is the density (g/cm^3), a and d are as shown (cm) in Fig. 2.6, S_n is the source term from Chapter 1 (Sv cm^2 GeV^{-1}), and λ_n (g/cm^2) is the attenuation length recommended for giant resonance neutrons. Values of λ_n are as follows for representative materials:

	λ_n (g/cm^2)
water	9 (g/cm^2)
concrete	42 "
iron	130 "
lead	235 "

The factor η_n is a dimensionless factor ($\eta_n \leq 1$) which gives an estimate of the efficiency for the production of neutrons by the target. Figure 2.7 taken from (Sc90) can be used to estimate this quantity:

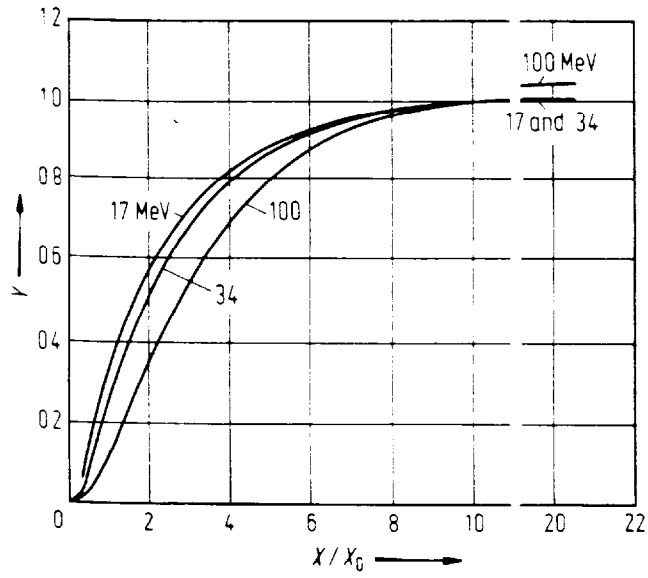

Fig. 2.7 Relative yield Y of neutrons released by electron beams incident on a lead target at energies E_o = 17, 34 and 100 MeV vs. target thickness measured in radiation lengths X_o. The curves are qualitatively similar for the other materials and energies but the initial rise will tend to be steeper, and saturation will be more quickly achieved, for higher E_o or greater Z. [Reproduced from (Sc90) as adapted from references cited therein.]

For the high energy particles:

In this case no correction for target thickness is generally employed. The formula for this is (starting with the De Staebler yield formula, Eq. (1.34)):

$$H_h = \frac{7.5 \text{ X } 10^{-13} E_o}{(1 - 0.75 \cos\theta)^2 A^{0.4}} \left(\frac{\sin\theta}{a + d}\right)^2 \exp\left(-\frac{\rho d}{\lambda_h \sin\theta}\right). \qquad (2.23)$$

In this formula H_h is the dose equivalent due to these particles (Sv), E is the beam energy (GeV), A is the atomic weight of the target and λ_h (g/cm^2) is the attenuation length typical of these particles. Table 2.3 taken from (Sc90) gives values of λ_h for representative materials. (Sc90) goes further and describes a variety of special cases.

Table 2.3 Attenuation lengths λ_h in g/cm^2 for the high energy particle component. [Adapted from (Sc90) and references cited therein.]

Material	Energy Limit > 14 MeV[1] or > 25 MeV[2] (g/cm^2)	Energy Limit > 100 MeV	Nuclear Interaction Length (g/cm^2)	Recommended λ_h [Eq. (2.23)] (g/cm^2)
Water			84.9	86
Aluminum			106.4	128
Soil (sand)	101...104*	117	99.2	117
	102...105+	96		
Concrete	101...105*	120	99.9	117
	91	105		
	82...100+	100		
Iron	139+		131.9	164
Lead	244+		194	253

*Attenuation lengths for the indicated values are slightly dependent on angle with the higher value at $\theta = 0^o$ and the smaller value in the backward direction for E > 15 MeV.

+Same remark but for E > 25 MeV.

IV. Theory of Radiation Transport and the Monte Carlo Method

The theoretical material in this section is largely the work of Mr. Keran O'Brien of the University of Northern Arizona, (OB80). It is included to show clearly the mathematical basis of the contents of shielding codes, especially those which use the Monte-Carlo method.

General Considerations

Stray and direct radiations at any location are distributed in particle type, direction, and energy. To determine the amount of radiation present for radiation protection purposes we must assign a magnitude to this multidimensional quantity. This is done by forming a double integral over energy and direction of the product of the flux and an approximate flux-to-dose or flux-to-dose-equivalent conversion factor, summed over particle type;

$$H(\mathbf{x},t) = \sum_i \oint_{4\pi} d\Omega \int_0^\infty dE\, f_i(\mathbf{x},E,\Omega,t)\, H_i(E) \qquad (2.24)$$

$$(i = p, n, e^{\pm}, \pi^{\pm}, \mu^{\pm}, \text{heavy nuclei}, \ldots)$$

where Ω is the direction vector of particle travel, $\mathbf{x}$ is the coordinate vector of the point in space where the dose or dose equivalent is to be calculated, E is the particle energy, t is time, and i is the particle type. (Here we adopt the conventional notation that bold-faced coordinates represent vector quantities.) $H_i(E)$ is the flux-to-dose or flux-to-dose-equivalent conversion factor expressed as a function of energy and particle type. The inner integral is over all energies while the outer integral is over all spatial directions which contribute to the radiation field at the location specified by $\mathbf{x}$. The result of the integration is H, the dose or dose-equivalent rate at location $\mathbf{x}$. Values of H_i are tabulated in (IC87). The angular flux, $f_i(\mathbf{x},E,\Omega,t)$, the number of particles of type i per unit area, per unit energy, per unit solid angle, per unit time at location $\mathbf{x}$, with a energy E, at a time t and traveling in a direction Ω is related to the scalar flux, or flux density by integrating over direction,

$$\phi_i(\mathbf{x},t) = \oint_{4\pi} d\Omega \int_0^\infty dE\, f_i(\mathbf{x},E,\Omega,t), \qquad (2.25)$$

to the fluence by integrating over the intervening period of time,

$$\phi_i(\mathbf{x}) = \oint_{4\pi} d\Omega \int_0^\infty dE \int dt f_i(\mathbf{x},E,\Omega,t), \qquad (2.26)$$

and to the energy spectrum at point $\mathbf{x}$ at time t by,

$$\phi_i(\mathbf{x},t,E) = \oint_{4\pi} d\Omega\, f_i(\mathbf{x},E,\Omega,t). \qquad (2.27)$$

To determine the proper dimensions and composition of a shield, the amount of radiation (expressed in terms of the dose or dose equivalent) which penetrates the shield and reaches locations of interest must be calculated. This quantity must be compared with the maximum permissible dose equivalent. If the calculated dose or dose equivalent is too large, either the conditions associated with the source of the radiation (e.g., the amount of beam loss allowed by the beam control instrumentation, the amount of residual gas in the vacuum system, or the amount of beam allowed to be accelerated) or the shield dimensions must be changed. It is difficult and expensive, especially in the case of the larger accelerators, to alter permanent shielding or operating conditions if the determination of shielding dimensions and composition has not been done correctly. The methods for determining these quantities have been investigated by numerous workers. The next section only summarizes the basics of this important work.

The Boltzmann Equation

The primary tool for determining the amount of radiation reaching a given location is the Boltzmann equation which, when solved, yields the angular flux: $f_i(\mathbf{x},E,\Omega,t)$; the distribution in energy and angle for each particle type as a function of position and time. The angular flux is then converted to dose equivalent by means of Eq. (2.24).

This section describes the theory that yields the distribution of radiation in matter, and discusses some of the methods for extracting detailed numerical values for elements of this distribution such as particle flux, or related quantities, such as dose, activation or instrument response. The basis for this theory is the stationary form of the Boltzmann equation (henceforth, referred to simply as the Boltzmann equation) which is a statement of all the processes that the corpuscles of various types that comprise the radiation field can undergo.

The Boltzmann equation is an integrodifferential equation describing the behavior of a dilute assemblage of corpuscles. It was derived by Ludwig Boltzmann in 1872 to study the properties of gases but applies equally to the behavior of those "corpuscles" which comprise ionizing radiation.

Boltzmann's equation is a continuity equation of the angular flux, $f_i(\mathbf{x},E,\Omega,t)$, in phase space which is made up of the three space coordinates of Euclidian geometry, the three corresponding direction cosines and the kinetic energy. The density of radiation in a volume of phase space may change in five ways:

1. Uniform translation; where the spatial coordinates change, but the energy-angle coordinates remain unchanged;

2. Collisions; as a result of which the energy-angle coordinates change, but the spatial coordinates remain unchanged, or the particle may be absorbed and disappear altogether;

3. Continuous slowing down; in which uniform translation is combined with continuous energy loss;

4. Decay; where particles are changed through radioactive transmutation into particles of another kind; and

5. Introduction; involving the direct emission of a particle from a source into the volume of phase space of interest: electrons or photons from radioactive materials, neutrons from an α-n emitter, the "appearance of beam particles, or particles emitted from a collision at another (usually higher) energy.

Combining these five elements yields

$$B_i f_i(\mathbf{x},E,\Omega,t) = Q_{ij} + Y_i \tag{2.28}$$

where the mixed differential and integral operator, B_i, is given by

$$B_i = \boldsymbol{\Omega} \bullet \mathbf{grad} \quad + \sigma_i \; + d_i \; - \left\{ \frac{\int dE}{\int EdE} \right\} S_i \; ; \tag{2.29}$$

$$Q_{ij} = \sum_j \oint_{4\pi} d\Omega \int_0^{E_{max}} dE_B \sigma_{ij}(E_B \rightarrow E, \boldsymbol{\Omega}' \rightarrow \boldsymbol{\Omega})\, f_i(\mathbf{x},e,\boldsymbol{\Omega}',t); \tag{2.30}$$

and

$$d_i \; = \frac{\left[\sqrt{1 - \beta_i^2}\right]}{T_i c \beta_i}. \tag{2.31}$$

B_i is the Boltzmann operator for particles of type i;

Y_i is the number of particles of type i introduced by a source per unit area, time, energy, and solid angle;

σ_i is the absorption cross section for particles of type i. To be dimensionally correct, this is actually the macroscopic cross section or linear absorption coefficient $\mu = N\sigma$ as defined in Chapter 1, Eq. (1.8) ;

d_i is the decay probability per unit flight path of radioactive particles (such as muons or pions) of type i;

S_i is the stopping power for charged particles of type i (assumed to be zero for uncharged particles);

Q_{ij} is the "scattering-down" integral, the production rate of particles of type i with a direction Ω, an energy E at a location **x**, by collisions with nuclei or decay of j-type particles having a direction Ω' at a higher energy E_B;

σ_{ij} is the doubly-differential inclusive cross section for the production of type-i particles with energy E and a direction Ω from nuclear collisions or decay of type-j particles with a direction E_B and a direction Ω';

β_i is the velocity of a particle of type i divided by the speed of light c ;

and T_i is the mean life of a radioactive particle of type i in the rest frame.

This equation is quite difficult to solve in general and special techniques have been devised to yield useful results. The Monte-Carlo method is the most common application to the field of radiation shielding.

The Monte Carlo method-general principles

The Monte Carlo method is based on the use of random sampling to obtain the solution of the Boltzmann equation. It is one of the most useful methods for evaluating radiation hazards for realistic geometries which are generally quite complicated to model using analytic techniques. The calculation proceeds by constructing a series of trajectories, each segment of which is chosen at random from a distribution of applicable processes.

In the simplest and most widely used form of the Monte Carlo technique, a history is obtained by calculating travel distances between collisions, then sampling from distributions in energy and angle made up from the cross sections

$$\sigma_{ij}(E_B \rightarrow E, \mathbf{\Omega}' \rightarrow \mathbf{\Omega}). \tag{2.32}$$

The result of the interaction may be a number of particles of varying types, energies, and directions each of which will be followed in turn. The results of many histories will be processed, leading, typically, to some sort of mean and standard deviation.

If p(x)dx is the probability of an occurrence at $x \pm \frac{1}{2} dx$ in the interval [a,b], then

$$P(x) = \int_a^x p(x')dx' \tag{2.33}$$

is the probability that the event will occur in the interval [a, x], and is monotonically increasing, satisfying P(a) = 0, P(b) = 1. If a random number R is chosen, uniform on the interval [0, 1] from a computer routine, the equation

$$R = P(x) \tag{2.34}$$

amounts to a random choice of the value of x, where the distribution function for the event P(x) can be inverted, as

$$x = P^{-1}(R) \tag{2.35}$$

As a simple illustration, to determine when an uncharged particle undergoes a reaction in a one dimensional system with no decays (d = 0) or competing processes (S = 0), we note from Eq. (1.6) and Eq (2.29) that the particle satisfies

$$B_i\phi = \left\{ \mathbf{\Omega} \cdot \mathbf{grad} + \sigma_i \right\}\phi$$

which in this simple situation reduces to the following (in view of the comment made above concerning the nature of σ_i), which is a continuity equation equivalent to Eq. (1.8):

$$B\phi = d\phi/dx + N\sigma\phi = 0. \tag{2.36}$$

The solution to this equation is the familiar

$$\phi = \phi_0 \exp(-x/\lambda), \tag{2.37}$$

where $\lambda = 1/N\sigma$ as in Chapter 1. One can replace x/λ as r, the number of mean-free-paths the particle travels in the medium. The differential probability per unit mean-free-path for an interaction is given by

$$p(r) = e^{-r} \tag{2.38}$$

$$\text{with} \quad P(r) = \int_0^r dr' e^{-r'} = -e^{-r'}\Big|_0^r = 1 - e^{-r} = R \tag{2.39}$$

Selecting a random number, R, then determines a depth r which has the proper physical distribution. By taking into account charged-particle slowing down during passage along r, the correct energy-dependent cross section can be chosen. Of course, quite analogous methods apply to other exponential processes such as radioactive decay. In this simple case, it is clear that one can solve the above for r as a function of R and thus obtain individual values of r from random numbers. For some process, the inversion that is so simple in the above might not be possible analytically. In those situations, other techniques exemplified by successive approximation and "table look-ups" must be employed.

The next sampling process might select which of several physical processes would occur. Another sampling might choose, for instance, the scattering angle which would then provide a new energy.

The Monte Carlo result is the number of times the event of interest occurred for the random steps through the relevant processes. As a counting process it has a counting uncertainty and the variance will tend to decrease as the square root of the run time. Thus high probability processes can be more accurately estimated than low probability processes such as passage through an effective shield in which the radiation levels are attenuated over many orders of magnitude.

It is by no means clear that the distributions obtained using the Monte Carlo method will be normally distributed, so that a statistical test of the adequacy of the mean and standard deviation may be required.

Monte-Carlo Example: A Sinusoidal Angular Distribution of Beam Particles

Suppose one has a distribution of beam particle particles such as exhibited in the following figure.

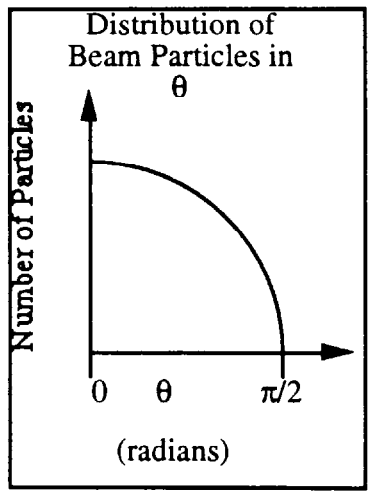

Say $p(\theta) = A \cos\theta$ for $0 < \theta < \pi/2$. Then, the fact that the integral of $p(\theta)$ over the relevant interval must be unity implies:

$$\int_0^{\pi/2} p(\theta)\, d\theta = 1;\ \int_0^{\pi/2} A\cos\theta\, d\theta = 1 \Rightarrow \int_0^{\pi/2} A\cos\theta\, d\theta = A\sin\theta\Big]_0^{\pi/2} = A = 1.$$

Then, $p(\theta) = \cos\theta$. The cumulative probability, $P(\theta)$, is given by:

$$P(\theta) = \int_0^{\theta} d\theta'\, p(\theta') = \int_0^{\theta} d\theta'\, \cos\theta' = \sin\theta'\Big]_0^{\theta} = \sin\theta.$$

If R is a random number, then $R = P(\theta)$ determines a unique value of θ; hence:

$$\theta = \sin^{-1}(R)$$

One can perform a simple Monte Carlo using, for example, 50 random numbers. To do this one should set up at table such as that given below. One can set up a set of bins of succesive ranges of θ-values. The second column is a "tally sheet" for collecting "events" in which a random number R results in a value of θ within the associated range of θ-values. θ_{mid} is the midpoint of the bin (0.1, 0.3,...). Column 4 is the normalized number in radians found from:

$$N = \frac{\text{Number Found in Bin in MC}}{\left(\text{Total Number of MC}\right)\left(\text{bin width}\right)} = \frac{\text{Number Found in Bin in MC}}{\left(50\right)\left(0.2\text{ radians}\right)}$$

θ (radians)	R (random #)	Total R's in Bin	N (norm. #)	$\cos\theta_{mid}$
0.0 - 0.199	~~1111~~ ~~1111~~ 1	11	1.1	0.995
0.2 - 0.399	~~1111~~ ~~1111~~ 111	13	1.3	0.955
0.4 - 0.599	~~1111~~ ~~1111~~ 1	11	1.1	0.877
0.6 - 0.799	1111	4	0.4	0.765
0.8 - 0.999	~~1111~~ 11	7	0.7	0.621
1.0 - 1.199	1111	4	0.4	0.453
1.2 - 1.399				0.267
1.4 - 1.57				0.086

One can calculate exactly the mean value of θ for the exact distribution:

$$\langle\theta\rangle = \frac{\int_0^{\pi/2} \theta\, p(\theta)\, d\theta}{\int_0^{\infty} p(\theta)\, d\theta} = \frac{\int_0^{\pi/2} \theta \cos\theta\, d\theta}{1} = \left[\cos\theta + \theta \sin\theta\right]_0^{\pi/2}$$

$$\langle\theta\rangle = \left[0 - 1 + \frac{\pi}{2} - 0\right] = \frac{\pi}{2} - 1 = 0.57$$

Multiplying the frequency of Monte-Carlo events for each eight angular bins from the table by the midpoint value of the bins, summing over the 8 bins and then dividing by the number of incident particles (50 in this example), one can determine the average value of θ, $< \theta >$ calculated by the Monte-Carlo technique:

$$<\theta>_{calc} = [(11)(0.1) + (13)(0.3) + (11)(0.5) + (4)(0.7) + (7)(0.9) + (4)(1.1)]/50 = 0.48.$$

It is easy to see from this simple example that the agreement is quite good in spite of the rather poor "statistics". This example also illustrates that the statistical errors are generally larger for the more rare events here represented by large values of θ (e.g., θ > 1 radian).

References

(Ba67) G. Barthow, E. Freytag, and K. Tesch, "Measurements on a 6.3 GeV electromagnetic cascades and cascade producing neutrons", Nucl. Phys. B2 (1967) 669-689.

(IC87) International Commission on Radiological Protection (ICRP) Report No. 51 (1987).

(Ne68) R. B. Neal, editor, *The Stanford Two Mile Accelerator* (Benjamin, New York, 1968) {Chapter 26 by H. De Staebler, T. M. Jenkins, and W. R. Nelson).

(Ne90) W. R. Nelson, H. Hirayama, and D. W. O. Rogers, "The EGS4 Code system", SLAC-265, Stanford Linear Accelerator Center (December, 1985). (EGS4 has been thoroughly reviewed in Kae, Bjarngard, and Attix, in *The Dosimetry of Ionizing Radiation,* Volume III (Academic Press, 1990)

(OB80) K. O'Brien, "The Physics of Radiation Transport" in *Computer Techniques in Radiation Transport Dosimetry*, W. R. Nelson and T. M. Jenkins, Editors, Ettore Majorana International Science Series (Plenum Press, New York, 1978), pp. 17-56.

(PR92) *Review of Particle Properties,* Physical Review D45 Part 2 (June, 1992).

(Ro41) B. Rossi and K. Greisen, "Cosmic-ray theory", Rev. Mod. Phy, 13 (1941) 240-309. and B. Rossi, *High Energy Particles* (Prentice-Hall, Englewood Cliffs, New Jersey, 1952).

(Sc90) H. Schopper (editor), A. Fassò, K. Goebel, M. Höfert, J, Ranft, and G. Stevenson, *Landolt-Börnstein Numerical Data and Functional Relationships in Science and Technology New Series; Group I: Nuclear and Particle Physics Volume II: Shielding Against High Energy Radiation* (O. Madelung, Editor in Chief, Springer-Verlag, Berlin, Heidelberg, 1990).

(Sw79) W. P. Swanson, "Radiological Safety Aspects of the Operation of Electron Linear Accelerators," Technical Report No. 188, Vienna, 1979.

(Te88) K. Tesch, "Shielding against high energy neutrons from electron accelerators-a review", Rad. Prot. and Dos. 22 (1988) 27-32.

(Va75) A. Van Ginneken and M. Awschalom, "High energy particle interactions in large targets", Vol. 1, Fermi National Accelerator Laboratory Report (1975).

(Va78) A. Van Ginneken, "AEGIS, a program to calculate the average behavior of electromagnetic showers", Fermilab Report FN-309 (1978).

1. In the discussion of the longitudinal development of electromagnetic showers, there are two different formulations (Rossi-Griesen and Bathow, and Van Ginneken). Using Van Ginneken's scaling method, calculate the value of λ_t (g/cm^2) for E_o = 1000 MeV, 10 GeV, and 100 GeV for copper and lead. Determine the number of radiation lengths to which λ_t, corresponds for each material at each energy.

2. Compare the results of Van Ginneken for the location of the longitudinal shower maximum with Bathow's result for copper and lead at the three energies given in problem 1. Is the agreement better or worse as the energy increases?

3. A hypothetical electron accelerator operates at either 100 MeV or 10 GeV and delivers a beam current of 1 μA. Using the results of (Sc90) calculate the dose equivelent rates in both Sv/sec and rem/h at the end of a 300 cm long aluminum beam stop; averaged over a 15 cm radius. (The beam stop is a cylinder much larger than 15 cm in radius.) Then assume that, in order to save space, a high-Z beam stop is substituted. How long of a high-Z beam stop is needed to achieve the same dose rates? (Assume lead is a suitable high-Z material.) Why is the length of high-Z shield different for the 2 energies? [In this problem, assume the results of (Sc90) are valid for energies as low as 0.1 GeV.]

4. In the accelerator and beam stop of problem 3, if the radius of the beam stop is 30 cm, what is the maximum dose equivalent rate (Sv/s and rem/h) on the lateral surface (at contact at r = 30 cm) of the beam stop for both energies, 100 MeV and 10 GeV, and both materials? Again assume approximate validity at 100 MeV of the (Sc90) results.

5. Calculate the dose equivalent rate outside a 1 meter thick concrete shield surrounding a radius tunnel (inner radius 1 meter) in which is located a copper target stuck by 1 μA beam of 100 GeV electrons. The geometry should be assumed to be optimized for producing giant resonance photoneutrons and the calculations should be performed at θ = 30, 60 and 90° (Concrete has ρ = 2.5 g/cm^3). Express the result as Sv/sec and rem/h.

6. This problem gives two elementary examples of Monte Carlo techniques that are almost "trivial". In this problem, obtaining random numbers from a standard table or from a hand calculator should be helpful.

a) First, use a random number table or random number function on a calculator along with the facts given about the cumulative probability distribution for exponential attenuation to demonstrate that, even for a sample size as small as, say, 15, the mean value of paths traveled is "within expectations" if random numbers are used to select those path lengths from the cumulative distribution. Do this, for example, by calculating the mean and standard deviation of your distribution.

b) An incident beam is subjected to a position measurement in the coordinate x. It is desirable to "recreate" incident beam particles for a shielding study using Monte-Carlo. The x distribution as measured is as follows:

x	#
0	0
1	1
2	3
3	3
4	4
5	5
6	4
7	3
8	2
9	1
10	0

Determine, crudely, p(x), P(x) and then use 50 random numbers to "create" particles intended to represent this distribution. Then compare with the original one which was measured in terms of the average value of X and its standard deviation. Do <u>not</u> take the time to use interpolated values of x, simply round off to integer values of x for this demonstration.